

**MODELING OF GAS NITRIDING USING
ARTIFICIAL NEURAL NETWORKS**

MODELING OF GAS NITRIDING USING ARTIFICIAL NEURAL NETWORKS

By

UMAR AFZAAL,

B.Sc.

A Thesis

Submitted to the School of Graduate Studies

in Partial Fulfillment of the Requirements

for the Degree

Master of Applied Science

McMaster University

© Copyright by UMAR AFZAAL, December 2006

MASTER OF APPLIED SCIENCE (2006)
(Mechanical Engineering)

McMaster University
Hamilton, Ontario

TITLE: Modeling of Gas nitriding using Artificial Neural Networks

AUTHOR: Umar Afzaal,
B.Sc. (University of Engineering and Technology, Lahore, Pakistan)

SUPERVISOR: Dr. M.S.Hamed
Department of Mechanical Engineering

NUMBER OF PAGES: xvi, 123

ABSTRACT

In North America, heat treating adds about \$15 billion per year in value to metal goods by imparting specific properties that are required if parts are to function successfully. Heat treating is an energy-intensive industry, requiring about 500 trillion BTUs (~ 0.5 trillion ft³ of natural gas) per year, which accounts for about 20% of the total cost of the business. Considering this huge demand on energy resources and its significant impact on the environment, in the year 1996, members of the heat treating industry represented by the ASM Heat Treating Society and the Metal Treating Institute (MTI) met and discussed the future of the heat treating industry in North America. A vision was developed known as “Heat Treating Industry Vision-2020”. In that vision, the industry identified key research areas among which was the development of integrated process models. The industry recognized that most current heat-treating procedures are based on the experience of the heat treater. Trial-and-error often results in operations or components that are functional but not optimized.

The present study is concerned with the development of process models of gas nitriding operations using Artificial Neural Networks (ANNs). Data required for the development of ANNs have been acquired from experiments carried out at the industrial partner site, VAC AERO International, Oakville, Ontario. Two types of ANNs have been developed and tested using the experimental data. The two models were able to predict

various case depths produced by the nitriding process with reasonable accuracy in the $\pm 20\%$ range. Predictions of the white layer thickness were in the $\pm 40\%$ range. The sensitivity of predictions due to measurement errors has been investigated. The range of measurement error of the current study did not have a significant effect on the ANNs predictions.

The effect of rate of cooling after the nitriding operation on the developed case depths has also been investigated. Cooling rates in the range of $3^\circ \text{F}/\text{min}$ to about $20^\circ \text{F}/\text{min}$ were tested. Results indicated that this range of cooling rates do not have a significant effect on the developed case depths.

The present study has confirmed that ANNs models have the ability to be trained and applied to multivariable systems which renders ANNs the most suitable tool to develop integrated models for heat treating processes.

ACKNOWLEDGEMENTS

I would like to dedicate this work to my parents and my wife who supported and encouraged me to overcome difficulties while undertaking this research work. I would also like to thank the following people for their contribution to this work:

Dr.M.S.Hamed for his patience, continuous guidance, support and encouragement throughout the course of the master's work.

Jeff Pritchard, Jerome Darbellay and Mark Passalent of VAC AERO International Inc. for their financial and technical support of this project.

I also acknowledge OCE – CMM (Centre for Materials and Manufacturing) for their financial support.

Friends and colleagues of the Thermal Processing Laboratory (TPL) and CSTP Centre for Solidification and Thermal Processing (CSTP) for their support and friendship.

TABLE OF CONTENTS

Abstract.....	iv
Acknowledgements.....	vi
Table of Contents.....	vii
Appendices.....	xi
List of Figures.....	xii
List of Tables.....	xv
Chapter 1:Introduction and Literature Review.....	1
1.1. Introduction.....	1
1.2. Literature Review.....	8
1.2.1 Investigations on gas nitriding.....	11
1.2.1.1 Nitriding case structure and properties.....	11
1.2.1.2 Control of gas nitriding process.....	13
1.2.1.3 Nitriding is a complex and multivariable process.....	14
1.2.1.4 Investigations on the two stage gas nitriding process.....	18
1.2.1.5 Investigations on the white layer reduction techniques.....	19
1.2.2. Modeling techniques used in thermal processing.....	20
1.2.3 Investigations on modeling and simulation of gas nitriding.....	22
1.2.4 Investigations on artificial neural network modeling.....	23
1.2.4.1 Structure and characteristics of Artificial Neural Networks.....	24

1.2.4.2	Investigations on the use of Artificial neural networks in material science.....	28
1.2.4.3	Artificial Neural Network (ANN) modeling of nitriding process.....	29
1.2.4.4	Techniques for evaluation of the performance of ANN modeling.....	29
1.2.4.5	Investigations on data preparation ,data availability and predictive power of Artificial Neural Network.....	30
1.2.5	Objective of the present study	31
Chapter 2:	The Experimental Facility	
2.1	Introduction.....	32
2.2	Experimental facility.....	33
2.2.1	Process and purging gas supply.....	33
2.2.2	Nitriding furnace and its control panel.....	36
2.2.2.1.	Heat source.....	37
2.2.2.2.	The Retort and the lid.....	37
2.2.2.3	The Control Panel.....	41
2.2.2.4	TheCooling stand.....	45
2.2.3	The ammonia dissociator.....	46
2.3	Furnace modification.....	48
Chapter 3:	Experimental Methodology.....	49
3.1.	Design of Experiments.....	51
3.2.	Sample Preparation.....	51
3.3.	Set up prior to running the test cycles.....	54
3.3.1	Specimen placement.....	54

3.3.2. Attachment of sample thermocouples.....	56
3.4. Typical experimental procedure.....	57
3.5 Data Collection.....	58
3.5.1 Rockwell superficial hardness testing.....	58
3.5.2 Micro hardness testing.....	59
3.5.2.1 Sample sectioning.....	59
3.5.2.2 Sample mounting.....	61
3.5.2.3 Grinding and polishing.....	62
3.5.2.3.1 Plane or coarse grinding.....	62
3.5.2.3.2 Fine grinding.....	63
3.5.2.3.3 Polishing.....	63
3.5.2.3.4 Vickers micro hardness testing.....	63
3.5.3 Metallographic examination.....	66
3.5.3.1 Etching.....	66
3.5.3.2 Storage after etching.....	66
3.5.3.3 Optical microscopy.....	67
3.6 Data compilation.....	68
Chapter 4: Results and Discussion.....	69
4.1. Artificial Neural Network(ANN) modeling.....	69
4.1.1 Introduction to Neural ware Predict.....	69

4.1.2	Modeling using neural ware predict.....	70
4.1.3	Modeling using Radial Basis function neural network.....	72
4.1.4	Characteristics of validation data for modeling.....	74
4.1.5	Reverse modeling.....	75
4.2	Investigation on non-uniform/discontinuous structure of white layer.....	77
4.2.1	Effect of cooling rate from nitriding temperature.....	78
4.2.2	Effect of pre treatment of Nitralloy bars.....	81
4.3.	Nitriding parameter variation profile during a typical cycle.....	84
4.4.	Sensitivity analysis.....	87
Chapter 5 :	Conclusions.....	89
Chapter 6:	Recommendations.....	92
List Of	References.....	94

APPENDICES

Appendix 1 a99
Appendix 1b.....100
Appendix 2.....101
Appendix 3.....102
Appendix 4103
Appendix 5.....106
Appendix 6.....109
Appendix 7.....112
Appendix 8.....115
Appendix 9.....119
Appendix 10.....120
Appendix 11.....121
Appendix 12.....122
Appendix 13.....123

LIST OF FIGURES

Figure 1.1 Characteristics of Thermo-chemical diffusion techniques.....	3
Figure 1.2 Iron-Nitrogen phase diagram.....	4
Figure 1.3 Area "A" of Fe-N phase diagram.....	4
Figure 1.4 Area "B" of Fe-N phase diagram.....	5
Figure 1.5 An Artificial neuron.....	7
Figure 1.6 A photomicrograph showing a nitrided case with white layer and diffusion case.....	10
Figure 1.7 Modified Lehrer diagram.....	12
Figure 1.8 Creation process of Nitrided layer.....	15
Figure 1.9 Structure of an artificial neural network.....	24
Figure 1.10 An Artificial Neuron.....	25
Figure 2.1 Schematic of experimental facility.....	34
Figure 2.2 Above ground liquid Ammonia container.....	35
Figure 2.3 Nitrogen gas storage tank and evaporator.....	35
Figure 2.4 A general view of gas nitriding furnace setup.....	36

Figure 2.5 retort being lowered in cooling stand.....	38
Figure 2.6 Interior view of retort showing load basket and ammonia inlet pipe.....	38
Figure 2.7 Retort lid with atmosphere circulation fan	39
Figure 2.8 A general view of load basket with liner.....	39
Figure 2.9 A cut away section of retort and lid assembly	40
Figure 2.10 A pictorial view of nitriding control panel model 9210	41
Figure 2.11 Flow sensor operational diagram.....	43
Figure 2.12 Hydrogen and oxygen sensors installed in control panel	44
Figure 2.13 A pictorial view of cooling stand with retort	45
Figure 2.14 Lindberg Ammonia dissociator	47
Figure 2.15 Ammonia dissociator gas cooler	47
Figure 2.16 A general view of modified furnace retort lid.....	48
Figure 3.1 A typical specimen of Nitralloy 135M.....	53
Figure 3.2 A pictorial view of furnace retort load basket.....	54
Figure 3.3 Load basket spokes with three specimens hanging.....	55
Figure 3.4 Furnace retort with fixture for thermocouples installation.....	56
Figure 3.5 Control panel user interface.....	57
Figure 3.6 Newage indentron superficial hardness tester with indenter	58

Figure 3.7 Enlarged view of sphero-conical diamondtype indenter for superficial hardness tester	59
Figure 3.8 IMPTECH EUROPE abrasive cutter powered by 2.2 Kw.2800 RPM motor	60
Figure 3.9 Exicut technique in operation	60
Figure 3.10 BUEHLER SIMPLIMET 3 hot mounting machine	61
Figure 3.11 STRUERS ROTOPOL-2 grinding/polishing machine.....	62
Figure 3.12 MITUTOYO MVK-HO Microhardness tester	64
Figure 3.13 Indents on nitrided case of Nitralloy 135M(x400).....	65
Figure 3.14 Vickers diamond indenter indentation profile	65
Figure 3.15 Calibration curve of Mitutoyo microhardness tester.....	66
Figure 3.16 ZEISS optical microscope	67
Figure 3.17 A photomicrograph of a sample nitrided for 20hrs at a K_N of 0.45 at 1050 °F with a white layer thickness of 12.1085 μ (x1000)	68
Figure 4.1a Aphotomicrograph showing non uniform portion of white layer with thickness of 30.7933 μ m(x1000)	77
Figure 4.1b A photomicrograph showing non –uniform portion of white layer with zero thickness(x 1000).....	77
Figure 4.2 A photomicrograph of white layer of thickness 16.38 μ m from sample(x1000).....	80

Figure 4.3 A photomicrograph of white layer of thickness 16.06 μ m from sample NN39S122(x1000).....	80
Figure 4.4 Bar 1 tempered marteniste grain structure (x1000).....	82
Figure 4.5 Bar 2 tempered marteniste grain structure.....	82
Figure 4.6 SEM image of Nitralloy 135M bar1(x5000).....	83
Figure 4.7 SEM image of Nitralloy 135M bar2(x5000).....	83
Figure 4.8 Temperature variation during 5 hrs of first stage of cycle NN29.....	84
Figure 4.9 Temperature variation during 10hrs of second stage of cycle NN29.....	85
Figure 4.10 K_N variation during 5hrs of first stage of cycle NN29.....	86
Figure 4.11 K_N variation during 10hrs of second stage of cycle NN29.....	86

LIST OF TABLES

Table 1.1 Characteristics of nitriding processes.....	6
Table 3.1 Percentage composition of Nitralloy 135M.....	50
Table 3.2 Values of process parameters used in experimentation.....	50
Table 4.1 Consolidated results of Neuralware modeling.....	71
Table 4.2 Consolidated results from Radial Basis function neural network	

modeling.....	73
Table 4.3 Results of reverse neural network modeling.....	76
Table 4.4 Cycle parameters for NN1.....	77
Table 4.5 Nitrided sample properties from two cycles NN29& NN39 to compare effect of cooling rate.....	79
Table 4.6 Hardening and tempering sequence of Nitralloy 135M bars.....	81

Chapter 1

INTRODUCTION AND LITERATURE REVIEW

1.1 Introduction

Steel is often called a “wonder metal” because of its tremendous flexibility in heat-treating and metal working to produce a wide variety of mechanical, physical and chemical properties, for example, the hardness can be increased by up to 500% just by changing the cooling rate from austenizing temperature from extremely slow to extremely fast. The generally accepted definition of heat treatment is; a combination of heating and cooling operations, timed and applied to a metal or alloy in the solid state in a way that will produce desired properties [1,2].

Surface treatment is a type of heat treatment and is also known as surface modification or surface engineering. It can be divided into two distinctive groups: deposition and diffusion techniques surface treatments. Deposition surface treatments are characterized as transporting a metallic substance from source metal and depositing it onto the surface of another metal. These techniques include electroplating, hard coating (thermal flame spray), physical vapour deposition (PVD) and chemical vapor deposition (CVD). Diffusion surface treatments involve surface and subsurface modification without any additional buildup or increase in part dimensions. They are further subdivided into two distinctive categories: thermo- chemical and thermal. Thermo-chemical diffusion

techniques, namely nitriding, carburizing, carbonitriding, ferritic nitrocarburizing and boronizing are characterized as diffusing an element, such as nitrogen, carbon, sulfur, boron, and oxygen, into the surface of the steel by the application of the appropriate amount of heat, time, and the steel surface catalytic reaction. Figure 1.1 shows the process temperature range and process characteristics of different thermo-chemical diffusion techniques. Thermal techniques, e.g. flame hardening, laser heat treatment, induction hardening treatment, etc., are those that modify the surface phases of steel containing sufficient carbon to allow the transformation from austenite to martensite when appropriate amount of heat is applied to the immediate surface [3].

Of the thermo-chemical diffusion techniques, nitriding is the introduction of nitrogen in the surface layers of ferrous alloys by holding the surface at a suitable temperature below the lower transformation temperature, (A_{c1}) as shown in Figure 1.2 for pure iron, in contact with a nitrogen- rich environment. Different phases (α , γ' and ϵ) formed during the process are shown in Figures 1.2, 1.3 and 1.4 and discussed in section 1.2.1.1. Nitriding can be classified into three types: gas, ion and salt bath nitriding (Table 1.1). They can be applied to all steels but the best results are obtained in those steels that contain one or more of the major nitride-forming alloying elements such as aluminum, vanadium, chromium, and molybdenum. The nitrogen must be supplied in the atomic or nascent form; molecular nitrogen will not react [1, 2, 4]. Gas nitriding seems to be more promising than the other methods from the standpoint of simplicity of equipment and variety of geometry and sizes of treated parts [5].

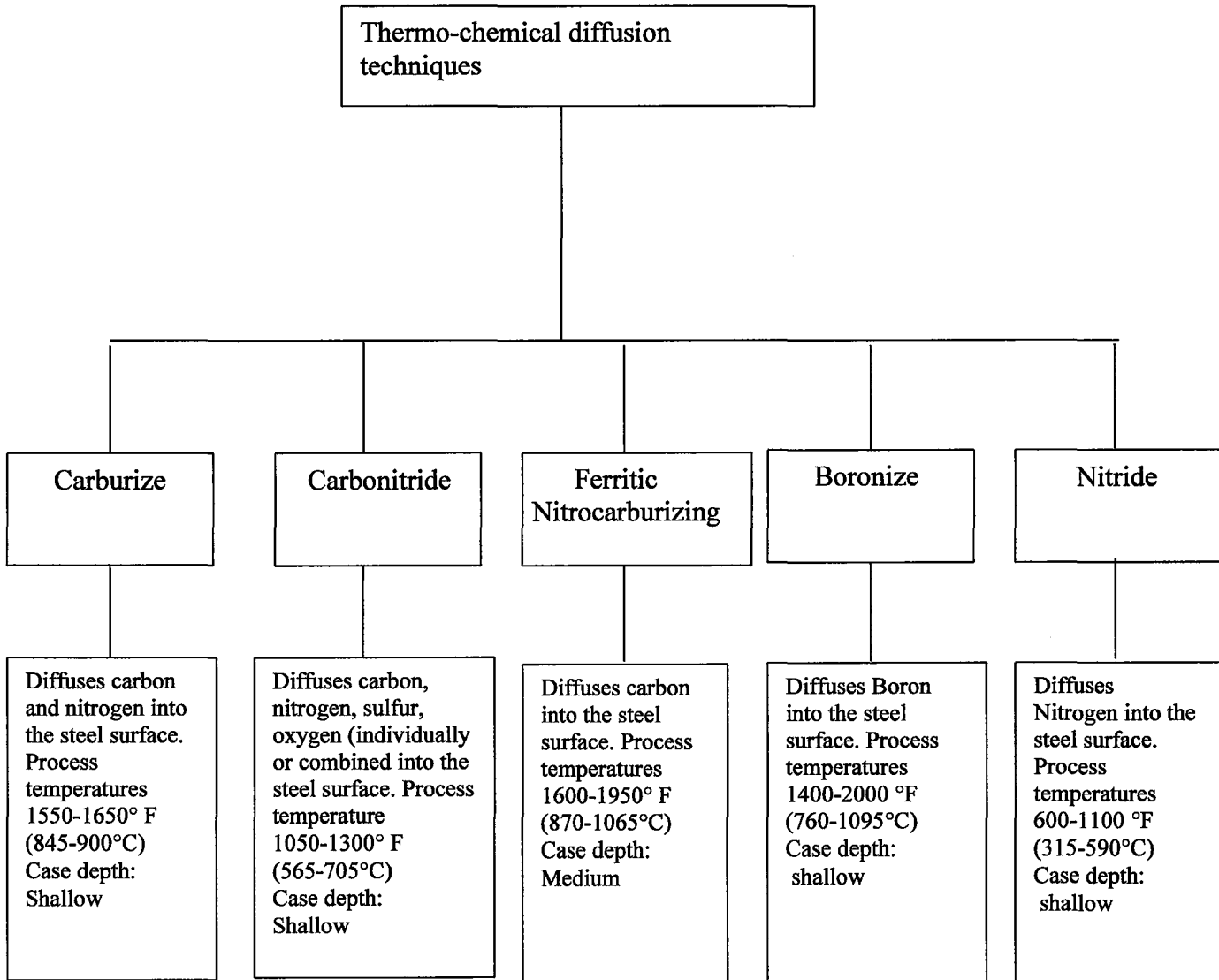


Figure 1.1: Characteristics of thermo-chemical diffusion techniques [4]

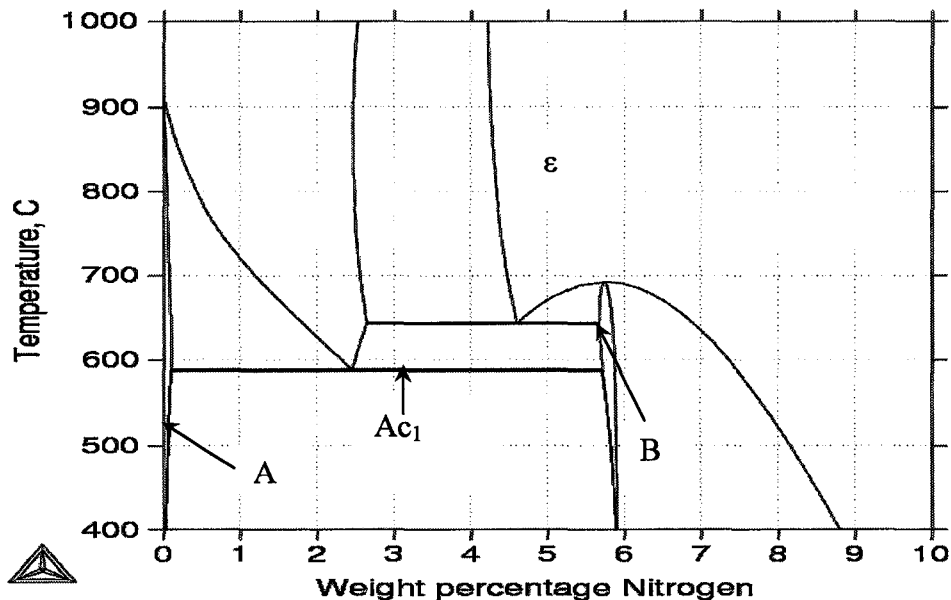


Figure 1.2: Iron-Nitrogen (Fe-N) phase diagram (Thermocalc[®] software)

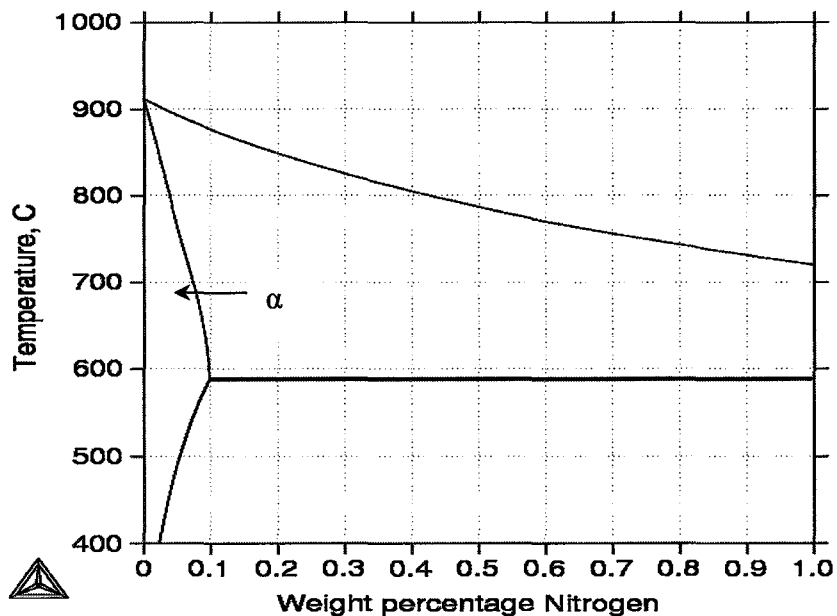


Figure 1.3: Area “A” of Fe-N phase diagram

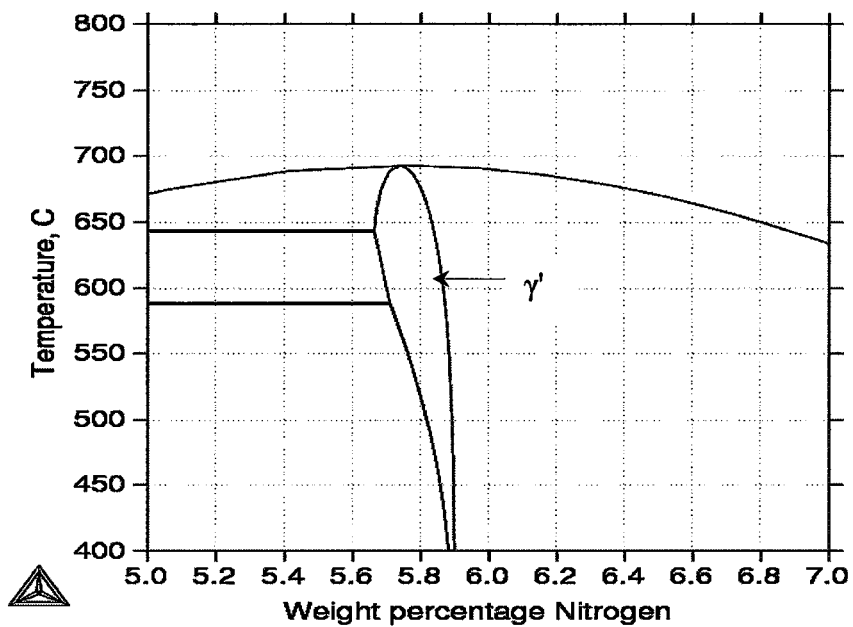


Figure 1.4: Area "B" of Fe-N phase diagram

Table 1.1: Characteristics of nitriding processes [4]

Process	Nature of case	Process temperature (°F)	Typical case depth (µm)	Typical base metals
Gas	Diffused Nitrogen and Nitrogen compounds	900-1100	125-750	Alloy steels, Stainless steels,
Ion	Diffused Nitrogen and Nitrogen compounds	650-1050	75-750	Alloy steels, Stainless steels,
Salt-bath	Diffused Nitrogen and Nitrogen compounds	950-1050	25-750	Most ferrous alloys including cast irons

For material scientists and engineers, a common goal is the determination of the relationship between the structure of a material and its properties. Obviously, the ability to predict the properties of materials prior to their synthesis and processing would be of tremendous value in optimizing the end product. To achieve the goal of properties prediction, modeling of heat treatment operations is required. Modeling is actually an approximation of reality. Practical processes and systems are generally very complicated and must be simplified through idealizations and approximations to make the problem solvable. A good model preserves all properties of interest. Different types of modeling techniques: analytical, numerical and empirical have been used in thermal processing of materials [6]. However,

there are situations in which the available models only deal with small part of the required problem [7]. Artificial Neural networks (ANNs) consist of artificial neurons discussed in reaction section 1.2.4.1, have emerged as new branch of computing that have shown remarkable performance when used to model complex linear and non-linear relationships. A neural network is a machine that is designed to model the way in which brain performs a particular task or function of interest; the network is usually implemented by using electronic components or is simulated in software on a digital computer [8]. This mathematical technique is especially useful for simulation of any correlation that is difficult to describe with physical models because of the neural network's ability to learn by example and recognize patterns in a series of input and output values from input data sets. Nowadays, ANNs are commonly used in the field of material science and physical metallurgy [9]. The main objective of the present study is to investigate the use of ANNs in modeling the gas nitriding surface treatment process.

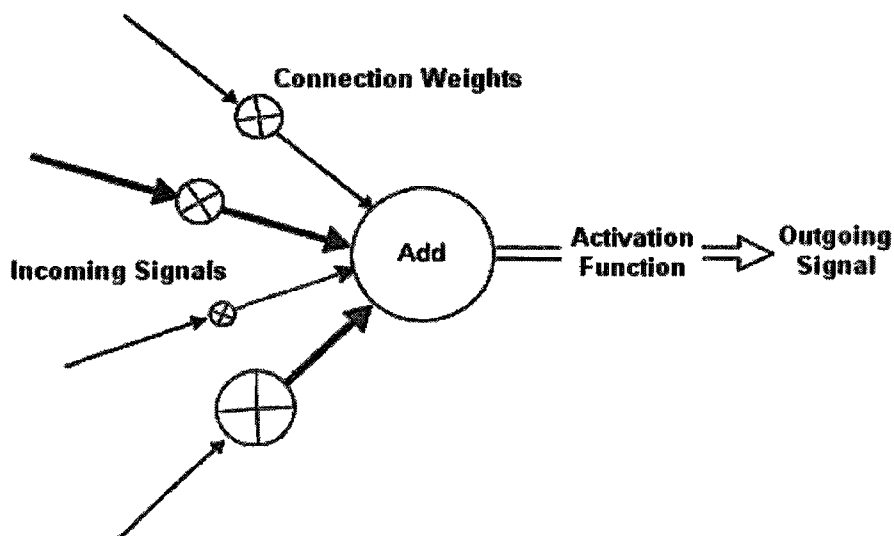


Figure 1.5: An artificial neuron [10]

1.2 Literature review

Gas Nitriding is a case-hardening process whereby nitrogen is introduced into the surface of a solid ferrous alloy by holding the metal at a suitable temperature (below A_{c1} for ferritic steels) as shown in figure 1.2 in contact with a nitrogenous gas, usually ammonia. The nitriding temperature for all steels is between 925 and 1100 ° F (495 and 590 °C) At these temperatures, the ammonia dissociates into its components according to the following reaction [5].



Nitrogen is very active at the moment of dissociation of the ammonia gas, combines with iron and alloying elements in the steel to form nitrides. These nitrides form on the steel surface as a fine dispersion and impart extremely high hardness to the surface without the need for quenching. Today cams, gear pinions, shafts, seals, cylinder barrels, clutches, piston rings, and many other devices are hardened by nitriding. The aircraft industry makes extensive use of nitrided parts when lubrication is marginal. With requirements for wear and fatigue resistance at relatively high temperatures becoming more and more severe in many fields, it seems certain that applications for nitriding will still increase in number in the future [11].

Advantages of the nitriding process are [4]:

1. To obtain high surface hardness
2. To increase wear resistance and anti-galling properties

3. To improve fatigue life
4. To improve corrosion resistance (except for stainless steels)
5. To obtain a surface that is resistant to the softening effect of heat treatment up to the nitriding temperature.

Gas nitriding can be employed as a single-stage process or a double-stage process. In single stage process, a temperature in the range of about 925 to 975°F (496 to 524°C) is used, and the ammonia dissociation by volume ranges from 15% to 30%. This process produces brittle “white layer”. The double-stage process known as the “Floe Process” was developed by Carl Floe in the middle of the twentieth century has the advantage of reducing the thickness of the white nitrided layer. In the first stage of the double-stage process the ammonia dissociation is held at 20 % by volume for a period of 5 to 10 hrs at 975 °F. During this period the white layer is established and the useful nitrides start to form by diffusion of nitrogen out of it. In the second stage, the ammonia dissociation is increased to 65 to 80% by volume, and the temperature is usually raised to 1010 -1050°F (543 - 565°C). During this second stage the gas composition (furnace atmosphere) is such that it maintains only a thin white layer on the finished part. A typical structure of the case produced by this method is shown in Figure 1.6. Generally, an external ammonia dissociator discussed in section 2.2.3 is necessary for obtaining the required second-stage dissociation [2].

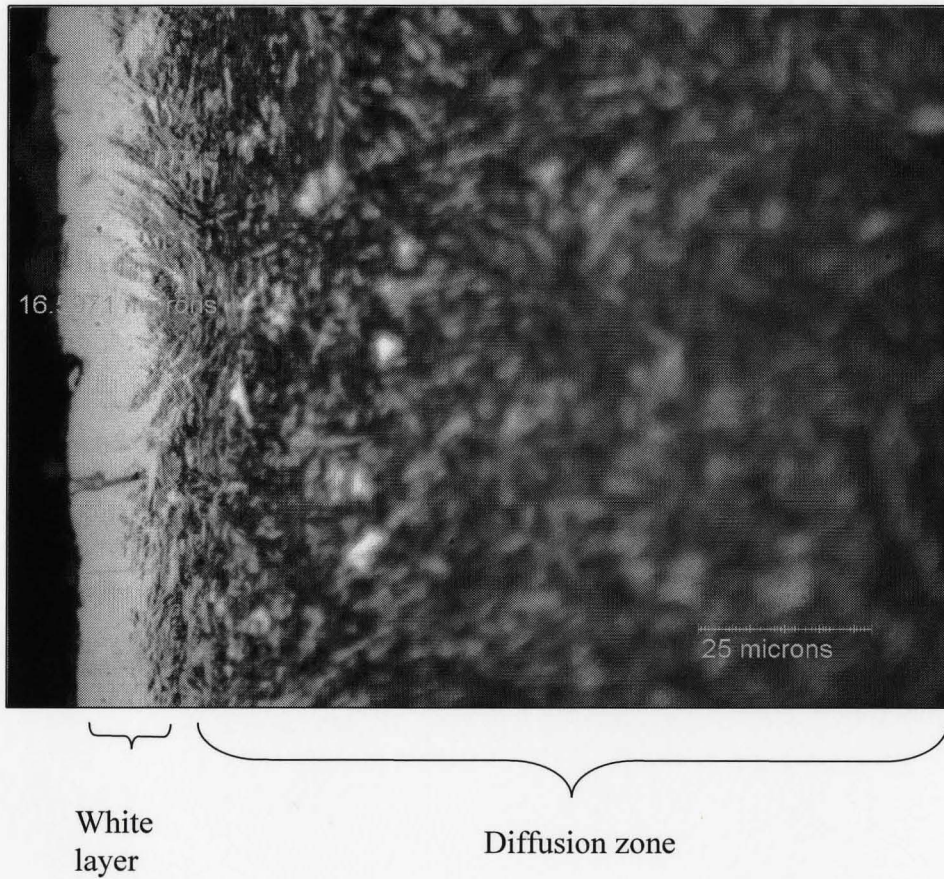


Figure 1.6: A photomicrograph showing a nitrided case with white layer and diffusion zone [12].

1.2.1 Investigations on gas nitriding

1.2.1.1 Nitrided case structure and properties

Ammonia decomposes or dissociates in accordance with equation (1.1). At the instant of decomposition, the liberated nitrogen will exist as nascent or atomic nitrogen and as such can be absorbed by the steel. Nitrogen has an atomic diameter of 0.142 nm and is dissolved in iron in interstitial positions in octahedral voids of the cubic lattice that have a maximum diameter of 0.038 nm in BCC (body centered cubic) alpha (α) ferrite iron and a maximum diameter of 0.104 nm in FCC (face centered cubic) gamma (γ) iron.

Depending on the values of the nitriding potential K_N to be discussed in section 1.2.1.2 and temperature T , nitriding of pure iron according to the binary Fe-N phase diagram shown in figure 1.2 and the modified Lehrer diagram shown in figure 1.7 leads to the formation of the following phases from core to surface of nitrided case.

1. Body-centered cubic α -iron, which dissolves .001 wt% N at room temperature and 0.115%N at 590 °C (1095 °F).
2. The face-centered cubic γ' phase exists at nitrogen concentrations from 5.3% to 5.75% N and consists of Fe_4N .
3. The ϵ -phase ($Fe_{2-3}N$) exists, at various temperatures, in the region of nitrogen concentrations from 4.35% to 11.0% by weight.
4. The ξ -phase (not shown) is formed at nitrogen concentrations not less than 11.0% and it consists of Fe_2N .

A typical nitrided case consists of two zones, a compound zone and a diffusion zone, the layer consisting of γ' and ϵ -phase is the compound zone commonly known as the “white layer” because of its appearance after a nital etch. The diffusion zone consists of α -solid solution of nitrogen in iron and alloy nitrides [13].

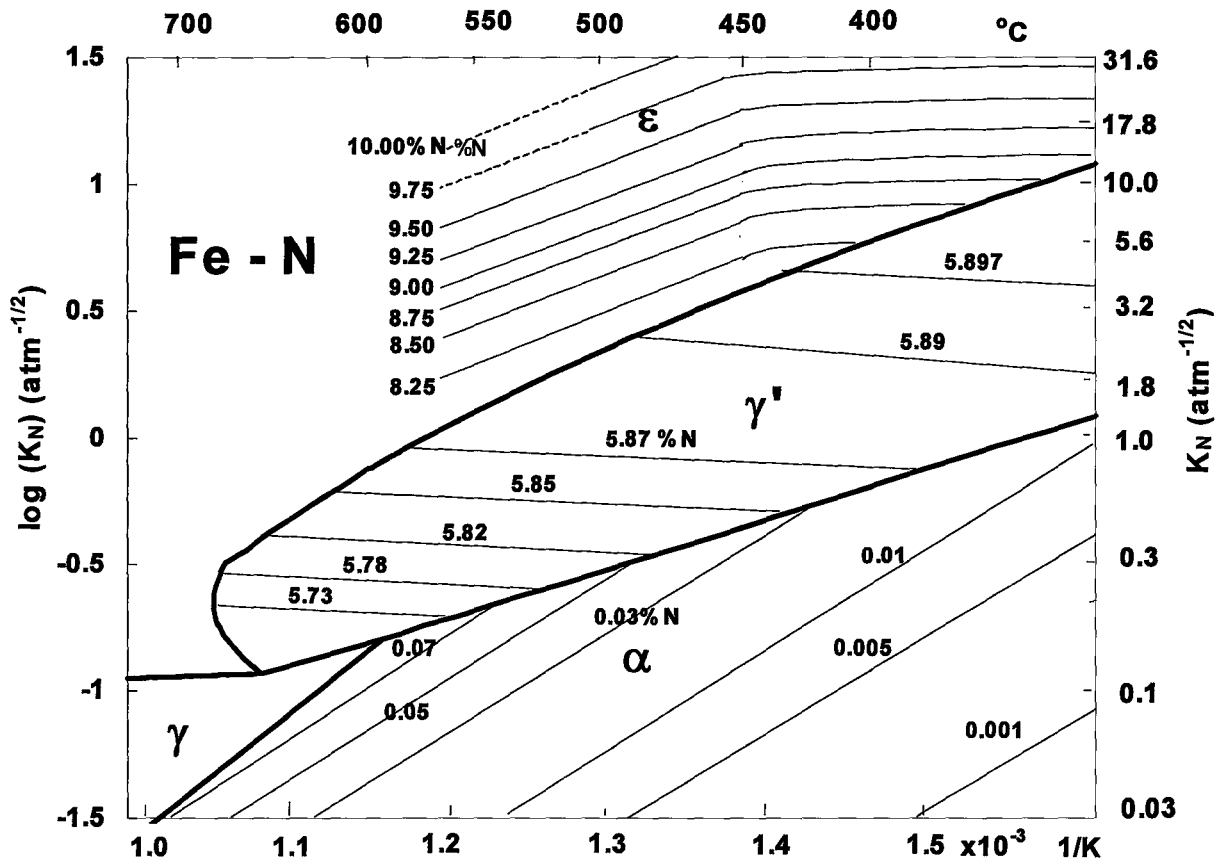


Figure 1.7: Modified Lehrer diagram showing the phases stable at a given K_N and T [14].

1.2.1.2 Control of gas nitriding process

Since the early beginnings of gas nitriding controlling, the percentage of the dissociated ammonia (PD) was considered the appropriate control parameter. This parameter is easily (but discontinuously) measured using the ammonia dissociation burette, which is calibrated directly in PD. This method has an inherent error in it [5], as the measured ammonia content is not equivalent to the actual degree of dissociation. In ammonia dissociation, Eq. 1.1, two molecules of ammonia gas dissociate to two atoms or one molecule of nitrogen gas and three molecules of hydrogen gas. This increase in volume dilutes the ammonia content, as do additional gases, and must be taken into account in determining the actual degree of dissociation.

In the 1990's, however, a new control parameter, the nitriding potential K_N , was introduced. This parameter is defined by the equation 1.2 [5].

$$K_N = \frac{P_{NH_3}}{\sqrt{P_{H_2}^3}} \quad (1.2)$$

where: P_{NH_3} is the partial pressure of Ammonia in the produced atmosphere and P_{H_2} is the partial pressure of Hydrogen in the produced atmosphere, the hydrogen being a product of the dissociated ammonia.

1.2.1.3 Nitriding is a complex and multivariable process [15-18]

Maldzinski et. al. [15] has indicated that in comparison with carburizing, nitriding is more difficult to describe from the point of view of thermodynamics and kinetic laws. The creation process of a nitrided layer comprises many stages as shown in figure 1.8, which include the following:

1. Transport of ammonia in the gas phase and adsorption of gas molecules at the solid surface,
2. Chemical reaction at the surface (ammonia dissociation), which depends on the pressures of the partial components of the atmosphere.
3. Desorption of reaction products (N_2 and H_2), which is influenced by the general rate of gas flow.
4. Transport of nitrogen atoms through the surface and diffusion into the material, and
5. Creation of multiphase nitrided layer (α -Fe (N), γ' , ϵ).

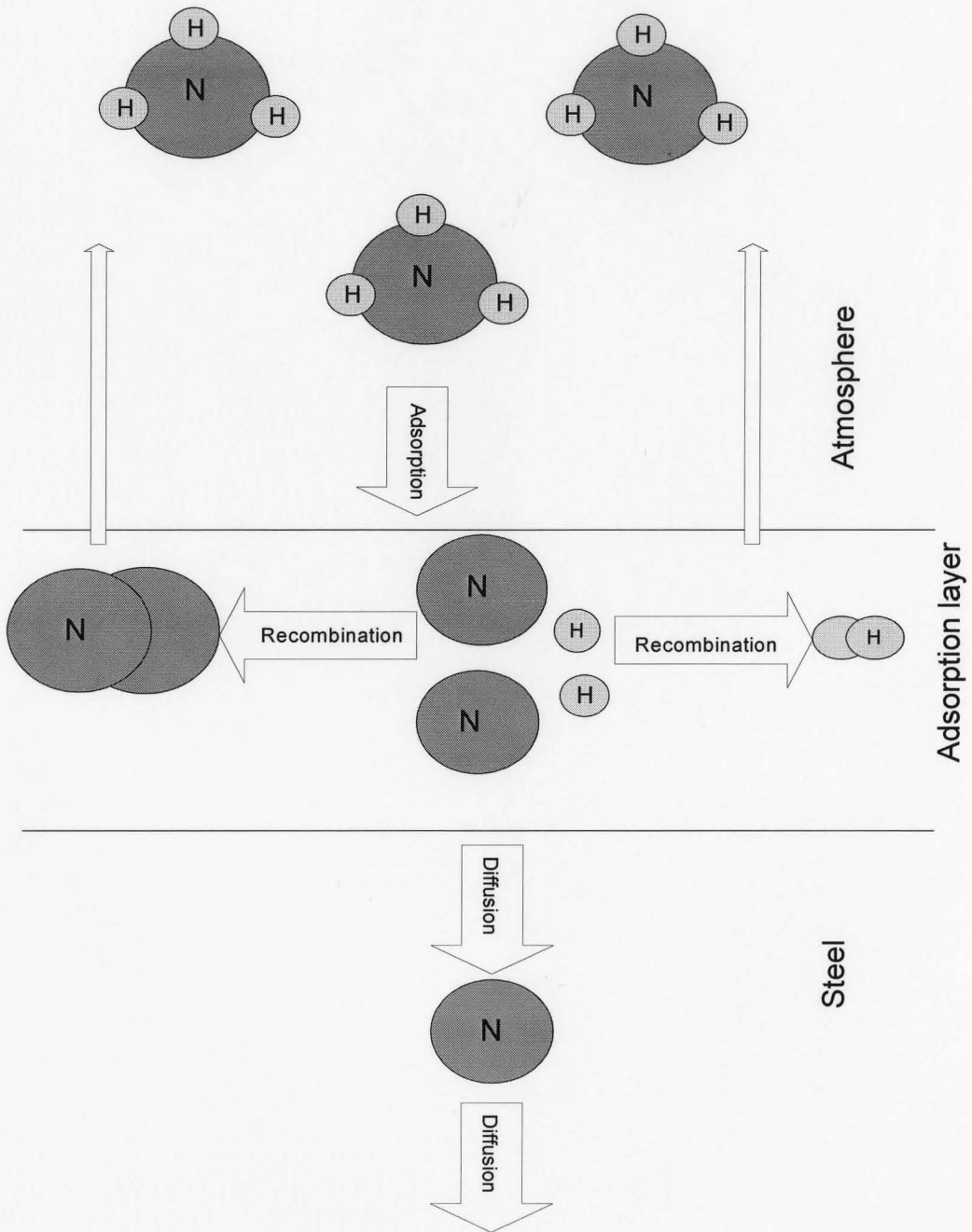


Figure 1.8: Creation process of nitrided layer

As a prerequisite for the predictability of properties obtained by a nitriding treatment of iron based work pieces, the relation between the process parameters and the composition and the structure of the surface layer produced must be known. Interaction between thermodynamics, kinetics and process control of nitriding revealed that thermodynamics of iron nitrides are governed by the ordering of nitrogen atoms on their sublattice. Kinetics provide data for the diffusion coefficients of nitrogen in ϵ and γ' iron nitrides.

A large number of variables influence the nitriding process including the method of nitriding (Gas, Ion, Salt-bath) temperature, duration of the process, cooling rate, depth of penetration, and type of material being processed, pre and post surface treatments [18]. Friehling et. al. [19] studied the effects of pre-oxidation on the nitriding kinetics and found that an oxidation treatment prior to nitriding dramatically reduces the incubation time. Enhanced nucleation is attributed to accelerated dissociation kinetics of NH_3 at the oxide surface as compared to the clean iron surface.

Baranowska et. al. [20] found that cathode sputtering used as pre-treatment before gas nitriding increases the rate of nitride layer formation. This phenomenon is also observed when the neutral gas (argon) is used as sputtering gas.

Thermodynamic description of gas nitriding given by Fe-N equilibrium diagram shown in figure 1.2 provides information about nitrogen concentration in α , γ' and ϵ at the α/γ' , $\alpha/\gamma'/\gamma'$, $\gamma'/\gamma'+\epsilon$ and $\gamma'+\epsilon/\epsilon$ phase boundaries. The Nitriding potential – temperature (K_N -T) diagram shown in figure 1.7 is an experimentally developed version of the Lehrer diagram (developed by E. Lehrer in 1930) with added adsorption isotherms

for nitrogen. It quantitatively describes correlations between concentration of nitrogen in α , γ' and ϵ phases on the one hand, and the nitriding potential of the atmosphere K_N and temperature on the other.

Maldzinski et al. [21] has indicated that there still are gaps in the state of knowledge that need to be filled in order to obtain a full description and understanding of the process of nitriding of iron. Despite the publication of various reports in the field of thermodynamics and kinetics of nitriding, there still remains lack of some data essential to the full description of layer growth during nitriding of iron.

Maldzinski indicated that his model does not take into account the intermediate period of nucleation of the γ' phase, coagulation of nuclei to continuously cover the ferrite surface with γ' , or the time period for the establishment of local equilibrium between the surface concentration of nitrogen and the atmosphere. Experimental research has revealed that at low values of nitriding potential γ' and ϵ phases nucleate very slowly and it is only after substantial amount of time (40 hrs at $K_N=0.25 \text{ bar}^{-1/2}$) that it becomes a continuous compact layer. Even more time is needed for the attainment of local equilibrium between the surface concentration of nitrogen and the atmosphere. With higher nitriding potential, these effect occur faster; only about 3 hours at $K_N=1.25 \text{ bar}^{-1/2}$. Maldzinski has also investigated growth kinetics of nitrified layers on pure iron and low carbon steels (up to 0.2%C) and found these layers to be the same, however higher carbon contents exert a certain effect on growth kinetics of the layer and on its zone structure as well as final phase composition. Greater differences in growth kinetics of nitrified layers should be expected on alloyed steels. The rate of growth of the α (diffusion) zone is determined by the content

of alloying elements; both nitride forming (Aluminum, chromium, vanadium, tungsten, and molybdenum) and non-nitride forming and growth rate falls with their increase. Maldzinski hypothesized that the growth of the compound layer does not appear to be affected by the content of nitride forming elements but does depend on the nickel content. Maldzinski also suggested that alloy steels require more evaluation of the effects of alloying elements on growth kinetics.

1.2.1.4 Investigations on the two stage nitriding process

Maldzinski et al. [21] suggested that nitriding of parts can be done in two processes, a single stage and a two stage process. The single stage process is carried out with a nitriding potential K_N that is constant in time and located on the K_N -T phase diagram shown in figure 1.7. The two stage process is carried out with the first stage at appropriately high nitrogen potential ($K_N: K_N^{\alpha/\gamma'} \ll K_N \ll K_N^{\gamma'/\epsilon}$) allowing rapid nucleation and growth of the γ' phase, and the second stage with K_N lowered in order to retard the growth of the γ' phase and perhaps to cause some reduction in its extent. They showed that the thickness of the γ' zone attained in a single stage process was the same as a two stage process but the total cycle time was less. They also argued that all types of morphologies of nitrided case could be obtained using a two stage process with economy.

In order to accelerate the nitriding process and eliminate embrittlement of the nitrided layer, and conserve ammonia, Lakhtin [22] recommended a nitriding regime in which the nitrogen potential of the atmosphere in the beginning of the process is

maintained at a high level for the first few hours (saturation period) and then decreased (diffusion period).

By changing the degree of dissociation of the ammonia (the nitrogen potential) in the furnace at all nitriding temperatures one can control the phase composition and the nitrogen concentration in the ϵ -phase, e.g. when the degree of dissociation of the ammonia in nitriding process is increased to 50-60%, a high hardness nitride layer is formed on the surface: for 80-90% dissociation only internal nitriding occurs.

The two stage process is an environmentally friendly as ammonia consumption is reduced as compared to the single stage process with similar case characteristics.

1.2.1.5 Investigations on the white layer reduction techniques

Rose et al. [23] found that the nitriding of ferrous materials has grown in popularity due to the ability to achieve significant surface hardness with minimal distortion.

However, due to the increased manufacturing competition and desire to eliminate post heat-treating operations the need for white layer reduction and control has increased dramatically. They have compared a number of techniques that were developed to solve the white layer quandary and divided these elimination techniques into two groups:

- Processes that function during the actual nitriding cycle
- Processes that function after the end of the nitriding cycle.

They rated each reduction technique using the following four criteria

1. Effectiveness
2. Case integrity , with respect to surface damage

3. Case hardness
4. Economics of the process

and appraised the two stage gas nitriding “Floer Process” as the best commercially available white layer reduction technique.

1.2.2 Modeling techniques used in thermal processing

Thermal processing of materials refers to the use of thermal energy (heating and cooling) in order to impart desired mechanical properties in manufactured metal components. With the substantial growth in new and advanced materials e.g. specialized alloys, composites, ceramics and semiconductor materials, thermal processing has become particularly important.

Modeling is one of the most crucial elements in the design and optimization of thermal materials processing systems. Practical processes and systems are generally very complicated and must be simplified through idealizations and approximations to make the problem solvable. This process of simplifying a given problem so that it may be represented in terms of a system of equations, for analysis, or a physical arrangement, for experimentation, is termed as modeling. There are different types of modeling techniques mathematical, statistical, empirical, numerical and artificial neural network modeling [6,24,25,26,27,28]. All are being used in thermal processing of materials.

Mathematical models form the basis for simulation, so that behaviour and characteristics of the system may be investigated without actually fabricating a prototype.

In addition, the simplifications and approximations that lead to a mathematical model also indicate the dominant variables in a problem.

Kang et al. [27] has used mathematical modeling in the modeling and simulation of load heating in heat treatment furnaces. He carried out two case studies for the heat transfer in the heat treatment of blades and drill bits.

Golodnikov et.al [24] used statistical models as tool to reduce time and cost associated with the development and selection of metallic alloys. A multiple regression model was developed which can accurately predict tensile yield strength of high strength low alloy steel based on its chemical composition and processing parameters. Quantile regression was used to model the fracture toughness response. Also discriminative analyses of steels using fitted regression models was done and the results were compared with the conclusions made solely on the basis of actual experimental data. The comparison showed that the statistical modeling approach yields results similar to those obtained by experiments.

Genel [25] made comparison of empirical modeling and Artificial neural networks modeling (ANNs) modeling, to be discussed in section 1.2.4. He used a case of relationship between ion nitrided case depth with chromium content as well as process time.

Numerical modeling and simulation is used in heat treatment operations to make metallurgical, thermal and thermoplastic calculations. Heat treatment and especially

quenching causes distortion and sometimes cracking of a quenched part .To eliminate these undesired effects the whole cycle of heat treatment was simulated by Slovacek [28] using FEM (Finite element modeling) .The goal of this simulation was to bring the whole cycle of heat treatment to optimum to reach the lowest level of residual stresses possible at the end and to meet the required mechanical properties .

1.2.3 Investigations on modeling and simulation of gas nitriding

Various attempts have been made for the numerical simulation of nitrided layer growth on pure iron and steels. Maldzinski et. al. [18] developed a mathematical model constituting a set of differential equations, correlating physical parameters such as diffusion coefficient, activation energy, nitrogen concentration, etc. These parameters in turn depend on certain process variables, such as temperature and nitriding potential. Numerical solution of these equations allowed the determination of variations in layer thickness as function of these parameters. The numerical results of the gas nitriding process demonstrated the influence of the nitriding potential of $\text{NH}_3\text{-H}_2$ atmosphere on the composition and growth kinetics of γ' and ϵ - nitride layers on pure iron. Their simulations made use of the recently developed $K_{\text{N-T}}$ phase diagram, figure 1.7, and growth kinetics models for both phases. Simulation results indicated optimum possibilities of process control for the formation of layers and predictable phase composition, thickness of particular zones, and surface nitrogen concentrations. Growth kinetics of the nitrided layers (ϵ/γ' and α solid solution) on alloy steels with reference to

the role of nitride forming and other alloying elements in process kinetics were also discussed.

Keddam et. al. [29] have shown that it is possible to predict both microstructural constitution nature and thicknesses of nitrated layers as well as the nitrogen profile within the formed phases during gas nitriding of pure iron. The numerical simulation results using diffusion equations as well as the experimental data from literature were presented and compared. No significant discrepancy was found between the computed results and those obtained experimentally within a certain range. They argued that their diffusion model can be extended to be applied to nitriding steels (steel containing nitride forming elements).

Krukovich [30] suggested that simulation of the nitriding process allows one to solve many practical problems of process control.

1.2.4 Investigations on Artificial neural network (ANN) modeling

Haque et.al. [31] reported that Artificial neural networks (ANNs) are revolutionary computing paradigms that try to mimic the biological brains. These ANNs are modeling techniques that are especially useful to address problems where solutions are not clearly formulated or where the relationships between inputs and outputs are not sufficiently known. ANNs have the ability to learn by example. Patterns in a series of input and output are recognized. This acquired ‘knowledge’ can then be used by the ANN to predict unknown output values for a given set of input values. Alternatively, ANNs can

also be used for classification. In this case, the ANN output is a discrete category to which the item described by the input values belongs.

Guanghui et. al.[32] used an artificial neural network model to predict flow boiling curves. Boiling is a complex, multi-variable phenomenon. So far there is no complete theoretical correlation to predict boiling heat flux during all boiling regions specifically as a function of wall superheat. To solve this problem the authors trained an artificial neural network using data of past four decades, the ANN was then used to predict the complete boiling curve. The heat flux as function of the wall superheat was predicted using the ANN model.

1.2.4.1 Structure and characteristics of Artificial neural networks

An artificial neural network as shown in Figure 1.9 is composed of simple interconnected elements called processing elements (PEs) or artificial neurons [31].

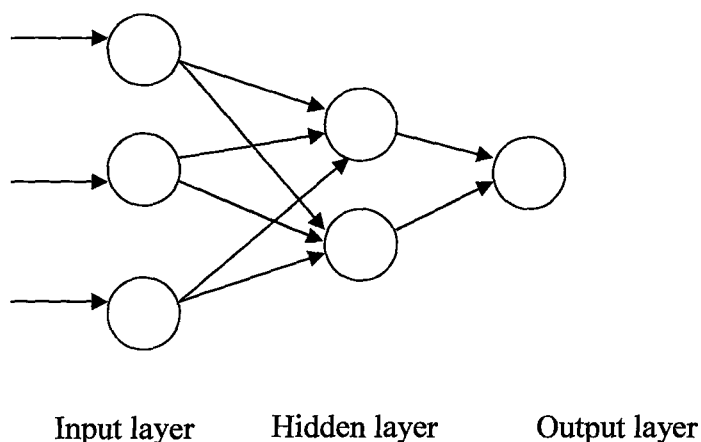


Figure 1.9: Structure of an artificial neural network

The structure of an artificial neuron is shown in Figure 1.10.

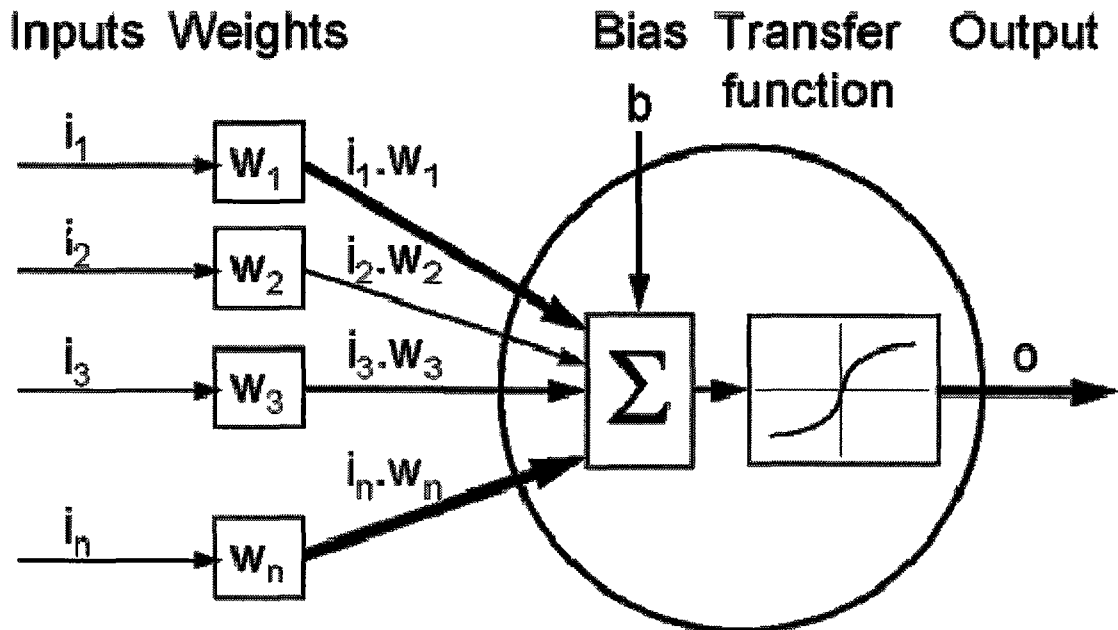


Figure 1.10: An artificial neuron [33].

Each PE has an input and an output side. The connections on the input side correspond to the dendrites of the biological neuron and provide the input from other PEs. The connections on the output side correspond to the axon and transmit the output. Synapses are mimicked by providing connection weights between the various PEs and transfer functions or bias within the PEs. The activation of the PE results from the sum of the weighted inputs and can be negative, zero, or positive. This is due to synaptic weights, which represent excitatory synapses when positive ($w_i > 0$) or inhibitory ones when

negative ($w_i < 0$). The PE output is computed by applying the transfer function to the activation, which is the result of the synaptic weights that can be negative, zero, or positive. The type of transfer function to be used depends on the type of ANN to be designed. Although several functions have been used as transfer functions, the most widely used is the sigmoid function.

The learning paradigm can be of ‘Supervised or Unsupervised learning’. The most widely used supervised learning algorithm/s is the back propagation algorithm.

Erb [34] characterized neural networks by their architecture, transfer function, and learning paradigm. The term ‘architecture of the neural network’ refers to the number of layers in the network and the number of the neurons in each layer. The number of neurons in the input layer and output layer are determined by the number of input and output parameters, respectively. In order to find the optimal architecture, different numbers of neurons in the hidden layer has to be attempted.

Genel [25] used a back propagation (BP) algorithm to train a multilayer, feed -forward ,neural network, which is simple, reliable ,and most commonly utilized for modeling of complex linear and non linear relationships. In order to decide on the optimum structure of the neural network, the rate of error convergence was checked by changing the number of hidden neurons and adjusting the learning rate and momentum coefficient. In essence, back-propagation training adapts a gradient decent approach of adjusting the ANN weights. During the training of an ANN, it is presented with the data thousand of times (called cycles). After each cycle, the error between the ANN output

(predicted) and the actual (or desired) values are propagated backward to adjust the weight in a manner mathematically guaranteed to converge.

Guo et. al. [35] used a BP algorithm and reported that the training time increases dramatically when the number of outputs increases. Therefore, setting up a series of ANN models where each model deals with only one output value significantly simplifies and speeds up the training of the ANN model. They reported that the back propagation algorithm might not always find the correct weights for the optimum solution, a number of re-initializations and re-trainings of the network were carried out to obtain the best solution.

Neural networks of other types may also be considered in model creation, such as radial basis function networks. Such networks may require more neurons than standard feed forward back propagation networks, but often they can be designed in a fraction of the time it takes to train standard feed forward networks.

1.2.4.2 Investigations on the use of Artificial neural networks in materials science

ANNs have been applied to model complicated processes in many engineering fields: aerospace, automotive, electronics, manufacturing, robotics, telecommunications etc. For the last few years, many researchers [26, 35-39] have used various types of ANN modeling techniques in materials science and engineering fields.

Bhadeshia [26] indicated that neural network analysis has had a liberating effect on material science, by enabling the study of incredibly diverse phenomena, which are not as yet accessible to physical modeling. The methodology is used extensively in process control, process design and alloy design. Over recent years the interest in the ANN modeling in the fields of physical metallurgy and materials science has increased rapidly.

Gou et. al. [35] used ANN to correlate between the processing parameters and properties of maraging steels (Steel developed mainly for aerospace and tooling applications). The input parameters of the model consisted of alloy composition, processing parameters including cold deformation degree, aging temperature, and ageing time, and working temperature. The outputs of the ANN model include property parameters namely: ultimate tensile strength, yield strength, elongation, and reduction in area, hardness, notched tensile strength, Charpy impact energy, fracture toughness, and martensitic transformation start temperature.

Genel [9] extracted tensile material data for seventy-three different types of steels for training four separate neural networks to model individual fatigue properties. Fatigue strength coefficient and fatigue ductility (strain) coefficient values, which primarily characterize the curves of the strain amplitude versus life reversals, were predicted with

high accuracy of approximately 99 and 98%, respectively. It was concluded, that predicted fatigue properties by the trained neural network model seem more reasonable compared to approximate methods, which were formerly suggested based on tensile material data. In ANN modeling there is no need to make a prior assumption about concerned material behaviour, making it superior to other conventional prediction techniques.

1.2.4.3 Artificial neural network modeling of nitriding processes

Filetin et.al. [40] indicated that the selection of the nitriding process parameters is based on experience . There are no successful mathematical and/or numerical models for the simulation of nitriding process simulation. ANN has proved to be a good choice for prediction of microstructure and hardness profiles as function of the nitriding parameters. Time, temperature, and nitriding-alloying level.

Zhecheva et. al. [36] indicated that ANN models can be created and used to correlate between processing parameters of nitriding and hardness of titanium alloys. It can also be used to optimize the processing parameters and alloy composition in order to achieve desired properties for various applications.

1.2.4.4 Techniques for evaluation of the performance of artificial neural network modeling

Different criteria can be used for judging ANN model performance. Haque et.al.[31] used the correlation coefficient, r , and the coefficient of multiple determination, R , squared.

Gou et al [35] used mean relative error and error deviation. However, the main quality indicator of a neural network is its generalization ability, i.e., its ability to predict accurately the output of unseen test data.

1.2.4.5 Investigations on data preparation, data availability and predictive power of artificial neural network

A neural network is usually trained using a large number of input and output data. Because ANN modeling is of statistical nature, so the performance of an ANN model is based on the size of the data used for model training [35].

Data is usually divided into a training set, which is about two thirds of the available data, and a validation set as the remaining one third of the available data. The validation data set is used to check the generalization ability of the ANN model. ANN modeling usually requires some trial and error to achieve a suitable and stable network. A good sampling of the data and proper selection of input parameters for the training data set improve prediction performance and reduce training time.

Velten et.al. [38] concluded that the quality of predictions based on ANN increases with increasing available data sets.

Filetin et. al.[40] used 275 data pairs in training and 93 data pairs in the validation of an ANN model developed to predict nitriding time. He also used 203 data pairs in training and 12 data pairs in the validation of an ANN model to predict surface hardness.

Zhecheva et. al. [36] used 116 data pairs with 78 in the training set and 38 in test set.

Genel [9] found that neural network can learn from experience (training), and can predict fatigue data with high accuracy throughout the range of experimental data, however, it cannot be used to extrapolate accurately. The prediction of an ANN is only valid in the range of tensile material data and its corresponding fatigue data.

Sukthomya [39] concluded that extrapolation is unreliable. He found that appropriate response of the trained network cannot be expected, when any of the inputs lie outside of the data ranges used in training.

1.2.5 Objective of the present study

The first objective of the present study is to use ANNs modeling in identifying which process parameters influence the outcome of the two stage gas nitriding of Nitralloy 135M low alloy steel. In addition to that ,using the nitriding potential , K_N , as the main control parameter, the second objective is to investigate the nitriding ability of ammonia gas as opposed to burette dissociation method while using dissociated ammonia as dilution gas .The aim is to achieve zero white layer thickness as demanded by the Aerospace Materials Specification (AMS) 2759/10, “Automated control of Gas Nitriding using nitriding potential”.

Chapter 2

The Experimental Facility

2.1 Introduction:

Gas nitriding is a case-hardening process in which machined and heat-treated steel components are subjected to the action of a nitrogenous medium, commonly ammonia gas, at temperatures ranging from 925° F -1050°F (490°C -565°C). Gas nitriding is performed in a gas-tight box furnace in such a way that ammonia gas can circulate freely around treated parts. Nitriding cycles can last for a day or longer according to the desired thickness of the nitrided case. Two stage Floe process gas nitriding test cycles were run based on a matrix of designed experiments (discussed in Chapter 3) to collect data for the development of the Artificial neural network model. The first stage of the nitriding cycles was run at using:

$K_N=8 \text{ bar}^{-1/2}$, time(t) = 5hrs , temperature(T) = 975 °F .The second stage of test runs was performed using different combinations of four values of K_N : 0.3,0.45,0.6 and $0.8 \text{ bar}^{-1/2}$,three values of t=10, 20 and 30 hrs, three values of T=1010,1030 and 1050 °F.

Gas nitriding facilities of the industrial partner in the present study, VAC AERO International Inc., Oakville, Ontario, were used to acquire all the experimental data needed for the investigation. Details of the experimental facility are discussed next.

2.2 Experimental facility

A schematic of the experimental facility used in this study is shown in Figure 2.1.

It is composed of the three following systems:

- The process and purging gas supply system
- The nitriding furnace with its control panel
- The ammonia cracker for the supply of the dissociated ammonia.

2.2.1 Process and purging gas supply

Metallurgical grade anhydrous ammonia liquid (max 35 ppm water) with a chemical formula NH_3 , was used as the process gas supply. It is stored in an above ground container as shown in Figure 2.2. The container was manufactured by Sparling Tank Company and has a capacity of 1375 U.S.W.G (5.2 cubic metres). Gaseous ammonia from the container is also supplied to ammonia dissociator (cracker) for dissociation to nitrogen (N_2) and hydrogen (H_2) gas.

Nitrogen is used as a purging gas and is supplied to the experimental facility from the common plant. The nitrogen gas header connected to the plant liquid nitrogen storage tank through an evaporator is shown in Figure 2.3.

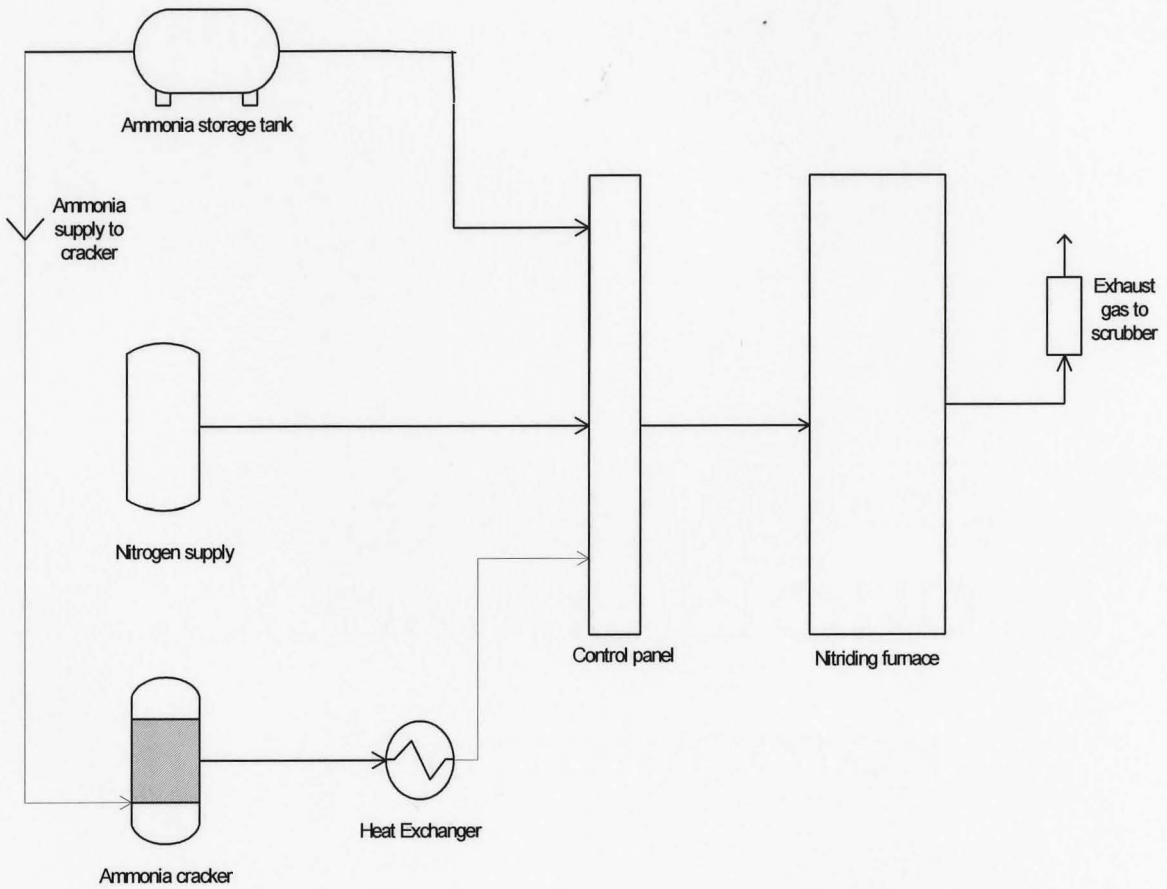


Figure 2.1: Schematic of the experimental facility

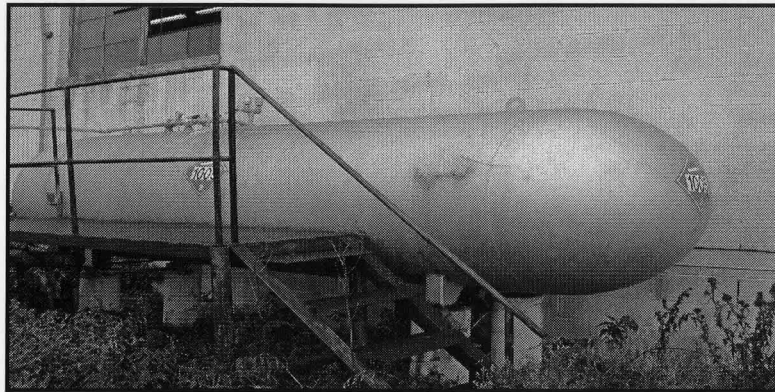


Figure 2.2: Above ground liquid ammonia container

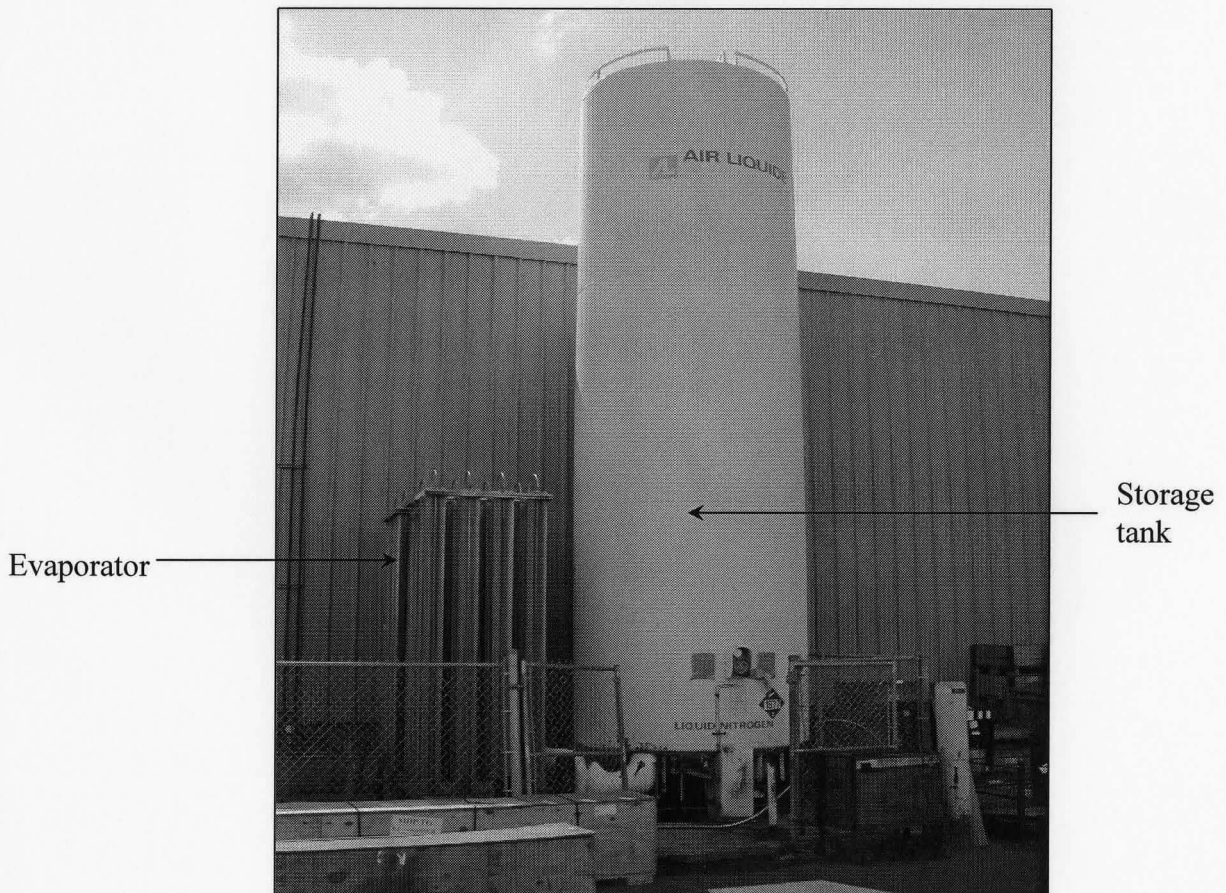


Figure 2.3: Liquid nitrogen storage tank and evaporator

2.2.2 Nitriding furnace and its control panel

Gas nitriding furnace is an electrically heated furnace and can be sub-divided into the following sections:

- Heat source
- The Retort and the retort lid, and the load basket
- Control panel
- Cooling stand

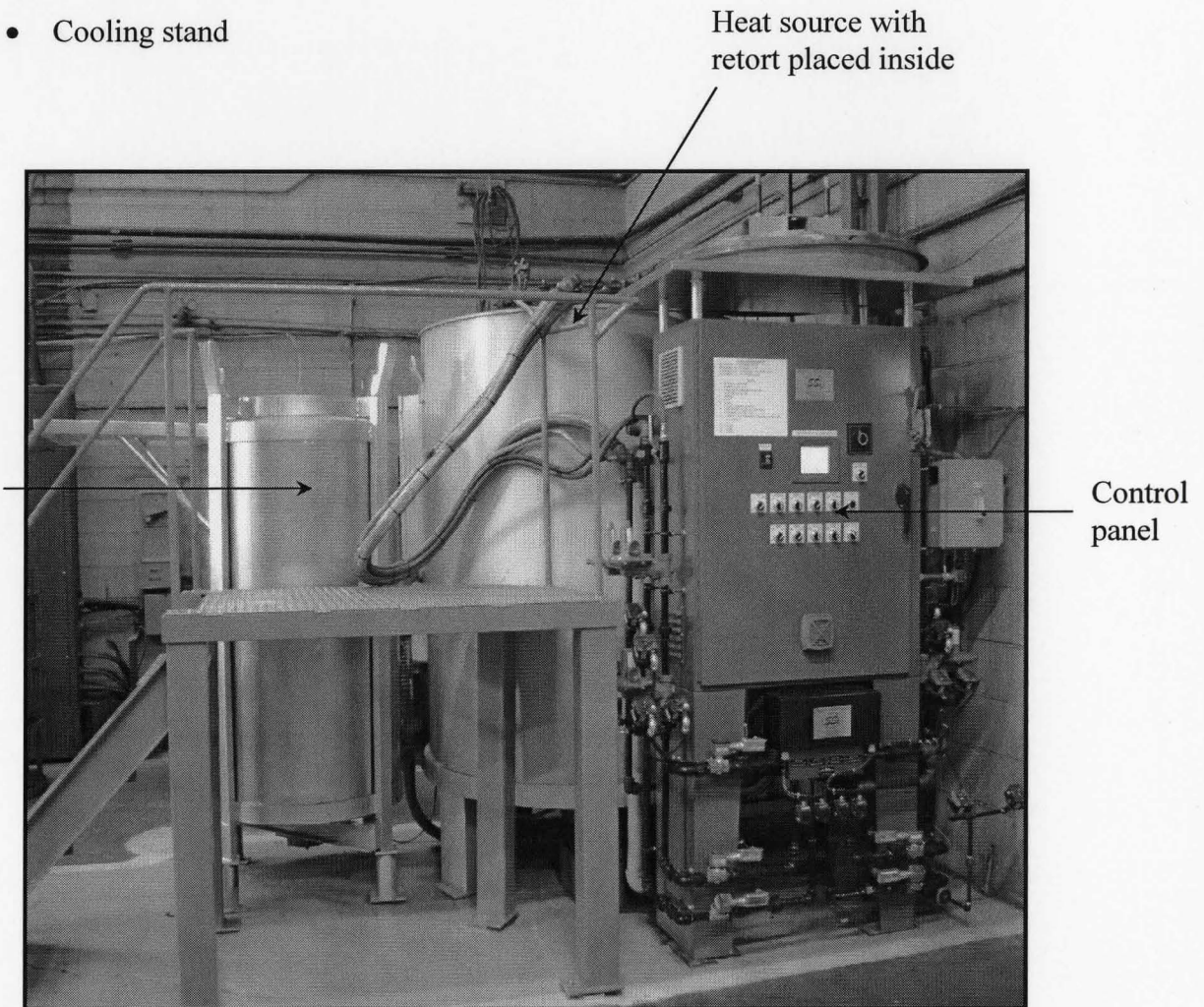


Figure 2.4: A general view of the gas nitriding furnace

2.2.2.1 Heat source

The electric heat source has a rating of 60 KVA.

2.2.2.2 The Retort, the lid, and the load basket

The retort and its lid shown in Figures 2.5 - 2.9 are made of Inconel 600. It holds the load basket and provide gas tight conditions during the nitriding cycle. The retort has an internal diameter of 23 3/4", height of 48 1/8" and volumetric capacity of 12.34 cubic feet. The lid has diameter of 22", height of 7 3/4" and a flange of diameter 29 1/4". The retort has piping arrangement for supply and exhaust of process, dilution and purging gases. The material to be nitrided is suspended or placed in the load basket shown in Figure 2.8. The basket is then lowered in the retort and covered with the lid shown. There is an atmosphere circulation fan and motor installed on the lid. This fan was added to the furnace as part of a furnace modification process that had to be implemented in order to improve the uniformity of the atmosphere distribution inside the furnace. More details will be discussed in section 2.3.

Figure 2.9 shows the path of circulation of nitriding gas inside the furnace. The flow is maintained by a centrifugal fan that discharges the gas and it is directed to flow in the annular gap of (7/8") between the retort and the liner by deflector shown in Figure 2.7. The gas is turned back after striking the base of retort and flows in the basket space where the parts to be nitrided are placed. The gas then flows into the eye of the fan. A part of the gas is discharged to the atmosphere to maintain a slight positive pressure of

25mbar in the retort. The pressure is maintained by a butterfly valve and P.I.D control loop discussed in section 2.2.2.3.

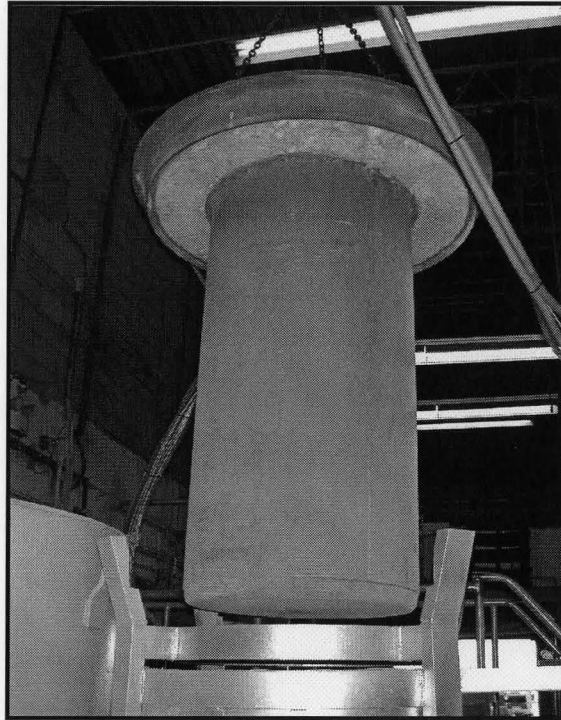


Figure 2.5: Retort being lowered in cooling stand

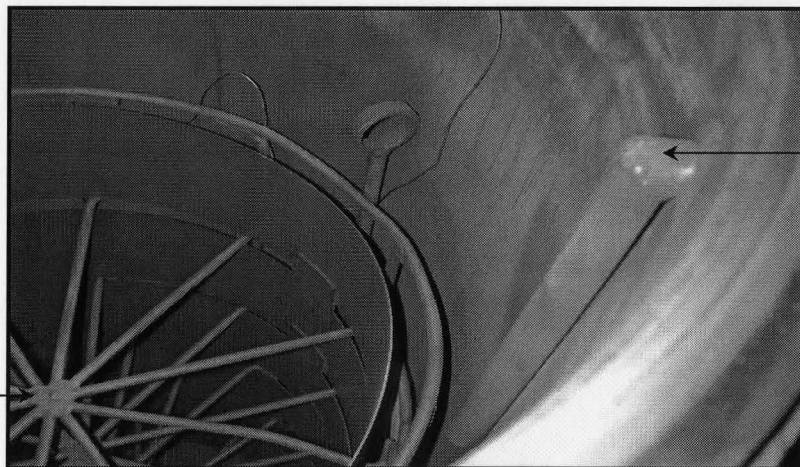


Figure 2.6: Interior view of retort showing load basket and ammonia inlet pipe

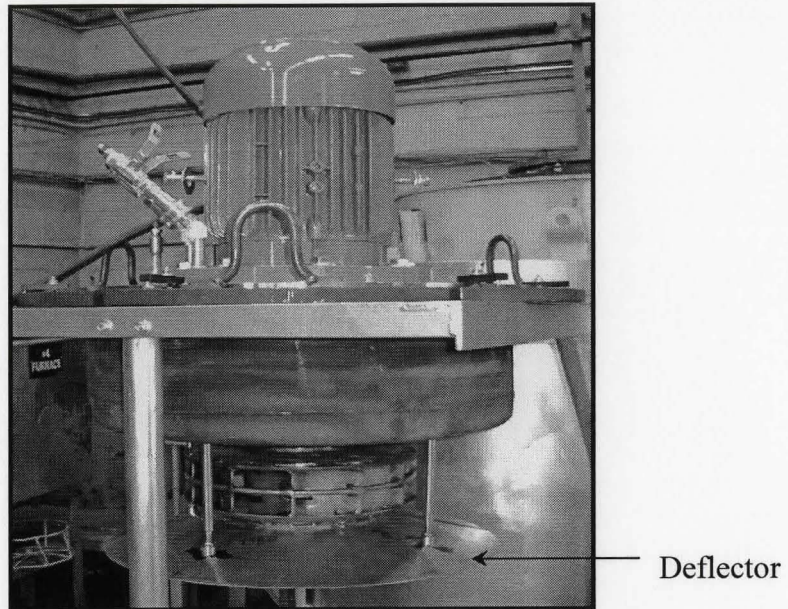


Figure 2.7: Retort lid with atmosphere circulation fan and deflector



Figure 2.8: A general view of load basket with liner

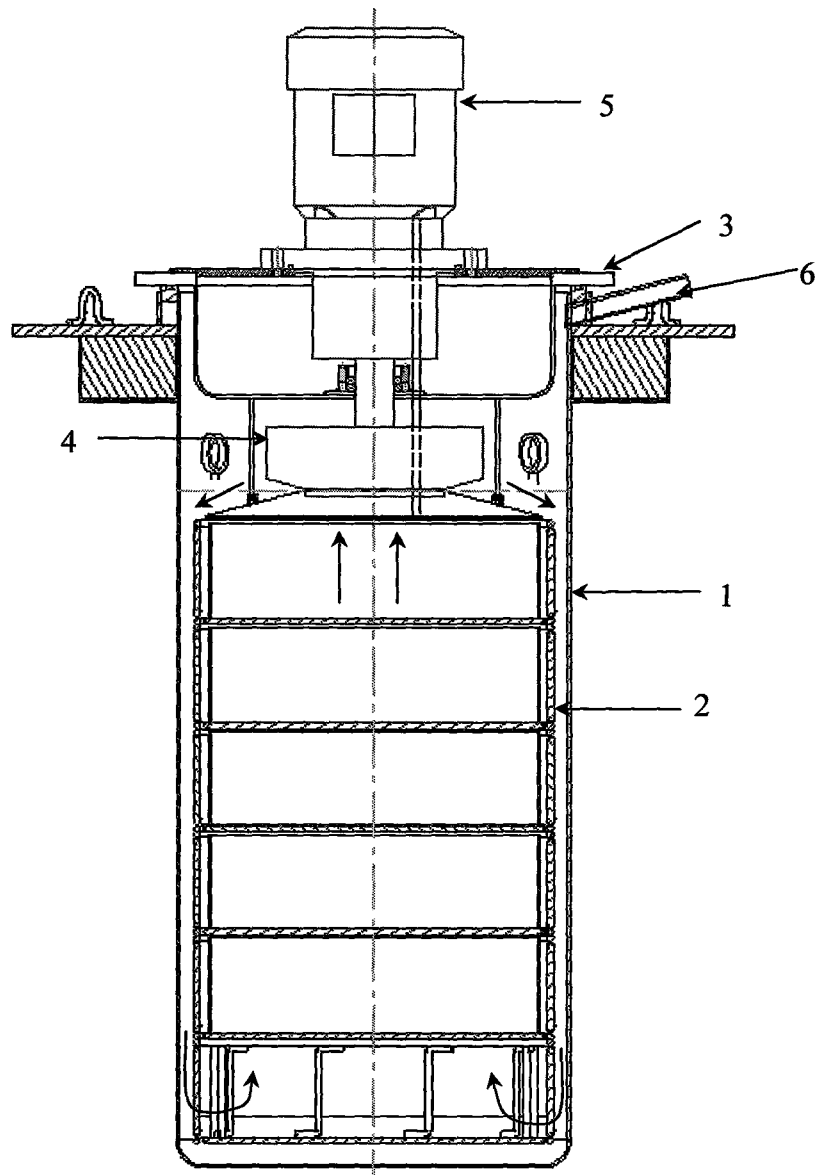


Figure 2.9: A section view of retort and lid assembly showing the gas circulation
1-Furnace retort, 2-Load basket with liner, 3-Retort lid, 4-Centrifugal circulation fan, 5-Fan motor, 6-Atmosphere exhaust pipe

2.2.2.3 The Control Panel

The control panel is model 9210 manufactured by Super Systems Inc. It is the heart of the gas nitriding operation and controls all parameters under investigation.

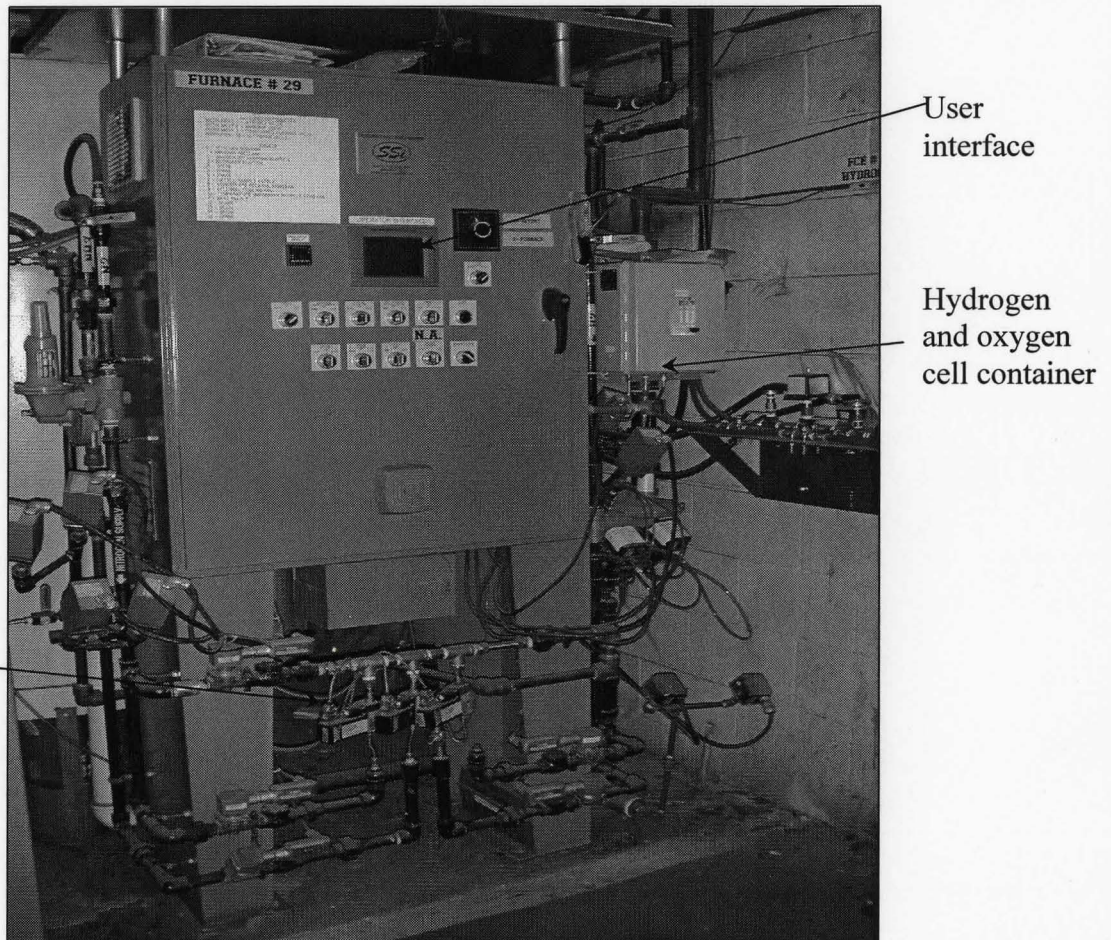


Figure 2.10: A pictorial view of nitriding control panel model 9210

There are three mass flow controllers installed in the control panel. One for the ammonia gas, the dissociated ammonia and the nitrogen gas. Only the ammonia and the

dissociated ammonia mass flow controllers were used during the experimentation. The mass flow controllers are based on thermal sensing technique and work as follows:

A precision power supply as shown in figure 2.11 provides a constant power input (P) at the heater, which is located at the midpoint of the sensor tube. At zero or no flow conditions, the amount of heat received by each temperature sensor (one upstream and one downstream of the heater) is equal; therefore the temperatures T_1 and T_2 are equal. When gas flows through the tube, the upstream sensor is cooled and the downstream sensor is heated producing a temperature difference. The temperature difference $T_2 - T_1$ is directly proportional to the gas mass flow.

The governing equation is:

$$\Delta T = A * P * C_p * m \quad (2.1)$$

where, ΔT = Temperature difference $T_2 - T_1$ ($^{\circ}\text{K}$), C_p = Specific heat of the gas at constant pressure ($\text{kJ/kg} \cdot ^{\circ}\text{K}$), P = Heater power (kJ/sec), m =mass flow (kg/sec) A =constant of proportionality ($\text{S}^2 \cdot \text{K}^2 / \text{kJ}^2$)

A bridge circuit interprets the temperature difference and a differential amplifier generates a linear 0-5 V dc signal directly proportional to the gas mass flow rate. The sensor tube has the same linear pressure drop/flow relationship. The ratio of the restrictor flow to the sensor tube flow remains constant over the range of the meter. Different restrictors have different pressure drops and produce controllers with different full scale flow rates. The mass flow controller also has an integral control valve and control circuit.

The control circuit senses any difference between set point and the flow sensor signal and adjusts the current in the modulating solenoid valve to increase or decrease the flow.

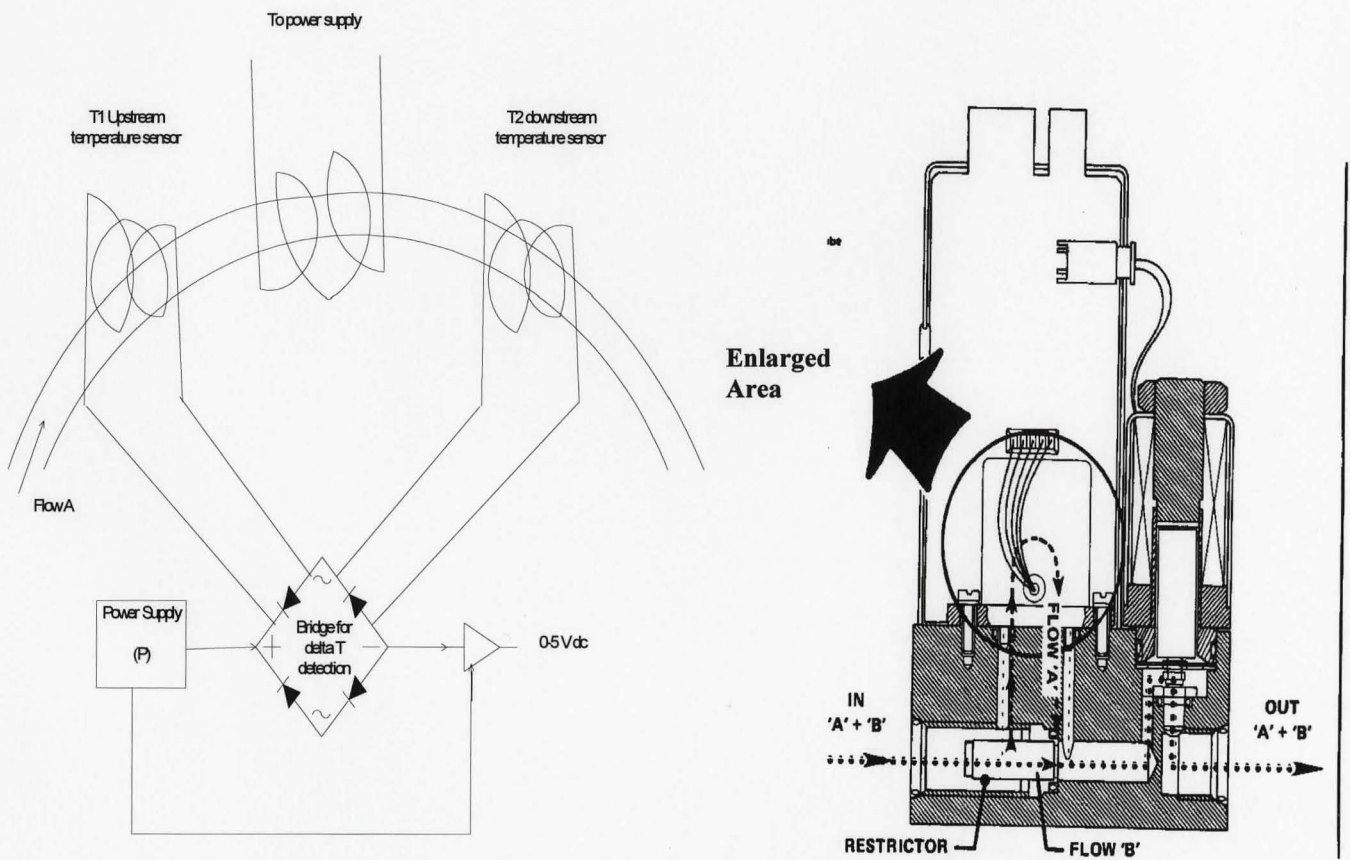


Figure 2.11: Flow sensor operational diagram [41]

Also there is a hydrogen sensor that is capable of measuring the hydrogen percentage in the dissociated ammonia and an oxygen sensor for measuring atmosphere oxygen content after nitrogen purging. Both sensors/cell are shown in figure 2.12.

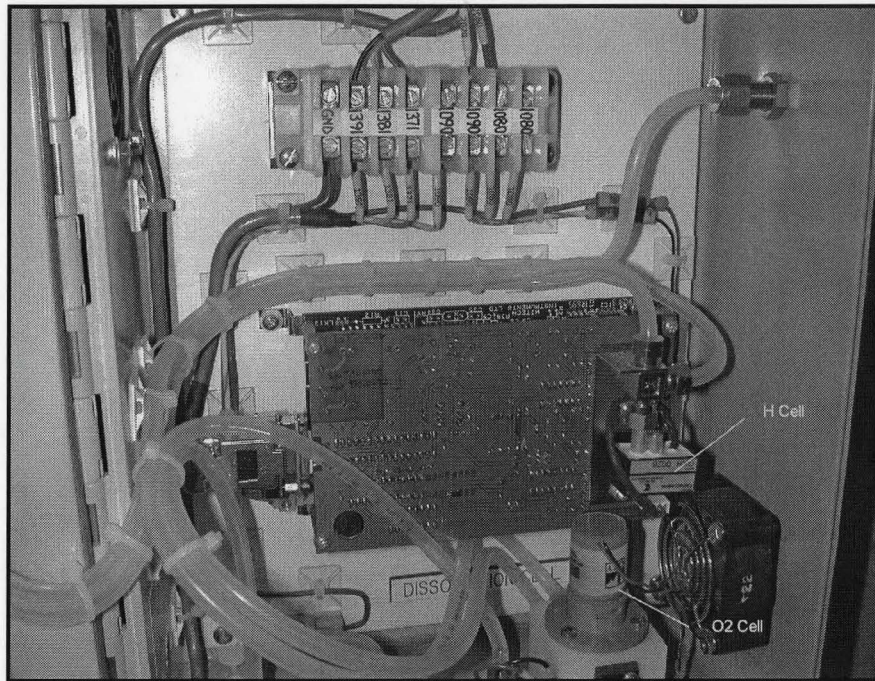


Figure 2.12: Hydrogen and oxygen sensors installed in the control panel

Three P.I.D (Proportional Integral Derivative) controllers are used. One each for the nitriding potential control, the back pressure control of the furnace, and the temperature control.

2.2.2.4 The Cooling stand

At the end of the second stage of the nitriding cycle the furnace retort is placed in the cooling stand. The cooling stand is a metal structure with a fan installed at its bottom directly driven by 1750 RPM motor to bring about forced air cooling.

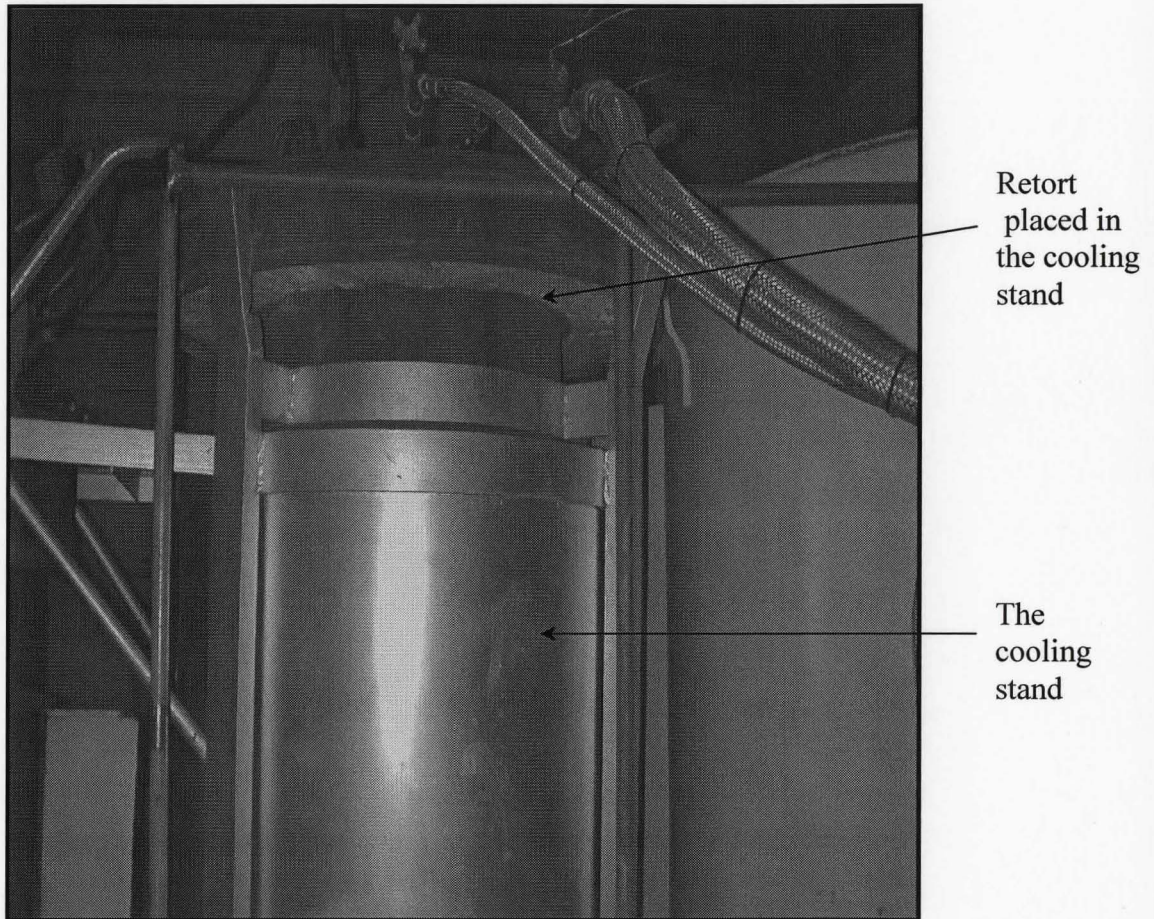
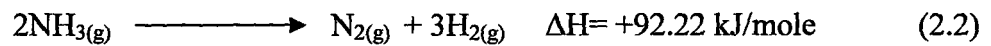


Figure 2.13: A pictorial view of the cooling stand with the retort inside

2.2.3 The Ammonia dissociator

The ammonia dissociation (cracking) takes place according to the following reaction. It is an endothermic reaction and takes place at 1700°F (927°C) in the presence of a nickel catalyst.



The above reaction is the preferred method of preparing the highest purity, oxygen-free nitrogen. This reaction was conducted in LINDBERG ammonia dissociator, shown in Figure 2.14. There are three main parts of the dissociator:

- Reaction chamber
- Gas cooler
- Instrument panel

Ammonia from storage tank is fed directly to the dissociator, which is heat resistant, electrically heated coiled pipe surrounded by refractory material. Hot dissociated ammonia is piped to an air-cooled heat exchanger and then goes to the nitriding furnace. The instrument panel carries the gauges for gas pressure and flow meter for the dissociated gas flow.

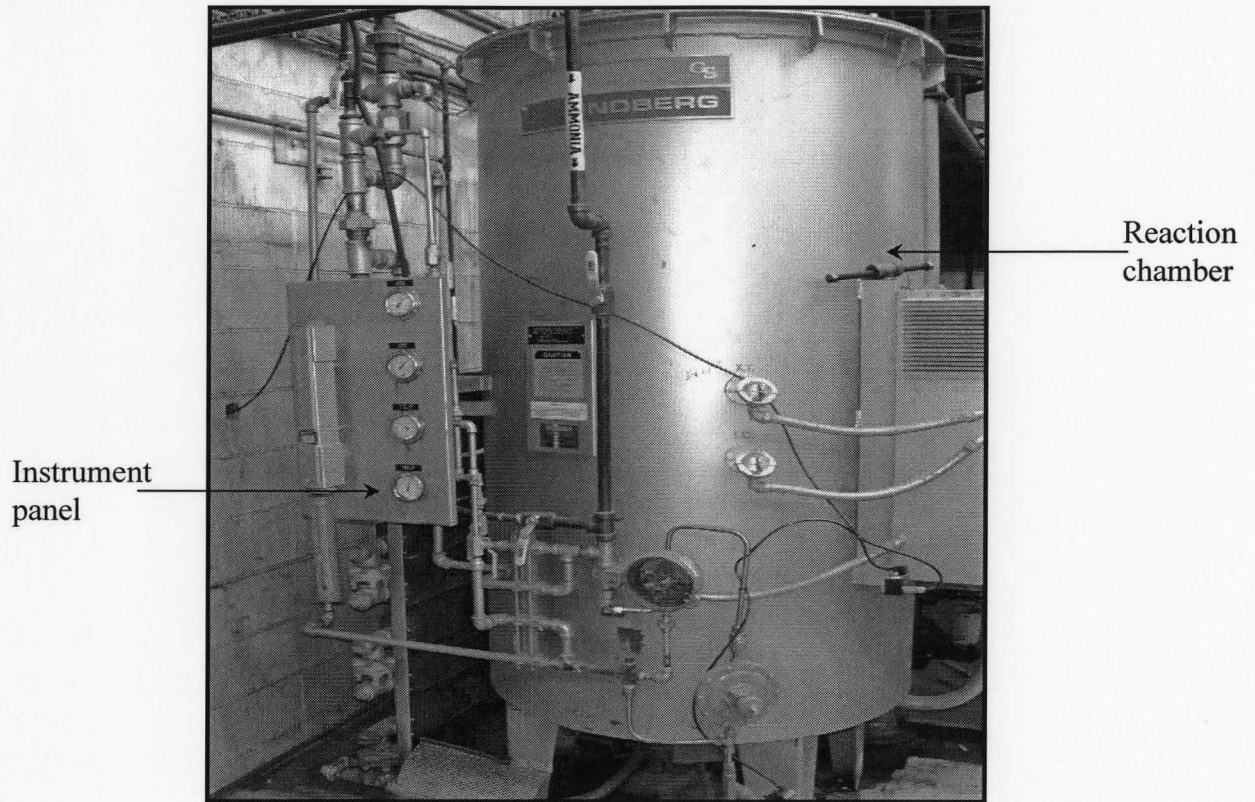


Figure 2.14: LINDBERG Ammonia dissociator

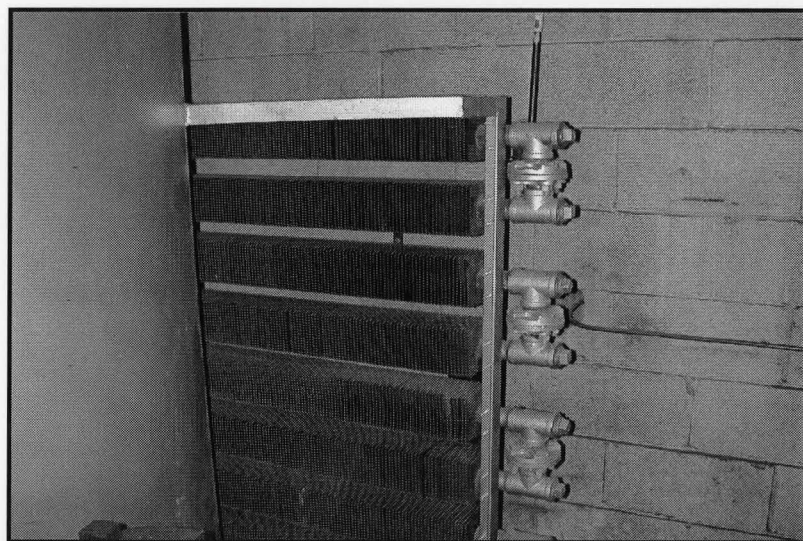


Figure 2.15: Ammonia dissociator gas cooler

2.3 Furnace modification

Originally i.e., before the start of the experimentation, the nitriding furnace was of overpressure circulation type. The results of the preliminary nitriding cycles indicated non-uniformity in the microstructure of the treated samples. A modification was implemented to install a furnace circulation fan to make the distribution of the nitriding gas inside the furnace uniform. A centrifugal fan with a diameter of 310 mm and made of AISI 310 SS was installed in the lid as shown in figure 2.16. The fan is powered by a directly coupled 2.2 KW, 3600 RPM motor. The fan can maintain a flow rate of 1483 ft³/min at nitriding temperature of 1100°F.

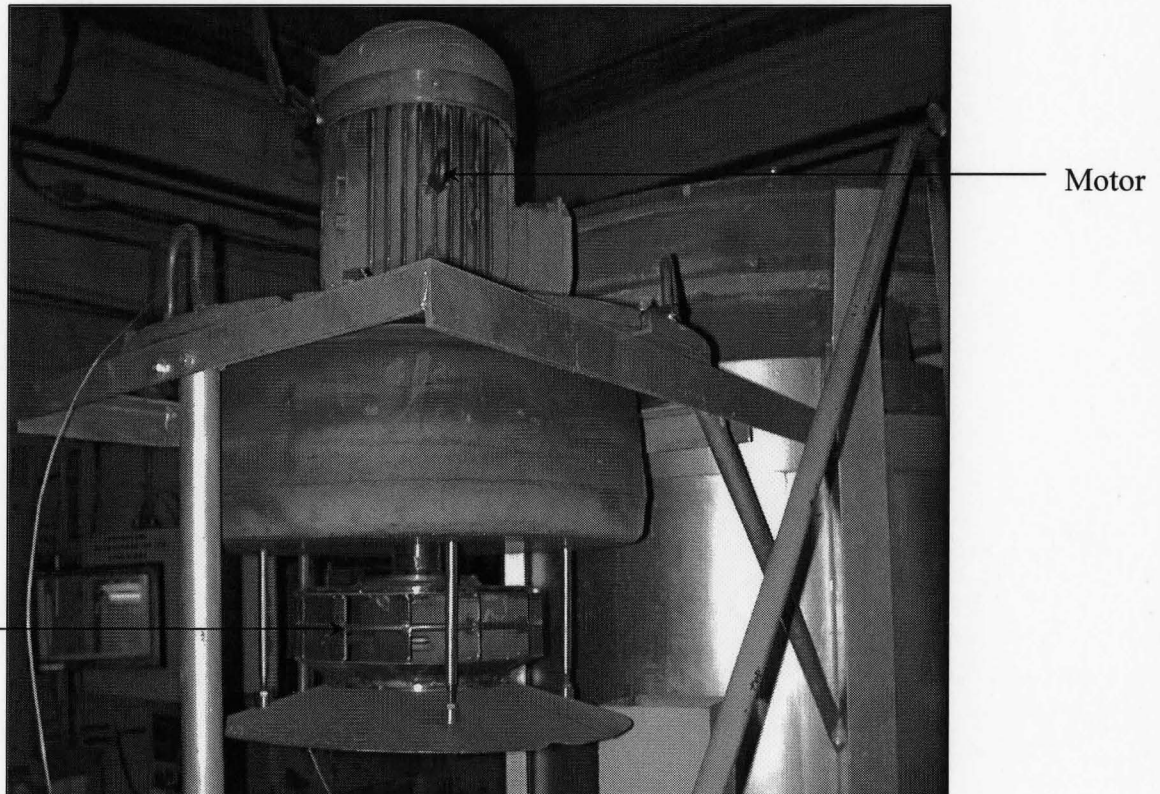


Figure 2.16: A general view of modified furnace retort lid

Chapter 3

Experimental Methodology

A set of two-stage Floe process gas nitriding test cycles was developed, planned, and run to collect the data for Artificial Neural network (ANN) modeling. The data was used to train the ANN model and the trained network was used to predict the nitrided case characteristics:

- The total case depth ($\mu\text{m}@ 40 \text{ HRC}$, Hardness Rockwell C scale),
- The effective case depth ($\mu\text{m}@ 50 \text{ HRC}$),
- The case depth in $\mu\text{m} @ 60\text{HRC}$,
- The compound (white) layer thickness in μm ,
- The superficial hardness (HR 15N).

Nitrided case properties are affected principally by input process parameters or factors:

- Nitriding potential (K_N),
- cycle time (t) ,
- cycle temperature (T) ,

- material composition.

Three geometrically uniform samples of low alloy steel (Nitalloy 135M) having a composition as given in Table 3.1 were nitrided in each cycle using a range of values of process parameters given in Table 3.2.

All steps in data collection from design of experiments to mechanical testing and metallographic examinations are discussed in the following sections.

Table 3.1: Percentage composition of Nitalloy 135M low alloy steel

Carbon	Manganese	Silicon	Chromium	Molybdenum	Aluminum
0.40	0.60	0.30	1.60	0.35	1.20

Table 3.2 : Values of process parameters used in experimentation.

Stage	Nitriding potential K_N (bar ^{-1/2})				Cycle time t(hrs)			Temperature °F		
	First	8				5			975	
Second	0.3	0.45	0.6	0.8	10	20	30	1010	1030	1050

3.1. Design of Experiments

The technique of defining and investigating all possible conditions in a set of experiments involving multiple factors (parameters) is known as the design of experiments. This technique is also referred to as factorial design. The motivation of design of experiments is to obtain more (or better) information with less work [42].

In the present study, experiments were planned to obtain data to investigate the effects of three factors in the second stage of the gas nitriding cycle, namely, the nitriding potential at four levels, the cycle time at three levels and the temperature at three levels. The same factors were kept constant in the first stage of the nitriding process, see Table 3.2.

Multilevel full factorial design of the study comes out to 36 combinations of all possible factors and levels. The experiments were designed using MINITAB[®] software. Also, a Taguchi partial factorial design was developed using the same software to get an orthogonal array; L₉ having 9 trial runs. An orthogonal array is a set of tables used to determine the least number of experiments and their conditions [42]. The cycles were designated using an alphanumeric symbol “NN (x)” where “x” denotes cycle run number. Both types of designs are included in appendix 1. Appendix 2 contains all the details of the actual cycles used in the study.

3.2. Sample preparation

Two rods of quenched and tempered Nitralloy 135M having core hardness of

34.6 HRC and 34 HRC were used to prepare the test samples. Test samples were 25.4 mm in diameter and 6.35 mm thickness as shown in Figure 3.1. For each cycle, six samples were used. Three of the samples were engraved with the sample number (to be discussed shortly) and were used for nitriding operation results. One side of each sample was slightly notched as shown in figure 3.1 to indicate its orientation in the furnace with the notched side facing the center of the furnace in all cycles. Both sides, plane and notched, of each sample were tested for case characteristics. The other three plane samples (without engraving) were used to attach three thermocouples to measure sample temperature, which was used to assess temperature uniformity in the furnace during each run. The samples were cleaned with methanol and dried before placement in furnace. The samples were designated using the cycle number as a prefix and alphanumeric characters "S (y)" where "y" denotes the sample number. For example three specimens S1, S2 and S3 nitrided in cycle NN1 are designated as: NN1S1, NN1S2 and NN1S3, respectively, and their respective notched sides are designated as: NN1S1N, NN1S2N and NN1S3N.

Notch made
in specimen

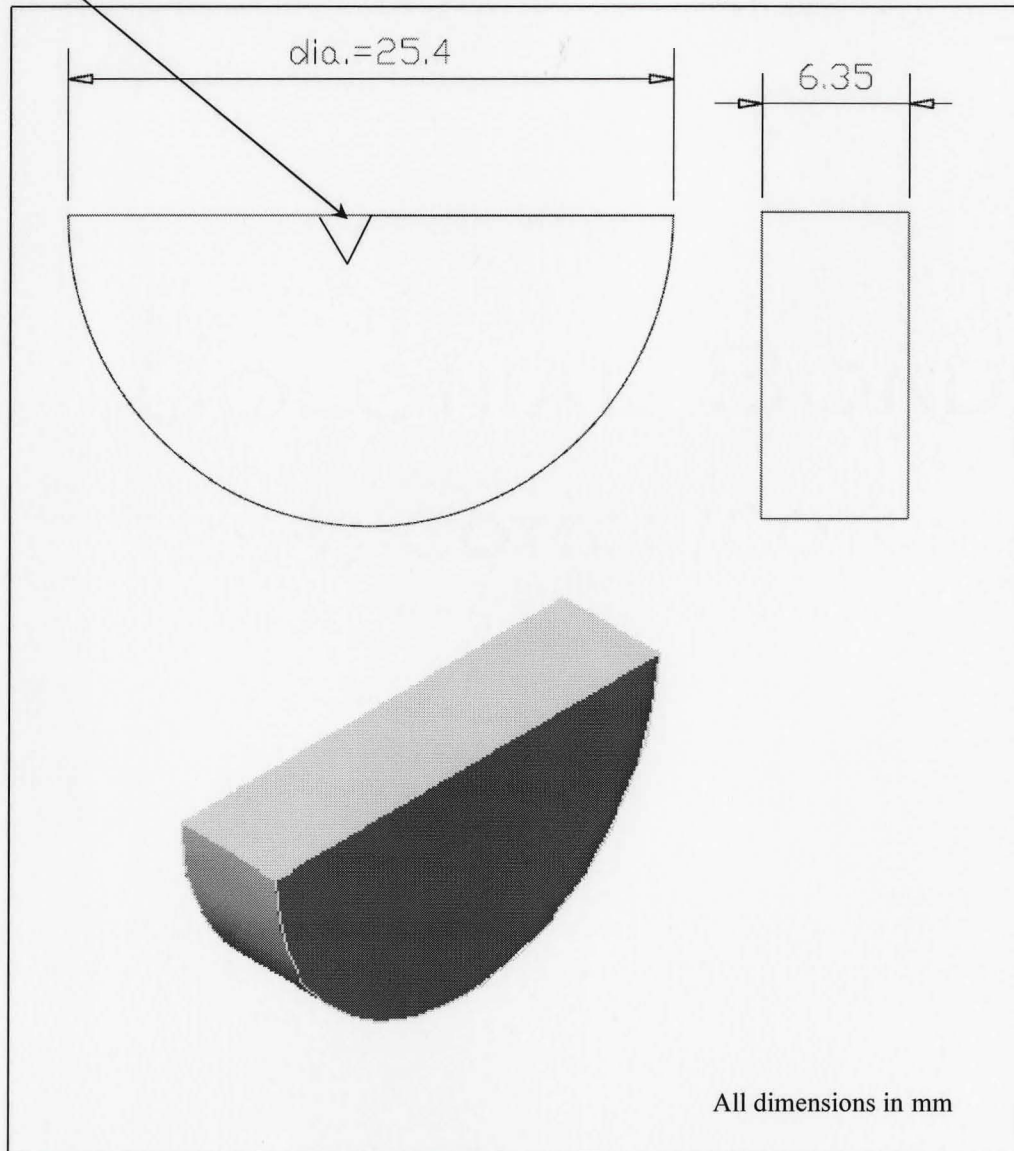


Figure 3.1: A typical specimen of Nitralloy 135M

3.3. Set up prior to running each test cycle

3.3.1. Specimen placement

The three engraved and the three unmarked specimens were hanged using steel wire to the load basket as shown in figure 3.2. Samples were oriented to hang from the spokes on the third basket at approximately 120° apart from each other, as shown in figure 3.3.

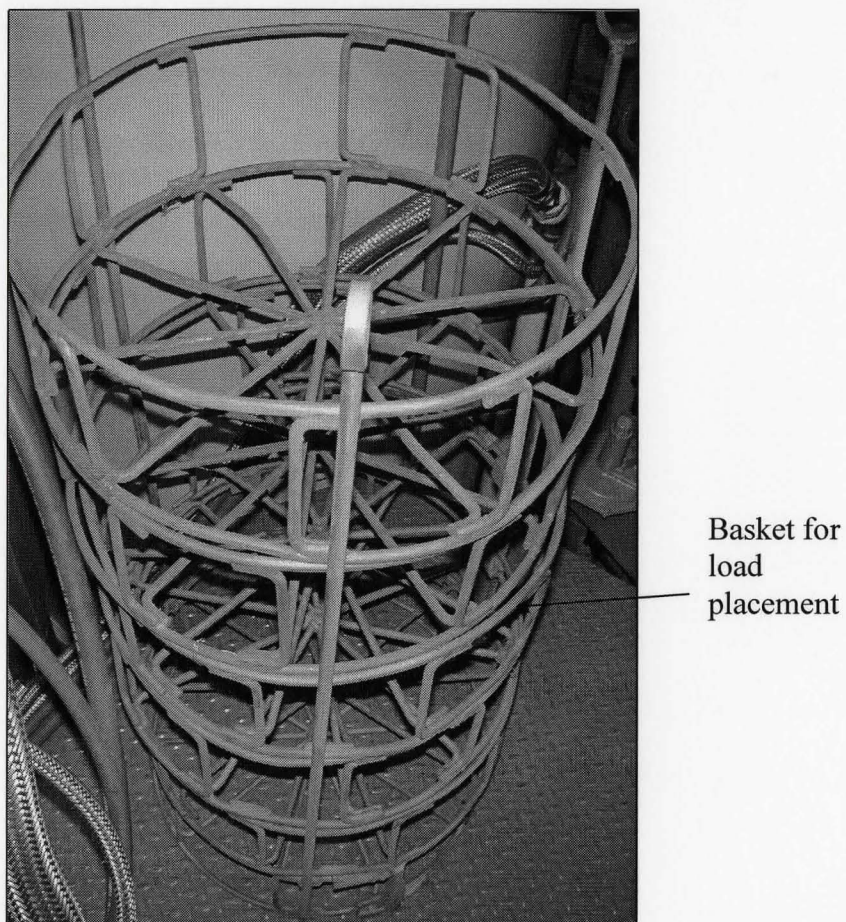


Figure 3.2 : A pictorial view of the furnace retort load basket

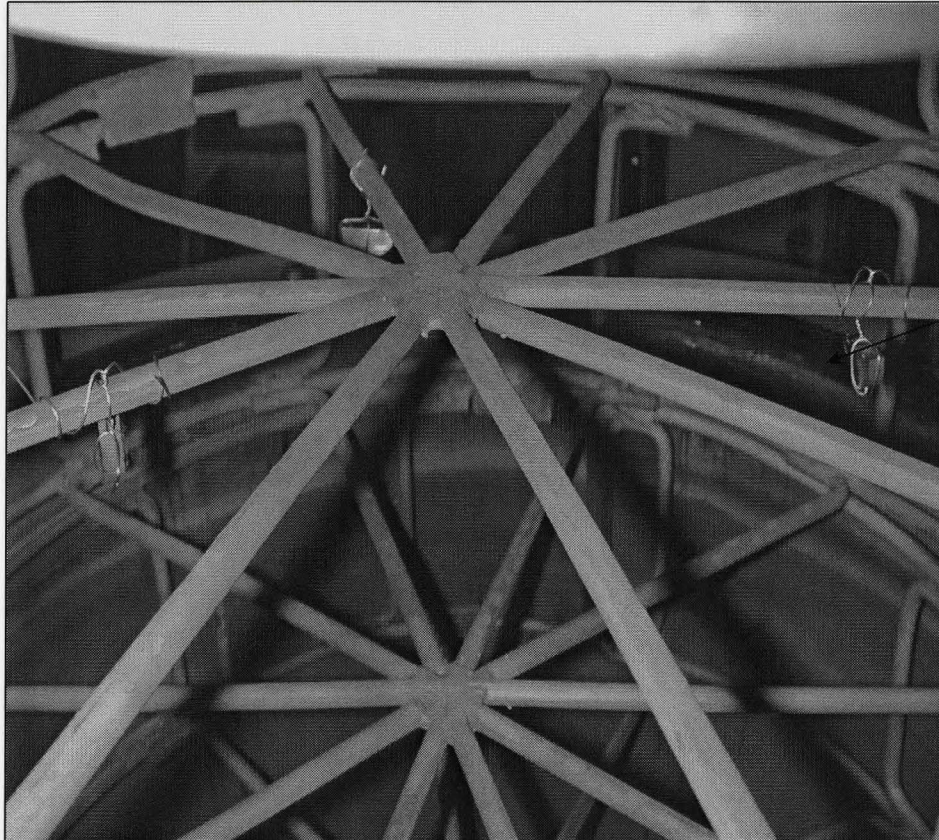


Figure 3.3: Load basket spokes with three specimens placed at 120° each.

3.3.2 Attachment of sample thermocouples:

Three type-K, 1/16" diameter thermocouple were attached to the three unnotched (plane) samples hanged from spokes adjacent to the three notched samples. Thermocouples were connected to the data acquisition system after emanating from the furnace through a manifold in the flange of the furnace retort ,as shown in figure 3.4.

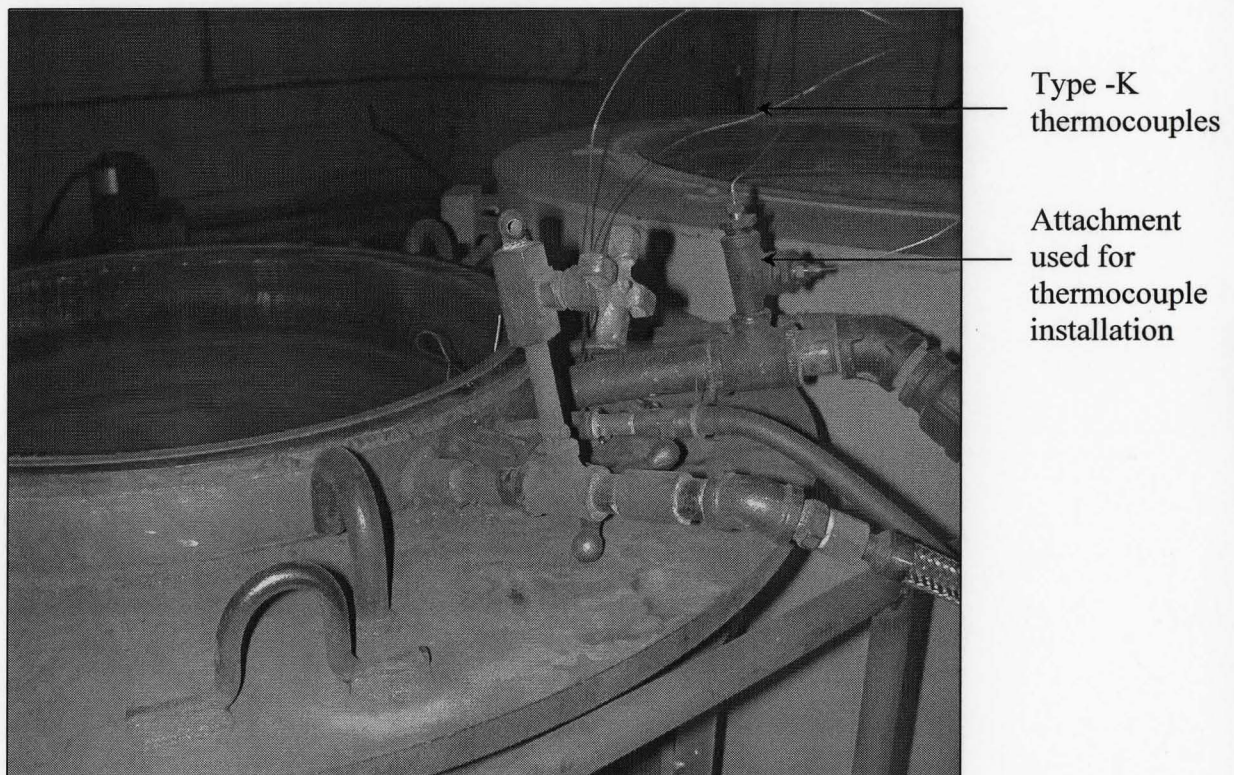


Figure 3.4: Furnace retort with fixture used for thermocouples installation.

3.4. Typical experimental procedure

- a) The basket is lifted with overhead crane and placed in the furnace retort.
- b) The furnace lid is placed and tied with bolts.
- c) Set points of input parameters of the designed run entered in the furnace control panel, see figure 3.5.
- d) The furnace circulation fan is set on and purging with Nitrogen is started and temperature is ramped up.
- e) As soon as the oxygen cell indicates less than 1% percent oxygen in the retort, ammonia supply is set on.
- f) P.I.D controllers control the furnace temperature, the nitriding potential, and maintain a slight positive pressure of 25 millibar in the retort.

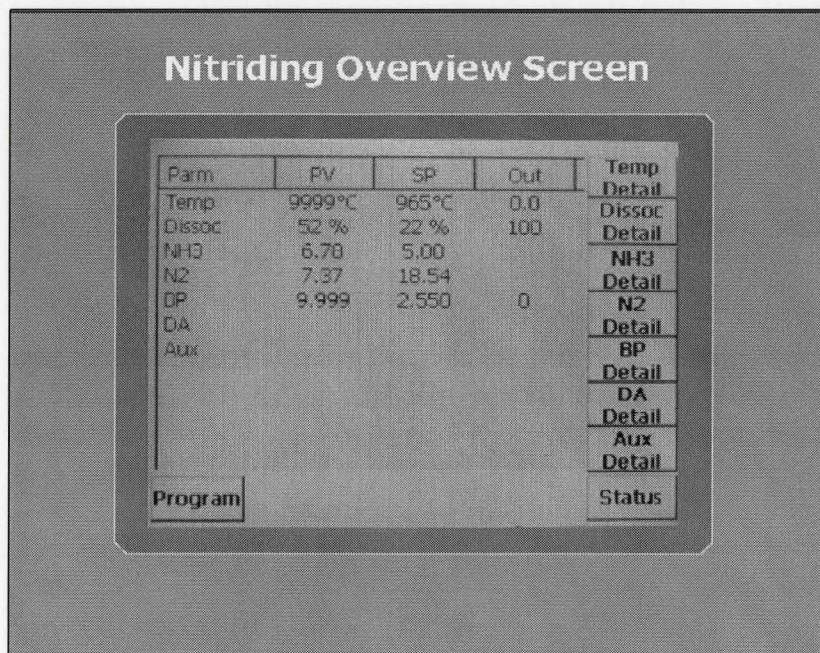


Figure 3.5: Control panel user interface

3.5 Data collection

Data collection is divided into the following sequential steps:

1. Superficial hardness testing
2. Micro hardness testing for the determination of the case depths at three hardness values 40, 50, and 60 HRC.
3. Metallographic examination for the determination of the white layer thickness.

3.5.1 Rockwell superficial hardness testing

Rockwell Superficial hardness testing using 15N scale was done by using a NEWAGE INDENTRON superficial hardness tester, shown in figure 3.6.

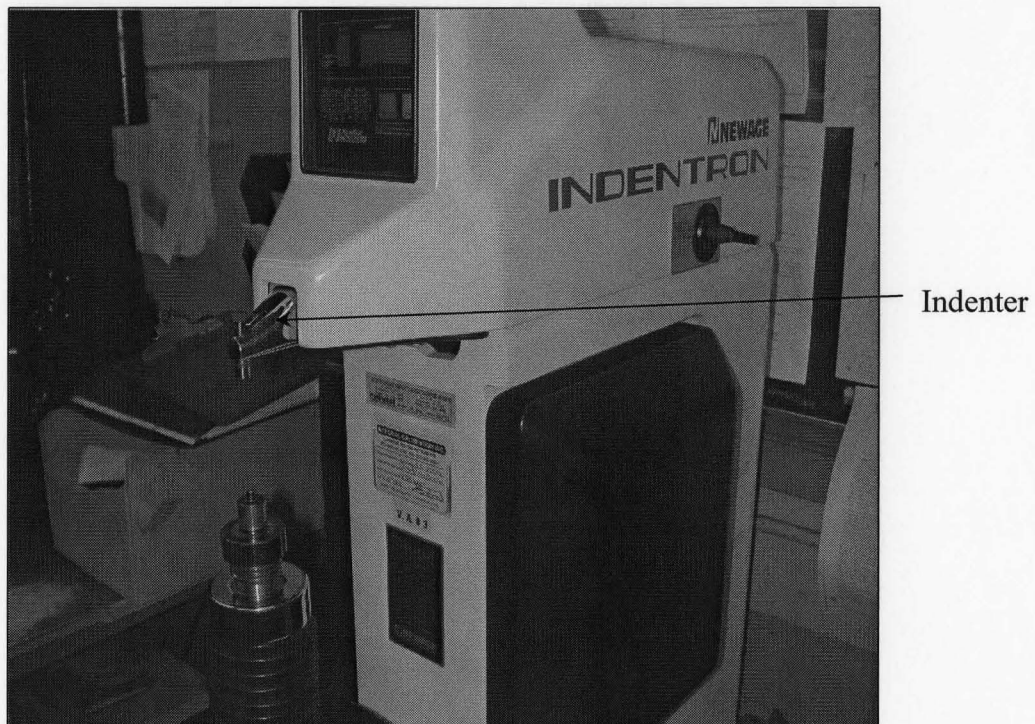


Figure 3.6: Newage Indentron superficial hardness tester with

The major load was 15 kgf; minor load was 3 kgf. The indenter used was of Sphero-conical diamond type as shown in figure 3.7.

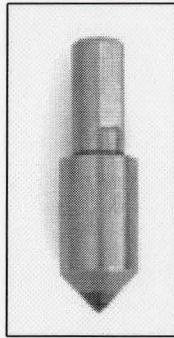


Figure 3.7 Enlarged view of Sphero-conical diamond type indenter for Superficial hardness tester [43].

3.5.2 Micro hardness testing

3.5.2.1 Sample sectioning

Samples were sectioned on an IMPTECH EUROPE Abrasive cutter shown in figure 3.8, using Exicut technique. In the exicut technique, the abrasive cutoff wheel moves forward and backward through the work piece while rotating. The result is simpler and faster cutting and a significant reduction in the consumption of abrasive cutoff wheels. The combined rotating and oscillating movements of the wheel improves the cooling by allowing easier access of the coolant to the surface being cut. Figure 3.9 shows the Exicut technique in operation.

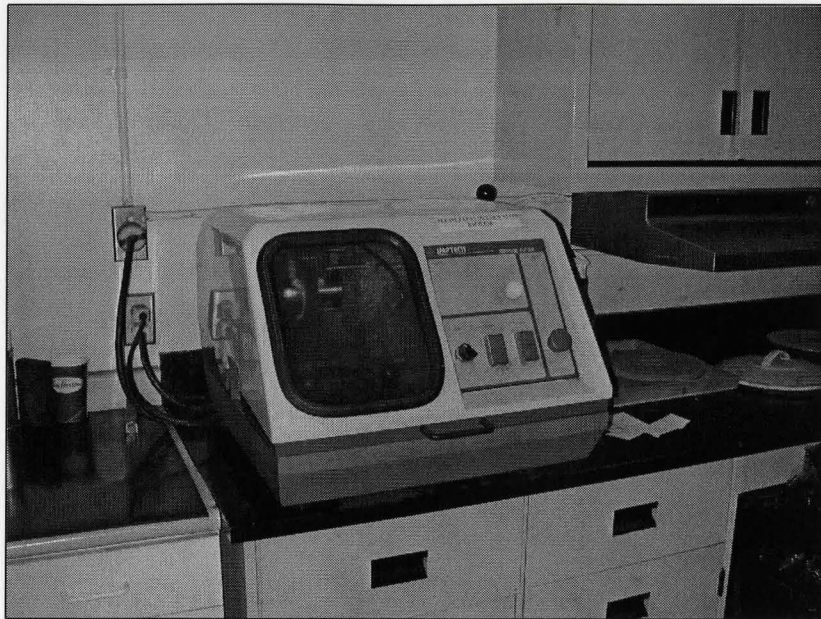


Figure 3.8. IMPTECH EUROPE abrasive cutter powered by a 2.2kW, 2800 RPM motor.

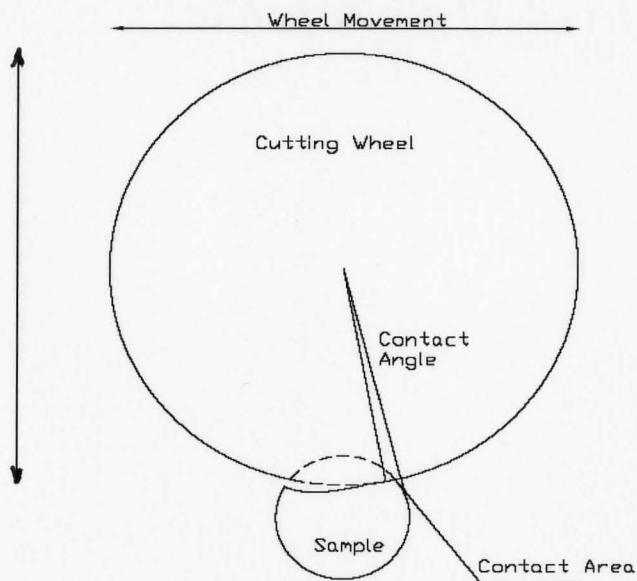


Figure 3.9. Excit technique in operation

3.5.2.2 Sample Mounting

Mounting of the samples is needed for various reasons: for storage, for use in the grinding /polishing machine and for edge retention in metallographic examination.

BUEHLER SIMPLIMET 3 hydro pneumatic mounting press, shown in figure 3.10 ,was used for hot mounting of the specimens. Struers Durofast black epoxy thermosetting resin was used as mounting material and the mold size used was of diameter 30 mm.

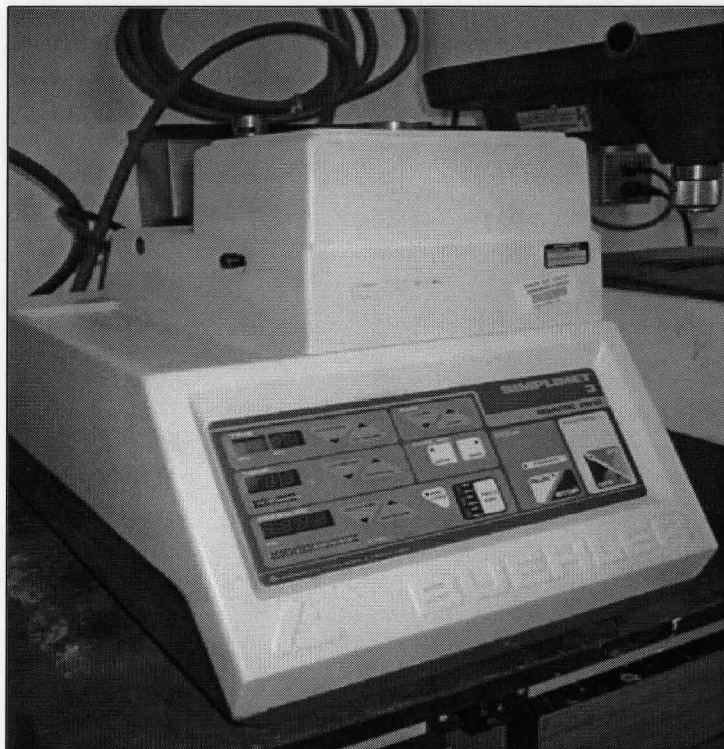


Figure 3.10. BUEHLER SIMPLIMET 3 hot mounting machine

3.5.2.3 Grinding and polishing

All steps involved in grinding and polishing operations were carried out on a STRUERS ROTOPOL-2 grinding/polishing machine, shown in figure 3.11.



Figure 3.11 STRUERS ROTOPOL-2 grinding /polishing machine

3.5.2.3.1 Plane or coarse grinding

The aim of plane grinding is to make the sample surface as a flat plane and to remove scratches and damaged layers produced during cutting. Scratches and disturbed layers produced in this stage should be easily removed during subsequent steps. Plane grinding was carried out with a surface named MD-Piano 600 (micro grit size 600= 13 microns) at 300 RPM with water as lubricant.

3.5.2.3.2 Fine grinding

The fine grinding stage is the most important of the entire preparation sequence. Any previously deformed layers from plane grinding not removed at the fine grinding stage and any excessive damage created at this stage are likely to remain to the end of the preparation process, which may cause misinterpretation of the microstructure. Therefore, the purpose of the fine grinding stage is to remove the entire deformed layer from plane grinding without introducing any more deformation than necessary. Fine grinding was carried out by using a combination of surface named MD-Allegro, abrasive diamond suspension size 9 microns at 150 RPM with lubricant DP Green.

3.5.2.3.3 Polishing

The purpose of the polishing stage is to remove all the scratches and deformed layer from the previous grinding steps. The resulting surface should be scratch free, relief free and planar.

Polishing was carried out in two steps using surfaces MD-Dur with 3 micron abrasive and DP Green lubricant and MD Nap with 1 micron abrasive and DP Green lubricant.

3.5.2.3.4 Vickers micro hardness testing

Micro- hardness testing was carried out to determine the case depths in microns (μm) at three values of hardness 40HRC, 50 HRC and 60 HRC. Case depth to 40 HRC and 50 HRC are termed as "total case" and "effective case", respectively. Vickers

Microhardness testing was performed using a MITUTOYO MVK-HO type of tester, shown in figure 3.12, and the results were interpreted into the desired case depth values using Clemex[®] CMT image analysis software and a high resolution camera. The load used was 100gf and dwell time was 15 sec. Figure 3.13 shows a typical profile of indents on a nitrided case. Figure 3.14 explains the geometry of the indent. Figure 3.15 gives the calibration curve of the Microhardness tester.

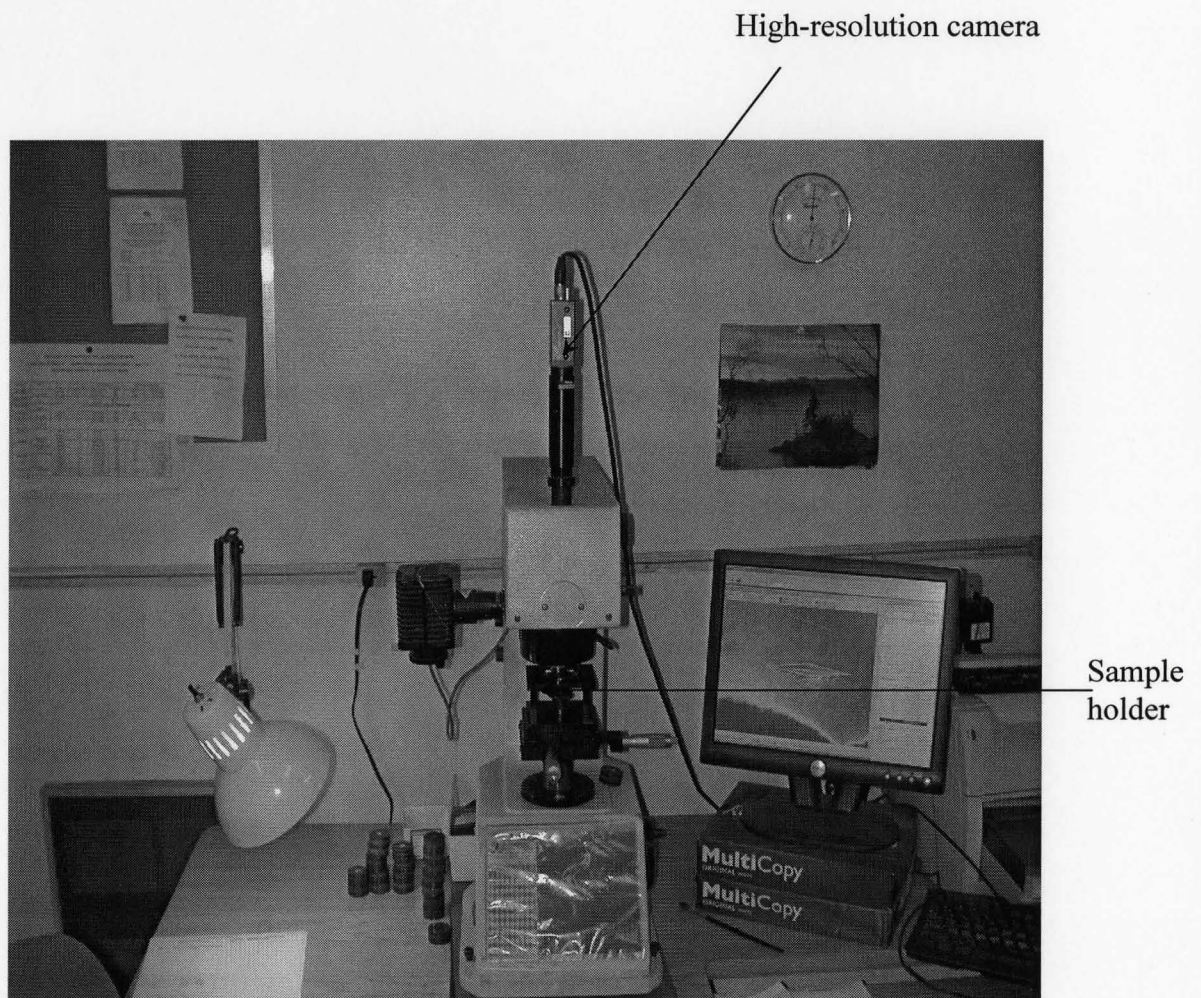


Figure 3.12: MITUTOYO MVK-HO Microhardness tester

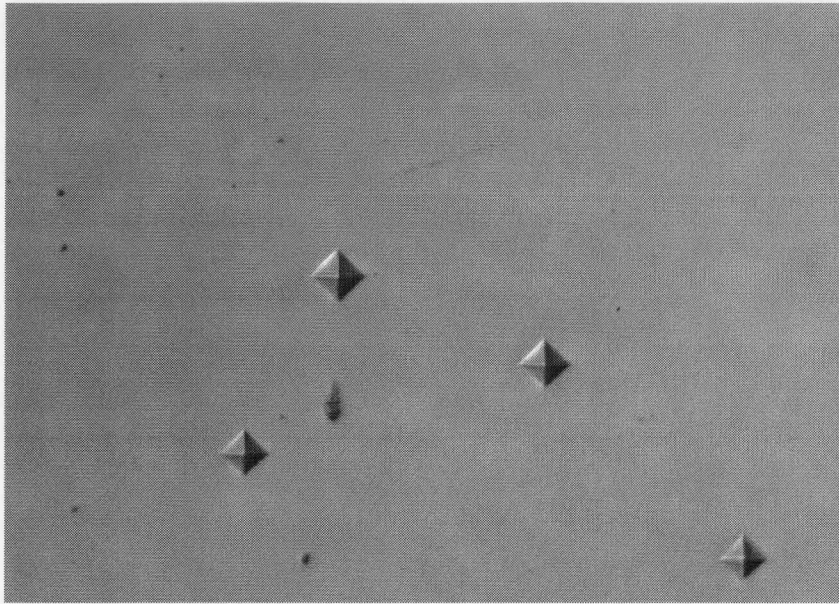


Figure 3.13: Indents on a nitrided case of Nitralloy 135M (x400)

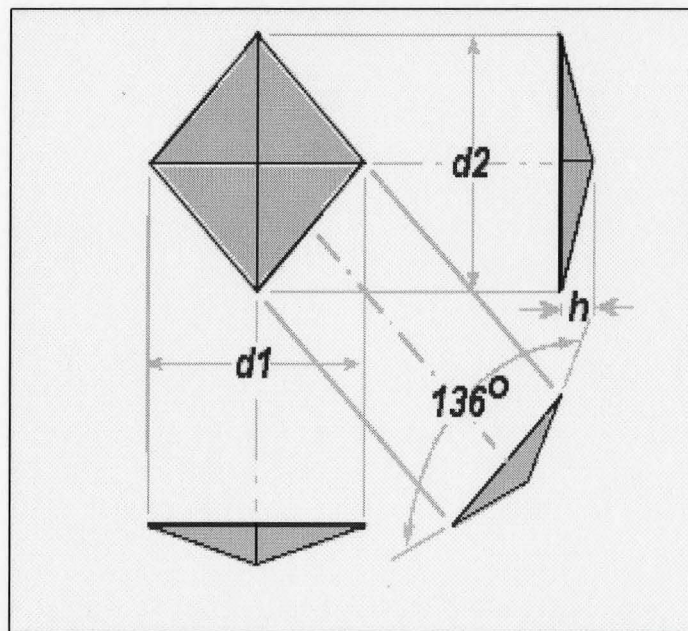


Figure 3.14: Vickers diamond indenter indentation profile [44]

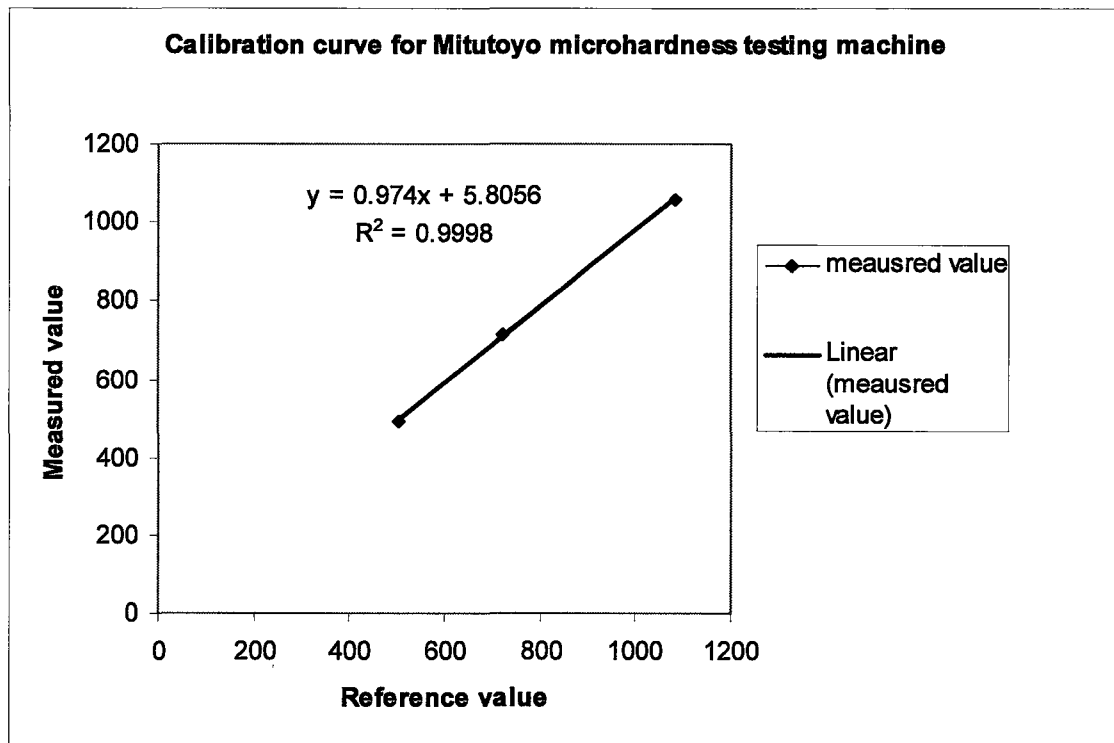


Figure 3.15: Calibration curve of Mitutoyo microhardness tester

3.5.3 Metallographic examination

The metallographic examination of the nitrided samples was conducted to determine the thickness of the white compound (layer) in microns (μm) developed during the process.

3.5.3.1 Etching

Specimens were etched using 3% Nital etchant having a volume-by-volume composition of 3ml HNO_3 in 97ml Methanol.

3.5.3.2 Storage after etching

After etching the specimens were ultrasonically cleaned to remove the etchant remaining in the pores, cracks, or interfaces between specimen and mount. Specimens were dried using an electric dryer and stored in desiccators.

3.5.3.3 Optical microscopy

White layer thickness examination of samples was conducted using a ZEISS optical microscope. Image analysis was done using a NORTHERN ECLIPSE[®] software as shown in the figure 3.16. A typical result from the white layer examination is shown in figure 3.17.

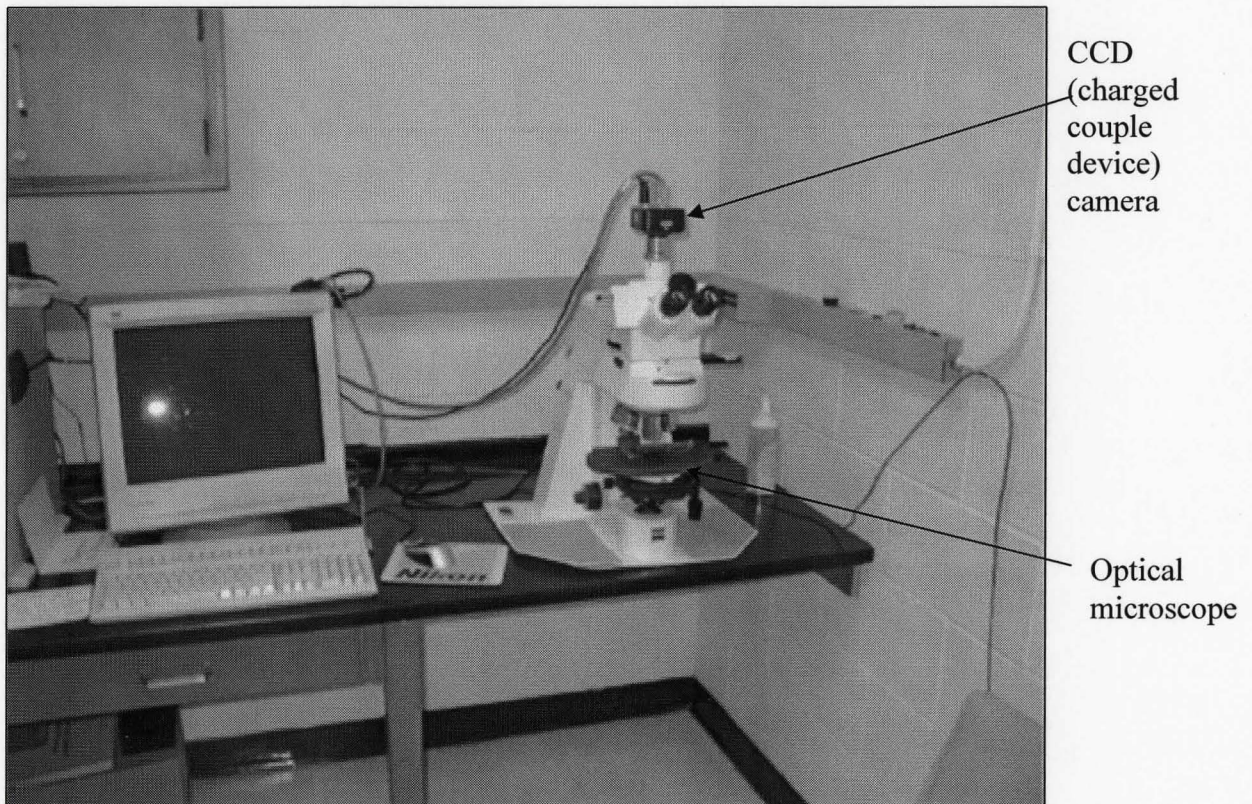


Figure 3.16: ZEISS optical microscope and computer with image analysis software.



Figure 3.17. A photomicrograph of sample “NN32S013” nitrided for 20 hrs at a K_N thickness of 0.45 and 1050 °F. White layer thickness is about 12.11 μm (x1000).

3.6. Data compilation

All the data collected was compiled in spreadsheet format, a sample of which is included in Appendix 3. Spreadsheets were prepared included in the Appendices 4-13 for the modeling of each of the five process parameters using the two ANN modeling techniques discussed in Chapter 4.

Chapter 4

Results and Discussion

Introduction

The main objective of the present study is to use real data collected from gas nitriding cycles to develop an Artificial neural network model that can predict case depths, white layer thickness, and superficial hardness of gas nitrided samples. Two ANN models have been developed and used in the present study. A multilayer perceptron (MLP) type model using Back-propagation adaptive gradient descent algorithm and a Radial basis function type neural network model were designed and tested using the same data. In addition to the development of the two ANN models, investigations of reverse modeling, non-uniformity of the microstructure due to effects of cooling rate and prior heat treatment of samples have also been considered and will be discussed below.

4.1. Artificial Neural Network (ANN) modeling

4.1.1. Introduction to NeuralWare® Predict

NeuralWare® Predict is an integrated, state-of-the-art tool for rapidly creating and deploying prediction and classification applications. Predict combines neural network technology with genetic algorithms, statistics, and fuzzy logic to automatically find optimal or near-optimal solutions for a wide range of problems.

Predict analyzes input data to identify appropriate transforms, partitions the input data into training and test sets, selects relevant input variables, and then constructs, trains, and optimizes a neural network tailored to the problem. In Microsoft® Windows environments NeuralWare® Predict can be run either as an add-in for Microsoft Excel to take advantage of Excel's rich data handling and graphing capabilities, or as a command line program that offers powerful batch mode processing [45].

4.1.2. Modeling using a (MLP) ANN model developed using NeuralWare® Predict

Prediction of nitriding case characteristics of total case depth (at 40HRC), effective case depth (at 50HRC), case depth (at 60HRC), superficial hardness and white layer thickness are presented in Table 4.1. Input to the model was the parameters of the second stage of the nitriding cycle, namely, K_N , t , and T .

Table 4.1. Consolidated results of NeuralWare modeling

Predicted Parameter	Number of data points		Maximum percentage difference based on experimental value
	Total	Number of data points used for model validation	
Case depth in μm at 60 HRC	111	20	14.00
Effective case in μm at 50 HRC	143	29	12.27
Total case in μm depth at 40HRC	122	19	13.48
Superficial hardness (HR 15N)	167	32	-4.78
White layer thickness in μm	148	30	> 40

NeuralWare Predict was trained and validated using the data for each of the characteristics of three types of case depths, superficial hardness and white layer thickness using values from Appendices 4-8. After training of the neural model it predicts the value of modeled characteristic for validation data (discussed in Section 4.1.4). The predicted values were compared with experimental values for each validation data point and the percentage difference based on the experimental value were calculated. The maximum percentage difference was noted.

It is evident from table 4.1 that more data points for training result in lower maximum percentage difference for three types of case depth with best prediction for effective case depth.

Superficial hardness prediction is the best of the five characteristics. It is over predicted i.e. the value predicted by the model is larger than the experimental value.

White layer thickness has more data points than any of the characteristics but has high value of error. This indicates that although number of data points used for training are more, the main factor is the process of gas nitriding itself i.e. the first stage of nitriding cycle. White layer is formed during the first stage and is diffused in the case during the second stage of the cycle. Since the parameters of first stage were not used as input parameters in the training of neural network model the prediction of white layer thickness has high percentage error as compared to other case characteristics prediction.

4.1.3. Modeling using Radial Basis Function (RBF)neural network

Nitriding cycles data was also used to build a Radial Basis function neural network using Mathworks® MATLAB 7.0 Newrbe function. Results of the (RBF) ANN model are summarized in table 4.2.

Table 4.2 Consolidated results of the Radial Basis Function neural network model.

Predicted parameter	Number of Data points		Maximum percentage difference based on experimental value
	Total	Number of data points used for validation	
Case depth in μm at 60 HRC	30	7	12.56
Effective case in μm at 50 HRC	30	7	6.57
Total case in μm depth at 40HRC	30	7	7.32
Superficial hardness (HR 15N)	30	7	-12.23
White layer thickness in μm	30	7	>50

Radial Basis Function neural network was trained and validated using the data for each of the characteristics of three types of case depths, superficial hardness and white layer thickness using values from Appendices 9-13. After training of the neural model it predicts the value of modeled characteristic for validation data (discussed in Section 4.1.4). The predicted values were compared with experimental values for each validation data point and the percentage difference based on the experimental value were calculated. The maximum percentage difference was noted.

Comparing Tables 4.1 and 4.2 one figures out marked difference in the number of datapoints used for the training and validation of neural networks. It is because as shown in Appendices 4-8 about the data used for training and validation of NeuralWare Predict,

Multilayer perceptrons can be trained on different values of outputs (case characteristics using same values of inputs (process parameters) work with same values of input and different outputs but Matlab 7.0 Newrbe function produces an error due to rank deficiency problem in this case. So the average values of case characteristics for all the 30 gas nitriding test cycles were used for training and validation.

It can be noted from table 4.2 that the prediction of three case depths is similar as using Multilayer perceptrons.

Prediction of superficial hardness is the best of all the case characteristics. But its over predicted.

White layer thickness prediction has high value of maximum percentage difference because of the reasons discussed in section 4.1.2.

4.1.4. Characteristics of validation data for modeling

Data sets used for the validation of both ANN models consisted of values of input process parameters that were within the range of values of data used to train the model. This is due to inherent ability of Artificial Neural Networks to interpolate as compared to extrapolation. Out of the 30 gas nitriding test cycles; 23 cycles were used for training and process parameters of 7 cycles qualified for usage as validation cycles.

4.1.5 Reverse modeling

Data of nitriding cycles of three types of case depth values (total, effective and case depth at 60 HRC), superficial hardness and white layer thickness were used to train MLP neural network model and the model was used to predict process parameters of K_N , t and T . This type of modeling is called reverse modeling. The models were then validated and results are presented in Table 4.3.

Reverse modeling was done using different combination of input parameters of case depth, superficial hardness and white layer thickness, consequently the following four cases were formed and modeled given by Table 4.3.

Table 4.3: Results of reverse neural network modeling

Case Number	Input Parameters	Number of datapoints		Maximum percentage error		
		Total	Validation	K_N	t	T
1	Total Case depth, Effective case depth, Case depth @60HRC	111	20	-23.52	-61.54	-1.84
2	Total Case depth, Effective case depth, Case depth @60HRC, Superficial hardness	111	20	-33.66	-101.3	-1.79
3	Total Case depth, Effective case depth, Case depth @60HRC, White layer thickness	111	20	-34.53	-71.0	-1.83
4	Total Case depth, Effective case depth, Case depth @60HRC, Superficial hardness, White layer thickness	111	20	-28.20	-82.56	-1.41

The results of reverse modeling have high percentage error because the data points used for training are not unique. The training data consist of results from 23 test cycles. To increase available data, case characteristics of three samples with two sides of each sample with some deletions were used a training data. Also the results indicate over prediction of the process parameters by the MLP neural network for all the cases.

Additionally the prediction of temperature is the best for all cases followed by Nitriding potential and cycle time.

4.2. Investigations of the non-uniform/discontinuous structure of white layer

The results of some nitrided case microstructure indicated non-uniform/discontinuous white layer. An example is shown in figures 4.1 (a) and (b). Both photomicrographs show portions of the microstructure of the same sample titled “NN11S31” nitrided in a cycle NN11 with the parameters listed in Table 4.2. The white layer variation from one portion of same side of sample to the other was 3000%.

Table 4.4: Cycle parameters for NN11

Parameter	Stage 1	Stage 2
K_N ($\text{bar}^{-1/2}$)	8.0	0.8
t (hrs)	5	20
T ($^{\circ}$ F)	975	1030



(a)



(b)

Figure 4.1: Two photomicrographs showing non-uniform portion of the white layer with thickness a) 30.79 μm . b) 0.0 μm (x1000) for the sample NN11S31

Two reasons for the above anomaly were investigated.

- Effect of cooling rate from nitriding temperature
- Effect of pre treatment of the used Nitralloy bars

4.2.1. Effect of cooling rate from nitriding temperature:

Two Nitriding cycles with identification number NN29 & NN39 were run using the same values of input parameters for both stages of the nitriding cycle. At the end of the cycle, the retort and the samples were cooled at the fastest and slowest possible cooling rates using the experimental setup. For the slowest cooling rate, the furnace heater was turned off and the retort was left to cool down inside the furnace from a temperature of 1030°F. The cooling rate recorded for the case was 3 °F/min. For the fastest cooling rate, the retort was lifted from the furnace and immediately placed on the cooling stand. The cooling rate recorded in this case was 19.68 °F/min, which is approximately 85% faster than the slowest cooling rate. The results of this investigation are shown in Table 4.5 and the white layer photomicrographs are presented in Figures 4.3 and 4.4.

Table 4.5: Nitrided sample properties from two cycles NN29&NN39 to compare effect of cooling rate

Sample number	NN29S92			NN39S122		
	Nitriding potential (bar ^{-1/2})	Cycle time (hrs)	Temperature (° F)	Nitriding potential (bar ^{-1/2})	Cycle time (hrs)	Temperature (° F)
First stage	8.00	5	975	8.00	5	975
Second stage	0.45	10	1030	0.45	10	1030
Average cooling rate for first 40 minutes after completion of cycle (° F/min)	3.00			19.68		
Total case depth (µm)	348.33			347.08		
Effective case depth (µm)	248.33			270.83		
Case depth at 60 HRC (µm)	168.33			171.25		
Superficial hardness (HR-15N)	94.5			94.7		
White layer thickness (µm)	16.81			16.77		



Figure 4.2. A photomicrograph of white layer of thickness $16.38\mu\text{m}$ from sample NN29S92 (x1000).



Figure 4.3: A photomicrograph of white layer of thickness $16.06\mu\text{m}$ from sample NN39S122 (x1000).

It is deduced from the afore mentioned results that the cooling rate from the nitriding temperature at the end of second stage of nitriding has no effect on the morphology of the white layer.

4.2.2. Effect of the pre treatment of the used Nitralloy bars

The nitriding test specimens were cut from two rods that were hardened and tempered in different cycles. The heat treatment recipes were the same as those shown in Table 4.6. The microstructure was studied using SEM (Scanning electron microscopy) and optical microscopy. As shown in Figures 4.5-4.8 .No difference was observed in the structure.

Table 4.6: Hardening and tempering sequence of Nitralloy 135M bars

Heat uniformly	Raise temperature	Quench	Temper	Average hardness (HRC)	
				Bar 1	Bar 2
1450° F hold for 20 minutes in Nitrogen atmosphere	1750° F hold for 1 hour	Oil	1175° F for 2 hours in air	34.6	34.0

Optical microscopy results are given below. The grain structure is not abnormally different.



Figure 4.4. Nitralloy 135M bar 1 tempered martensite grain structure (x1000)

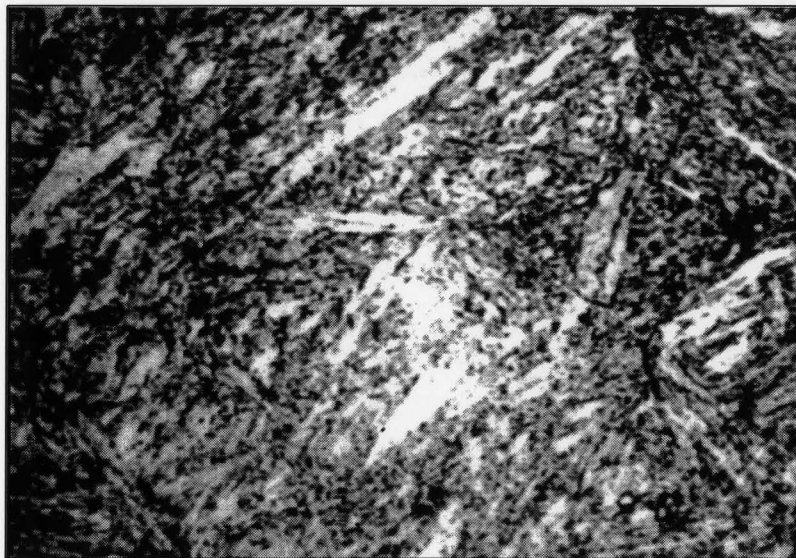


Figure 4.5. Nitralloy 135M bar 2 tempered martensite grain structure (x1000).

The microstructure of samples was observed using SEM microscopy using five times more magnification than optical microscope and results are given below.

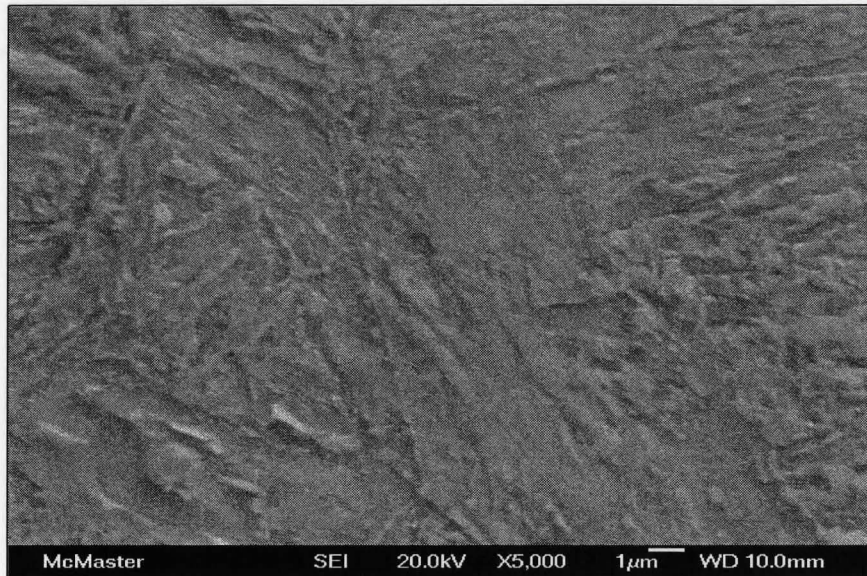


Figure 4.6. SEM image of Nitralloy 135M bar 1(x5000).

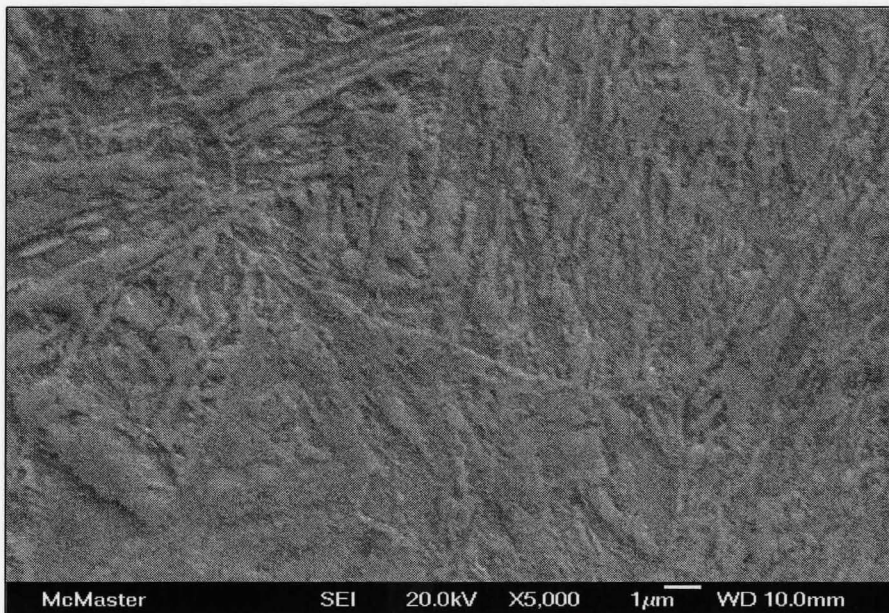


Figure 4.7. SEM image of Nitralloy 135M bar 2 (x5000).

No variation to suggest difference in white layer non-uniformity was noted.

4.3. Nitriding parameter variation profile during a typical cycle

Figures 4.8 , 4.9, 4.10 and 4.11 show a typical profile of parameters T and K_N variation during the first stage (5hrs) and second stage (10hrs) of the nitriding NN29cycle .The set points for K_N were 8 and 0.45 bar^{-1/2} and T were 975 °F and 1030 °F for first and second stages, respectively. As can be seen from figures 4.8 and 4.9 the temperature variation as indicated by one furnace atmosphere and two load thermocouples is ± 5 °F which is within the specified limits set by AMS 2759 series specifications.

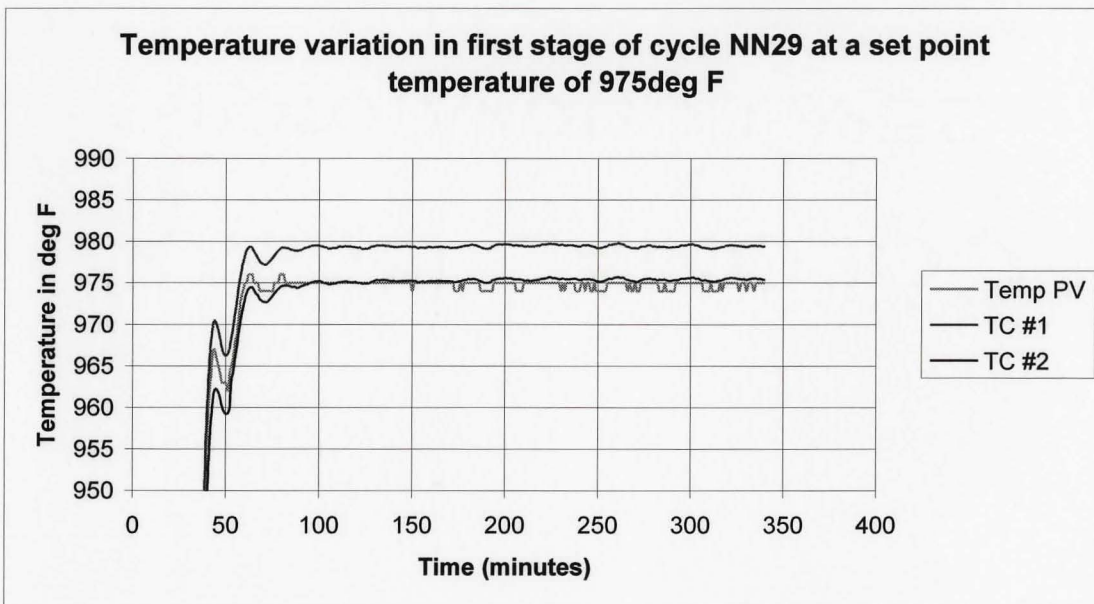


Figure 4.8. Temperature temporal variation during 5 hrs of first stage of cycle NN29

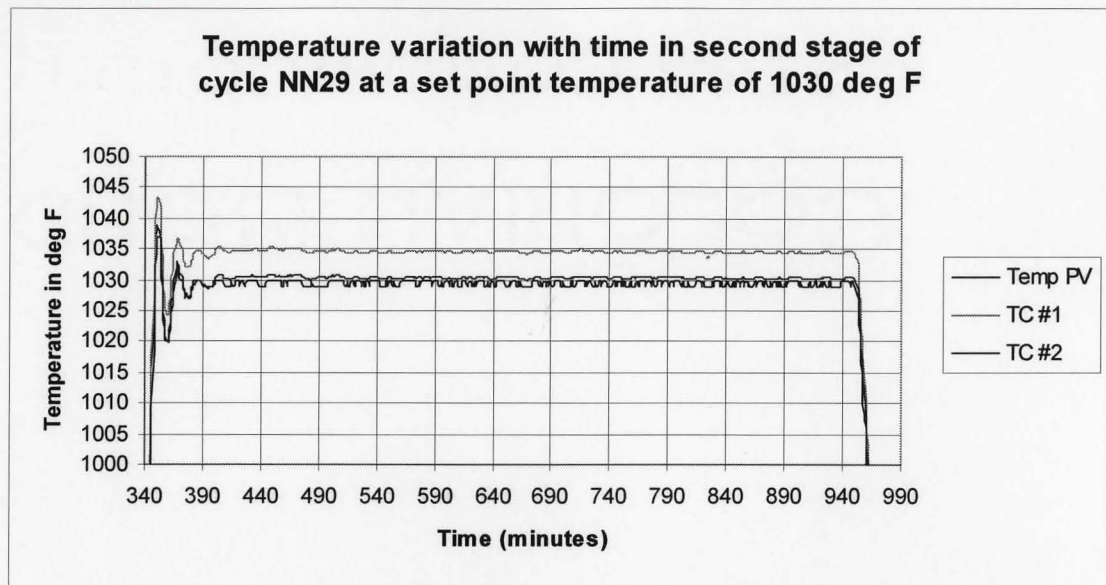


Figure 4.9. Temperature temporal variation during 10 hrs of second stage of cycle NN29

Also from figures 4.10 and 4.11 the nitriding potential variation is within $\pm 0.1 \text{ bar}^{-1/2}$ for the first stage and within $0.05 \text{ bar}^{-1/2}$ for the second stage of nitriding cycle. The variation in nitriding potential is within the limits specified by AMS specification 2759/10.

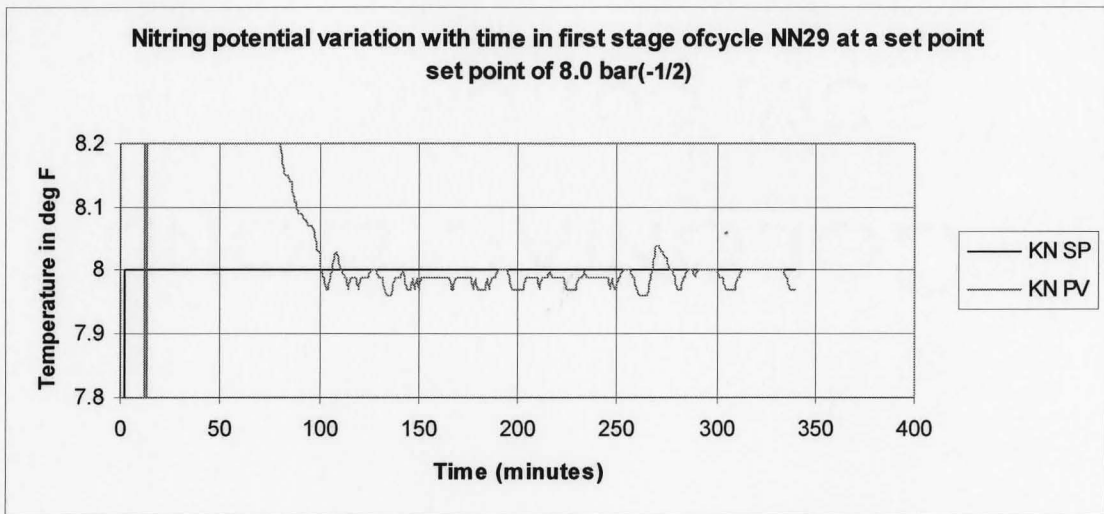


Figure 4.10: Nitriding potential temporal variation during 5 hrs of first stage of cycle NN29

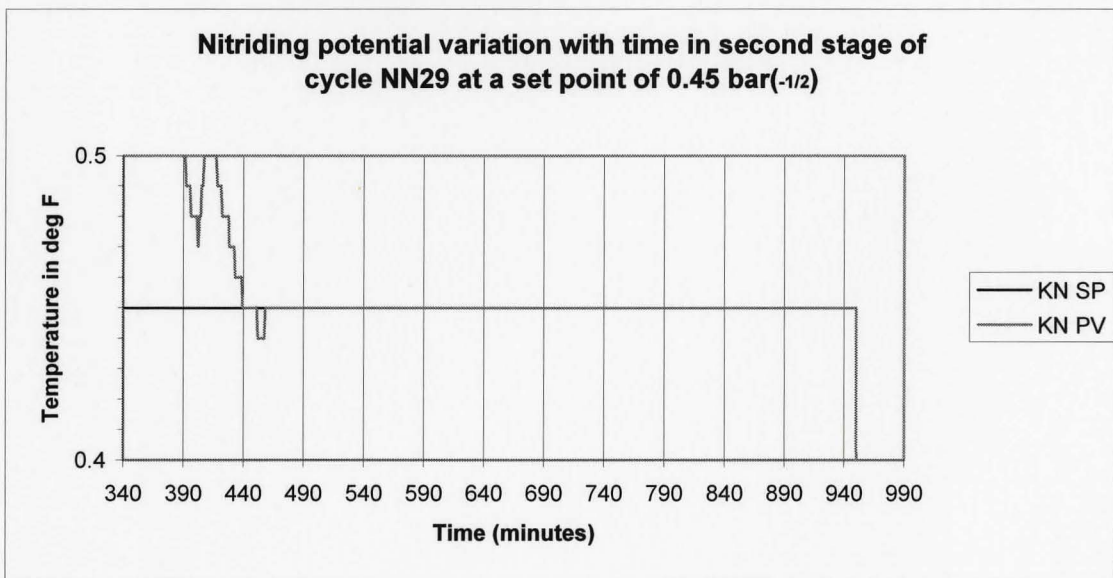


Figure 4.11: Nitriding potential temporal variation during 10 hrs of second stage of cycle NN29

4.4 Sensitivity analysis

Predictions obtained from the MLP artificial neural network model developed using the NeuralWare® Predict were subjected to a sensitivity analysis.

The resolution of the control system for K_N is $\pm 0.01 \text{ bar}^{-1/2}$, and temperature is $\pm 1^\circ\text{F}$. The altered values of K_N as given by table 4.7 were used in the training of the MLP neural network model. The effect of the altered values on the accuracy of the prediction of the case depth at 60 HRC were examined. The maximum percentage error on the validation set was found to be 14.80 % whereas the maximum percentage error on validation set using the actual (not altered) values was 14.00 %. No significant variation was found.

Table 4.7 : Nitriding potential values used in the sensitivity analysis

Parameter varied	Actual value $\text{bar}^{-1/2}$	Altered values $\text{bar}^{-1/2}$
K_N	0.3	0.295
	0.45	0.445
	0.6	0.595
	0.8	0.795

Also for the case of temperature there was $\pm 2.2^\circ\text{F}$ deviation in load thermocouples readings and $\pm 5.0^\circ\text{F}$ in temperature uniformity as measured by

furnace atmosphere thermocouple. Due to this it was almost impossible to gauge the effect of temperature on sensitivity analysis.

As part of sensitivity analysis a calibration curve of the Microhardness tester was obtained as shown in figure 3.15.

Chapter 5

Conclusions

Multivariate two-stage gas nitriding process for Nitralloy 135M was studied and significant parameters affecting the process; and characteristics defining the nitrided case were identified. AMS 2759/10 specification was used as a guide for controlling the process using Nitriding potential (K_N) parameter as opposed to percentage dissociation. A set of experimental data of process input and output parameters of nitriding test cycles were collected. Data was analyzed and partitioned into training and validation sets. The data sets were used to develop Multilayer Perceptron type ANN models using NeuralWare® Predict software. Another type of neural network model called Radial Basis function was also built using MATLAB 7.0 Newrbe function. The results and discussion of model prediction using validation data were presented in Chapter 4.

In addition the data sets were used for reverse modeling i.e. prediction of process control parameters (K_N , t and T) using case characteristics (case depths, superficial hardness and white layer thickness).

Further to that investigation on the effects of cooling rate after nitriding and prior heat treatment; on the microstructure of nitrided material i.e. Nitralloy 135M was done. A summary of investigations and neural network modeling of gas nitriding are given.

Parameters affecting gas nitriding process:

Four parameters were identified as having greatest effect on the process:

1. Nitriding potential
2. Cycle time
3. Cycle temperature

Effect of data points on the Neural network modeling:

Artificial Neural modeling results using Multilayer perceptron and Radial Basis Function structure are strongly dependant on the data points available for training.

This is evident from the modeling results of case depths in which effective case depth, with most number of data points for training has lowest value of maximum percentage difference i.e. 12.27 and 6.57% for MLP and RBF network respectively.

Prediction of white layer thickness:

The prediction of white layer thickness was poor. Although the number of data points for training was higher as compared to those used for the other parameters (case depths and superficial hardness). This is attributed to the fact that white layer formed on the case, is the result of process during the first stage of gas nitriding operation and we did not use first stage input parameters at all in the building of artificial neural network model. Also deficiencies in metallographic examination and the effects of kinetics of gas nitriding contributed to poor prediction.

Results of reverse modeling:

Reverse modeling i.e. prediction of process parameter for a particular case characteristic has great significance for heat treatment industry. The scarcity of unique data points used for reverse modeling caused poor reverse modeling results.

Effect of prior heat treatment on the microstructure of nitrided case:

Nitralloy 135M bars used for preparing samples for the nitriding cycles were hardened and tempered to achieve a specific hardness value. The heat treatment was done in separate cycles for both bars. Microhardness testing and metallographic examination of bars was done to determine the effect of non-uniformity of microstructure prior to gas nitriding. The microstructure was found to be similar. Prior heat treatment has no effect on gas nitrided case results.

Chapter 6

Recommendations and Future work

The following are the recommendations of the project:

1. More cycles should be run as the Artificial Neural Network performance (Prediction power) is dependant on the number of data points.
2. The scope of design of experiments for data collection should be increased to include parameters from the first stage of the gas nitriding cycle because the prediction of white layer is principally dependant on the conditions prevalent during the first stage of nitriding cycle.
3. Thermocouples should be spot welded to the sample to be nitrided rather than on samples placed adjacent to the test coupons.
4. All cycles should be of total duration (first stage plus the second stage) longer than 15 hours, equal or shorter cycles result in non-uniform case structure with regards to white layer morphology.
5. Microhardness testing using the Vickers Hardness method should be done with load greater than 100gf (used in the current experimentation), as this load is at the borderline of load at which the hardness value is dependant on the load.
6. New and better a metallographic techniques for sample testing should be explored.

7. Modeling of gas nitriding using other multivariate modeling methods like PCA (Principal Component Analysis) and PLS (Projection to latent structures) should be explored.

List of References

1. Boyer, E. H., "Practical heat treating", American Society of Metals International, 1999.
2. Avner, S., "Introduction to physical metallurgy", McGraw Hill International, 1974.
3. Pye, D., "Diffusion surface treatment techniques: A review", Industrial Heating magazine No.3, pp.139-144, 2001.
4. Handbook of the American Society of Metals International, "Heat Treating", Vol.4, 1991.
5. Pye, D., "Practical Nitriding and Ferritic Nitrocarburizing", ASM International, 2003.
6. Jaluria, Y., "Thermal processing of materials: from basic research to engineering", Journal of Heat transfer, Vol. 125, pp 957-979, 2003.
7. Barber Z., "Introduction to materials modeling", Maney publishers, 2005.
8. Haykin, S., Neural networks: a comprehensive foundation, Prentice Hall, 1999
9. Genel, K., "Application of Artificial neural network for predicting strain-life fatigue properties of steels on the basis of tensile tests", International Journal of Fatigue, Vol. 26, pp1027-1035, 2004.
10. <http://www.generation5.org/content/2000/nnintro.asp>

11. Fast, J., "Interaction of metals and gases", Publisher: Philips technical library, 1964.
12. Nitriding cycle number "NN6" Sample 16.
13. Karpenko, G.V., "Influence of diffusion coatings on the strength of steel", Freund publishing house, 1979.
14. https://engineering.purdue.edu/MSE/Fac_Staff/grad_students/Brayshaw.html
15. Maldzinski, L., Liliental, W., Tacikowski, J., Tymowski, G., "Modeling and control of nitride layer growth kinetics on the Nitralloy 135M alloy", Proceedings of 20th ASM Heat treating society conference, Vol.17, pp. 208-216, 2000.
16. Ratajski, J., "Model of growth kinetics of nitrated layer in the binary Fe-N system", Z. Metallakd. (Journal), Vol.95, No.9, pp-823-829, 2004.
17. Mittemeijer, E.J., Somers, M.A.J., "Thermodynamics, kinetics, and process control of Nitriding", Surface Engineering (Journal), Vol.13, No.6, pp.483-497, 1997.
18. Lambda Research, "Qualitative phase analysis of nitrated steels", Diffraction notes, No.22, 1998.
19. Friehling, P.B, Poulsen, F.W., Somers, M.A.J., "Nucleation of iron nitrides during gaseous nitriding of iron; effect of a preoxidation treatment", Z.Metallakd. (Journal), vol.92, No.6, pp-589-595, 2001.
20. Baranowska, J., Szczecinski, K., Wysiecki, M., "Increasing of gas nitriding kinetics via surface pre-treatment", Surface and coatings technology, (Journal) No. 151-152, pp 534-539, 2002.

21. Maldzinski, L, Liliental, W, Tymowski, G, Tacikowski, J., “New possibilities for controlling gas nitriding process by simulation of growth kinetics of nitride layers”, *Surface Engineering*, Vol.15, No.5, pp.377-384, 1999.
22. Lakhtin, Y.,”Control of the phase composition and nitrogen content in the nitride layer in the nitriding of steel 38Kh2MyuA”, *Metal science and heat treatment*, Vol. 38,Nos.1-2, pp 6-11,1996.
23. Rose, T., Manriquez, A., “White layer reduction techniques for gas nitriding”, *Proceedings of 16th ASM Heat treating society conference*, March 19-21, pp. 307-315, 1996.
24. Golodnikov, A., Macheret, Y., Trindade, A.,Uryasev, S., Zrazhevsky, G., “Statistical modelling of composition and processing parameters for alloy development”, *Modelling Simul. Mater. Sci. Eng.* Vol.13, pp. 633–644, 2005.
25. Genel, K., “Use of artificial neural network for prediction of ion nitrided case depth in Fe-Cr alloys”, *Materials and design*, Vol.24, pp 203-27, 2003.
26. Bhadeshia, H., “Neural networks in materials science”, *ISIJ International*, Vol.39, No.10, pp.966-979, 1999.
27. Kang, J., Rong, Y. “Modeling and simulation of load heating in heat treatment furnaces”, *Journal of Materials Processing Technology* , Vol.174, pp.109–114,2006.
28. Slovacek, M., “Application of numerical simulation of heat treatment in industry”, *J.Phys.IV*, Vol.120, pp 753-760, 2004.

29. Keddam, M., Djeghlal, M.E., Barrallier, L., Salhi, E., “Computer simulation of nitrated layers growth for pure iron”, *Computational Materials Science*, Vol. 29, pp. 43–48, 2004.
30. Krukovich, M.,G., “Simulation of the nitriding process”, *Metal science and heat treatment*, Vol.46,Nos.1-2,2004.
31. Haque, M.E., Sudhakar,K.V., “ANN back-propagation prediction model for fracture toughness in microalloy steel” *International Journal of Fatigue*, Vol. 24, No. 9, pp.1003-1010,2002.
32. Guanghui SU, Kenji FUKUDA, Koji MORITA, Mark PIDDUCK, Dounan JIA, Tatsuya MATSUMOTO and Ryo AKASAKA, “Applications of Artificial Neural Network for the Prediction of Flow Boiling Curves”, *Journal of nuclear science and technology*, Vol:39 ,No.11 pp:1190 –1198, 2002.
33. <http://www.warwick.ac.uk/atc/tig/whatwedo/interests/neuralnetworks.php>
34. Erb,R., “Introduction to backpropagation neural network computation”, *Pharmaceutical Resaerch*, Vol.10,No.2,pp.165-170,1993.
35. Guo, Z., Sha, W., “Modelling the correlation between processing parameters and properties of maraging steels using artificial neural network”, *Computational Materials Science*, Vol. 29, No. 1, pp.12-28, 2004.
36. Zhecheva, A., Malinov, S., Sha, W. “Simulation of microhardness profiles of titanium alloys after surface nitriding using artificial neural network”, *Metal Science and Heat Treatment*, Vol. 200, No. 7, pp. 2332-2342, 2005.

37. Hancheng, Q., Bocai X, Shangzheng L, Fagen W, "Fuzzy neural network modeling of material properties", Journal of Materials Processing Technology, Vol. 122, Nos.2-3, pp. 196-200,2002.
38. Velten, K., Reinicke, R., Friedrich,K., "Wear volume prediction with artificial neural networks", Tribology International, Vol. 33, No.10, pp 731-736,2000.
39. Sukthomya, W., Tannock, J., "The training of neural networks to model manufacturing processes" Journal of Intelligent Manufacturing, Vol.16, No. 1, pp 39-51,2005.
40. Filetin, T., Zmak I., Novak, D. "Determining nitriding parameters with neural networks", Journal of ASTM International, Vol. 2, No.5, pp.133-143, 2005.
41. Brooks Instrument model 5850i mass flow controller Installation and Operation manual 2001.
42. Ranjit R. "A Primer on the Taguchi Method" Society of Manufacturing; 1st edition 1990.
43. <http://www.hardnesstesters.com/hardness-indenters.htm>
44. <http://www.gordonengland.co.uk/hardness/>
45. Neuralware® Predict User manual,2002

Appendix-1(a)				
Taguchi partial factorial design(original design)				
Nitriding Potential	Cycle time	Temperature	Cycle number	Repeat cycle
0.3	10	1010	NN4	
0.3	20	1030	NN15	NN25
0.3	30	1050	NN17	
0.5	10	1030		
0.5	20	1050		
0.5	30	1010		
0.8	10	1050	NN5	
0.8	20	1010	NN8	NN23
0.8	30	1030	NN16	
With revised Nitriding potential to include 0.45				
Nitriding Potential	Cycle time	Temperature	Cycle number	Repeat cycle
0.3	10	1010	NN4	
0.3	20	1030	NN15	NN25
0.3	30	1050	NN17	
0.45	10	1030	NN29	
0.45	20	1050	NN32	
0.45	30	1010	NN33	
0.8	10	1050	NN5	
0.8	20	1010	NN8	NN23
0.8	30	1030	NN16	

Appendix-1(b)		
Multilevel full factorial design		
Nitriding Potential	Cycle time	Temperature
0.80	30.0	1030.0
0.30	20.0	1030.0
0.45	20.0	1030.0
0.80	30.0	1050.0
0.60	10.0	1010.0
0.60	10.0	1050.0
0.30	20.0	1050.0
0.60	20.0	1030.0
0.60	30.0	1030.0
0.80	10.0	1050.0
0.60	10.0	1030.0
0.80	20.0	1030.0
0.45	10.0	1010.0
0.45	20.0	1010.0
0.30	10.0	1010.0
0.60	20.0	1010.0
0.30	10.0	1030.0
0.80	20.0	1010.0
0.45	30.0	1050.0
0.60	30.0	1010.0
0.30	30.0	1010.0
0.80	10.0	1010.0
0.30	30.0	1050.0
0.80	10.0	1030.0
0.30	20.0	1010.0
0.80	30.0	1010.0
0.80	20.0	1050.0
0.60	20.0	1050.0
0.30	10.0	1050.0
0.45	10.0	1050.0
0.45	30.0	1010.0
0.60	30.0	1050.0
0.45	10.0	1030.0
0.30	30.0	1030.0
0.45	30.0	1030.0
0.45	20.0	1050.0

Appendix -2				
Details of all the actual cycles used in the study				
Cycle identification number #	Date	Samples	Cycle Parameters	
			Stage 1	Stage 2
NN1	6-Jun-05	S1, S2, S3	975F, 5hrs, Kn=8	1010F, 10hrs, Kn=0.6
NN2	16-Jun-05	S4, S5, S6	975F, 5hrs, Kn=8	1010F, 10hrs, Kn=0.6
NN3	17-Jun-05	S7, S8, S9	975F, 5hrs, Kn=8	1010F, 10hrs, Kn=0.8
NN4	20-Jun-05	S10, S11, S12	975F, 5hrs, Kn=8	1010F, 10hrs, Kn=0.3
NN5	22-Jun-05	S13, S14, S15	975F, 5hrs, Kn=8	1050F, 10hrs, Kn=0.8
NN6	23-Jun-05	S16, S17, S18	975F, 5hrs, Kn=8	1050F, 10hrs, Kn=0.3
NN7	26-Jun-05	S19, S20, S21	975F, 5hrs, Kn=8	1050F, 10hrs, Kn=0.6
NN8	28-Jun-05	S22, S23, S24	975F, 5hrs, Kn=8	1010F, 20hrs, Kn=0.8
NN9	30-Jun-05	S25, S26, S27	975F, 5hrs, Kn=8	1010F, 20hrs, Kn=0.6
NN10	2-Jul-05	S28, S29, S30	975F, 5hrs, Kn=8	1010F, 20hrs, Kn=0.3
NN11	4-Jul-05	S31, S32, S33	975F, 5hrs, Kn=8	1050F, 20hrs, Kn=0.8
NN12	6-Jul-05	S34, S35, S36	975F, 5hrs, Kn=8	1050F, 20hrs, Kn=0.3
NN13	8-Jul-05	S37, S38, S39	975F, 5hrs, Kn=8	1050F, 20hrs, Kn=0.6
NN14	10-Jul-05	S40, S41, S42	975F, 5hrs, Kn=8	1030F, 20hrs, Kn=0.8
NN15	13-Jul-05	S43, S44, S45	975F, 5hrs, Kn=8	1030F, 20hrs, Kn=0.3
NN16	15-Jul-05	S46, S47, S48	975F, 5hrs, Kn=8	1010F, 30hrs, Kn=0.8
NN17	18-Jul-05	S49, S50, S51	975F, 5hrs, Kn=8	1050F, 30hrs, Kn=0.3
NN18	20-Jul-05	S52, S53, S54	975F, 5hrs, Kn=8	1050F, 30hrs, Kn=0.8
NN19	27-Jul-05	S55, S56, S57	975F, 5hrs, Kn=6.9	1010F, 10hrs, Kn=0.8
NN20	28-Jul-05	S58, S59, S60	975F, 5hrs, Kn=6	1010F, 10hrs, Kn=0.8
NN21	30-Jul-05	S61, S62, S63	950F, 5hrs, Kn=8	1010F, 10hrs, Kn=0.8
NN22A [NN7 dupl]	9-Nov-05	S64, S65, S66, S67, S68	975F, 5hrs, Kn=8	1050F, 10hrs, Kn=0.6
NN22 [NN7 dupl]	11-Nov-05	S69, S70, S71, S72, S73	975F, 5hrs, Kn=8	1050F, 10hrs, Kn=0.6
NN23 [NN8 dupl]	12-Nov-05	S74, S75, S76	975F, 5hrs, Kn=8	1010F, 20hrs, Kn=0.8
NN24 [NN12 dupl]	14-Nov-05	S77, S78, S79	975F, 5hrs, Kn=8	1050F, 20hrs, Kn=0.3
NN25 [NN15 dupl]	18-Nov-05	S80, S81, S82	975F, 5hrs, Kn=8	1030F, 20hrs, Kn=0.3
NN26	18-Nov-05	S83, S84, S85	975F, 5hrs, Kn=8	1030F, 6.6hrs, Kn=0.6
NN27	9-Dec-05	S86, S87, S88	975F, 5hrs, Kn=8	1010F, 13hrs, Kn=0.3
NN28 [NN4 dupl]	24-Feb-06	S89, S90, S91	975F, 5hrs, Kn=8	1010F, 10hrs, Kn=0.3
NN29	26-Feb-06	S92, S93, S94	975F, 5hrs, Kn=8	1030F, 10hrs, Kn=0.45
NN27_A	5-Mar-06	S95A, S96A, S97A	975F, 5hrs, Kn=8	1010F, 2.25hrs, Kn=0.3
NN30	6-Mar-06	S95, S96, S97	975F, 5hrs, Kn=8	1010F, 17.75hrs, Kn=0.3
NN31	14-Mar-06	S98, S99, S100	975F, 5hrs, Kn=8	1010F, 30hrs, Kn=0.3
NN32	23-Mar-06	S101, S102, S103	975F, 5hrs, Kn=8	1050F, 20hrs, Kn=0.45
NN33	25-Mar-06	S104, S105, S106	975F, 5hrs, Kn=8	1010F, 30hrs, Kn=0.45
NN34	27-Mar-06	S107, S108, S109	975F, 5hrs, Kn=8	1030F, 30hrs, Kn=0.8
NN35	30-Mar-06	S110, S111, S112	975F, 5hrs, Kn=8	1010F, 20hrs, Kn=0.45
NN36	2-Apr-06	S113, S114, S115	975F, 5hrs, Kn=8	1030F, 20hrs, Kn=0.45
NN37	4-Apr-06	S116, S117, S118	975F, 5hrs, Kn=8	1030F, 20hrs, Kn=0.6
NN38	6-Apr-06	S119, S120, S121	975F, 5hrs, Kn=8	1030F, 10hrs, Kn=0.8
NN39	1-Jun-06	S122, S123, S124	975F, 5hrs, Kn=8	1030F, 10hrs, Kn=0.45

Appendix-3						
Typical spreadsheet of data collected for samples in each cycle						
Cycle29: Hardness Test						
Superficial Hardness						
Diamond cone Indenter [HR15N]						
Sample	NN29 S92	NN29 S92N	NN29 S93	NN29 S93N	NN29 S94	NN29 S94N
Measurements	94.2	94.6	94.7	94.7	94.6	94.7
	94.6	94.7	94.7	94.6	95.0	94.8
	94.2	94.4	94.7	94.8	94.7	94.4
	94.4	94.5	94.7	94.5	94.8	94.2
	94.4	94.9	94.1	95.0	94.4	94.5
	94.1	94.7	94.8	94.5	94.8	94.6
	94.2	94.6	94.4	94.6	94.3	94.5
94.5	94.5	94.3	94.4	91.2	94.7	
Min	92.8	94.4	94.1	94.4	91.2	94.2
Max	94.6	94.9	94.8	95.0	95.0	94.8
Average	94.3	94.6	94.6	94.6	94.2	94.6
Std Dev	0.18	0.16	0.25	0.19	1.24	0.19
Micro Hardness						
Vickers Indenter [HV 100gf]						
Depth	Hardness					
	NN29 S92	NN29 S92N	NN29 S93	NN29 S93N	NN29 S94	NN29 S94N
1	1083	1060	1060	1060	1131	1106
2	1060	1038	1060	1083	1060	1060
4	920	902	885	902	920	938
6	736	711	749	724	749	749
8	622	622	612	633	654	633
10	495	510	517	510	517	455
15	360	352	388	347	369	365
20	360	331	388	335	3434	347
25	352	327	360	331	347	339
125	339	339	343	335	343	335
Maximum value						
Samples	NN29 S92	NN29 S92N	NN29 S93	NN29 S93N	NN29 S94	NN29 S94N
Case Depth (40HRC) mils	13.8	13.7	14.8	13.6	14.2	13.5
Effective Case Depth (50HRC) mils	9.8	10.0	10.2	10.0	10.2	9.4
(60HRC) mils	6.7	6.3	6.8	6.6	7.1	6.9
60/50 HRC ratio [%]	68.4	63.0	66.7	66.0	69.6	73.4
White layer thickness(microns)	16.39	17.33	13.99	18.68	12.53	17.22
Notes on White layer						

Appendix-4					
Training and validation data for case depth at 60HRC prediction using NeuralWare Predict					
	Sample	Nitriding potential (bar - 1/2)	Cycle time (hrs)	Furnace temp (deg F)	case depth at 60HRC (microns)
1	NN27 NN27A S95A	0.3	2.25	1010	127.50
2	NN27 NN27A S95AN	0.3	2.25	1010	127.50
3	NN28 S89	0.3	10	1010	147.50
4	NN28 S89N	0.3	10	1010	147.50
5	NN28 S90	0.3	10	1010	147.50
6	NN28 S90N	0.3	10	1010	142.50
7	NN28 S91	0.3	10	1010	142.50
8	NN28 S91N	0.3	10	1010	140.00
9	NN6 S16	0.3	10	1050	170.00
10	NN6 S17	0.3	10	1050	177.50
11	NN27 S86N	0.3	13	1010	152.50
12	NN27 NN30 S95	0.3	17.75	1010	165.00
13	NN27 NN30 S95N	0.3	17.75	1010	170.00
14	NN10 S28N	0.3	20	1010	157.50
15	NN10 S29N	0.3	20	1010	153.00
16	NN25 S80	0.3	20	1030	182.50
17	NN25 S80N	0.3	20	1030	170.00
18	NN25 S81	0.3	20	1030	167.50
19	NN25 S81N	0.3	20	1030	160.00
20	NN25 S82	0.3	20	1030	180.00
21	NN25 S82N	0.3	20	1030	170.00
22	NN24 S77	0.3	20	1050	172.50
23	NN24 S78	0.3	20	1050	180.00
24	NN24 S78N	0.3	20	1050	182.50
25	NN24 S79	0.3	20	1050	187.50
26	NN31 S98N	0.3	30	1010	160.00
27	NN17 S49	0.3	30	1050	165.00
28	NN17 S50	0.3	30	1050	165.00
29	NN17 S50N	0.3	30	1050	167.50
30	NN17 S51	0.3	30	1050	162.50
31	NN17 S51N	0.3	30	1050	165.00
32	NN29 S92	0.45	10	1030	167.50
33	NN29 S92N	0.45	10	1030	157.50
34	NN29 S93	0.45	10	1030	170.00
35	NN29 S93N	0.45	10	1030	165.00
36	NN29 S94	0.45	10	1030	177.50
37	NN29 S94N	0.45	10	1030	172.50
38	NN35 S110	0.45	20	1010	172.50
39	NN35 S110N	0.45	20	1010	165.00
40	NN35 S112	0.45	20	1010	160.00
41	NN35 S112N	0.45	20	1010	167.50
42	NN36 S113	0.45	20	1030	175.00
43	NN32 S101	0.45	20	1050	182.50
44	NN32 S101N	0.45	20	1050	177.50
45	NN32 S102	0.45	20	1050	202.50
46	NN32 S102N	0.45	20	1050	210.00
47	NN32 S103	0.45	20	1050	212.50
48	NN33 S104	0.45	30	1010	202.50
49	NN33 S104N	0.45	30	1010	230.00

Training and validation data for case depth at 60HRC prediction using NeuralWare Predict					
50	NN33 S105	0.45	30	1010	202.50
51	NN33 S105N	0.45	30	1010	202.50
52	NN33 S106	0.45	30	1010	202.50
53	NN33 S106N	0.45	30	1010	210.00
54	NN2 S4	0.6	10	1010	152.50
55	NN2 S4N	0.6	10	1010	167.50
56	NN2 S6	0.6	10	1010	157.50
57	NN2 S6N	0.6	10	1010	152.50
58	NN26 S83	0.6	6.6	1030	162.50
59	NN26 S83N	0.6	6.6	1030	167.50
60	NN26 S84	0.6	6.6	1030	160.00
61	NN26 S84N	0.6	6.6	1030	167.50
62	NN26 S85	0.6	6.6	1030	172.50
63	NN26 S85N	0.6	6.6	1030	165.00
64	NN22 S69	0.6	10	1050	195.00
65	NN22 S69N	0.6	10	1050	182.50
66	NN22 S70	0.6	10	1050	180.00
67	NN22 S70N	0.6	10	1050	202.50
68	NN22 S71	0.6	10	1050	190.00
69	NN22 S71N	0.6	10	1050	187.50
70	NN22 S72N	0.6	10	1050	177.50
71	NN22 S73	0.6	10	1050	170.00
72	NN22 S73N	0.6	10	1050	187.50
73	NN9 S25	0.6	20	1010	190.00
74	NN9 S27N	0.6	20	1010	207.50
75	NN37 S117	0.6	20	1030	220.00
76	NN37 S117N	0.6	20	1030	225.00
77	NN37 S118	0.6	20	1030	220.00
78	NN37 S118N	0.6	20	1030	220.00
79	NN13 S37	0.6	20	1050	227.50
80	NN13 S39	0.6	20	1050	227.50
81	NN3 S7	0.8	10	1010	180.00
82	NN3 S7N	0.8	10	1010	177.50
83	NN3 S8	0.8	10	1010	182.50
84	NN3 S8N	0.8	10	1010	172.50
85	NN3 S9	0.8	10	1010	182.50
86	NN3 S9N	0.8	10	1010	182.50
87	NN38 S119	0.8	10	1030	187.50
88	NN38 S119N	0.8	10	1030	187.50
89	NN38 S120	0.8	10	1030	190.00
90	NN38 S120N	0.8	10	1030	205.00
91	NN38 S121	0.8	10	1030	202.50
92	NN38 S121N	0.8	10	1030	187.50
93	NN5 S13	0.8	10	1050	220.00
94	NN5 S13N	0.8	10	1050	220.00
95	NN5 S14	0.8	10	1050	222.50
96	NN5 S14N	0.8	10	1050	225.00
97	NN5 S15	0.8	10	1050	212.50
98	NN5 S15N	0.8	10	1050	210.00
99	NN23 S74	0.8	20	1010	202.50
100	NN23 S74N	0.8	20	1010	215.00
101	NN23 S75	0.8	20	1010	202.50
102	NN23 S75N	0.8	20	1010	222.50
103	NN23 S76N	0.8	20	1010	215.00

Training and validation data for case depth at 60HRC prediction using NeuralWare Predict					
104	NN14 S41	0.8	20	1030	257.50
105	NN14 S41N	0.8	20	1030	242.50
106	NN11 S33	0.8	20	1050	272.50
107	NN16 S47N	0.8	30	1010	207.50
108	NN16 S48	0.8	30	1010	215.00
109	NN34 S108N	0.8	30	1030	240.00
110	NN18 S53	0.8	30	1050	242.50
111	NN18 S54	0.8	30	1050	267.50

Appendix-5					
Training and validation data for effective case depth prediction using NeuralWare Predict					
	Sample	Nitriding potential (bar - 1/2)	Cycle time (hrs)	Furnace temp (deg F)	Effective case depth at 50HRC (microns)
1	NN27 NN27A S95A	0.3	2.25	1010	160.00
2	NN27 NN27A S95AN	0.3	2.25	1010	162.50
3	NN28 S89	0.3	10	1010	212.50
4	NN28 S89N	0.3	10	1010	222.50
5	NN28 S90	0.3	10	1010	212.50
6	NN28 S90N	0.3	10	1010	212.50
7	NN28 S91	0.3	10	1010	210.00
8	NN28 S91N	0.3	10	1010	197.50
9	NN6 S16	0.3	10	1050	245.00
10	NN6 S16N	0.3	10	1050	237.50
11	NN6 S17N	0.3	10	1050	212.50
12	NN6 S18N	0.3	10	1050	225.00
13	NN27 S86N	0.3	13	1010	270.00
14	NN27 NN30 S95	0.3	17.75	1010	277.50
15	NN27 NN30 S95N	0.3	17.75	1010	282.50
16	NN10 S28	0.3	20	1010	283.00
17	NN10 S28N	0.3	20	1010	285.00
18	NN25 S80	0.3	20	1030	310.00
19	NN25 S80N	0.3	20	1030	312.50
20	NN25 S81	0.3	20	1030	300.00
21	NN25 S81N	0.3	20	1030	300.00
22	NN25 S82	0.3	20	1030	312.50
23	NN25 S82N	0.3	20	1030	302.50
24	NN24 S77N	0.3	20	1050	320.00
25	NN24 S78N	0.3	20	1050	327.50
26	NN24 S79	0.3	20	1050	340.00
27	NN31 S99	0.3	30	1010	315.00
28	NN31 S99N	0.3	30	1010	312.50
29	NN31 S100	0.3	30	1010	310.00
30	NN31 S100N	0.3	30	1010	312.50
31	NN17 S49	0.3	30	1050	400.00
32	NN17 S49N	0.3	30	1050	382.50
33	NN17 S50	0.3	30	1050	400.00
34	NN17 S50N	0.3	30	1050	402.50
35	NN17 S51	0.3	30	1050	407.50
36	NN29 S92	0.45	10	1030	245.00
37	NN29 S92N	0.45	10	1030	250.00
38	NN29 S93	0.45	10	1030	255.00
39	NN29 S93N	0.45	10	1030	250.00
40	NN29 S94	0.45	10	1030	255.00
41	NN29 S94N	0.45	10	1030	235.00
42	NN35 S110	0.45	20	1010	285.00
43	NN35 S110N	0.45	20	1010	277.50
44	NN35 S112	0.45	20	1010	265.00
45	NN35 S112N	0.45	20	1010	272.50
46	NN36 S113	0.45	20	1030	300.00
47	NN36 S113N	0.45	20	1030	302.50
48	NN36 S114	0.45	20	1030	305.00
49	NN36 S114N	0.45	20	1030	305.00
50	NN36 S115	0.45	20	1030	300.00

Training and validation data for effective case depth prediction using NeuralWare Predict					
51	NN36 S115N	0.45	20	1030	295.00
52	NN32 S101	0.45	20	1050	337.50
53	NN32 S101N	0.45	20	1050	335.00
54	NN32 S102	0.45	20	1050	345.00
55	NN32 S102N	0.45	20	1050	347.50
56	NN32 S103	0.45	20	1050	320.00
57	NN32 S103N	0.45	20	1050	327.50
58	NN33 S104	0.45	30	1010	317.50
59	NN33 S104N	0.45	30	1010	325.00
60	NN33 S105	0.45	30	1010	327.50
61	NN33 S105N	0.45	30	1010	312.50
62	NN33 S106	0.45	30	1010	325.00
63	NN33 S106N	0.45	30	1010	312.50
64	NN2 S4	0.6	10	1010	222.50
65	NN2 S4N	0.6	10	1010	230.00
66	NN2 S6	0.6	10	1010	222.50
67	NN2 S6N	0.6	10	1010	227.50
68	NN26 S83	0.6	6.6	1030	220.00
69	NN26 S83N	0.6	6.6	1030	230.00
70	NN26 S84	0.6	6.6	1030	225.00
71	NN26 S84N	0.6	6.6	1030	227.50
72	NN26 S85	0.6	6.6	1030	225.00
73	NN26 S85N	0.6	6.6	1030	227.50
74	NN22 S69	0.6	10	1050	310.00
75	NN22 S69N	0.6	10	1050	302.50
76	NN22 S70	0.6	10	1050	285.00
77	NN22 S70N	0.6	10	1050	307.50
78	NN22 S71	0.6	10	1050	297.50
79	NN22 S71N	0.6	10	1050	295.00
80	NN22 S72	0.6	10	1050	287.50
81	NN22 S72N	0.6	10	1050	287.50
82	NN22 S73	0.6	10	1050	295.00
83	NN22 S73N	0.6	10	1050	282.50
84	NN9 S25	0.6	20	1010	287.50
85	NN9 S27	0.6	20	1010	297.50
86	NN9 S27N	0.6	20	1010	292.50
87	NN37 S116	0.6	20	1030	327.50
88	NN37 S116N	0.6	20	1030	320.00
89	NN37 S117	0.6	20	1030	312.50
90	NN37 S117N	0.6	20	1030	312.50
91	NN37 S118	0.6	20	1030	312.50
92	NN37 S118N	0.6	20	1030	322.50
93	NN13 S37	0.6	20	1050	332.50
94	NN13 S38N	0.6	20	1050	330.00
95	NN13 S39	0.6	20	1050	340.00
96	NN13 S39N	0.6	20	1050	332.50
97	NN3 S7	0.8	10	1010	242.50
98	NN3 S7N	0.8	10	1010	247.50
99	NN3 S8	0.8	10	1010	242.50
100	NN3 S8N	0.8	10	1010	247.50
101	NN3 S9	0.8	10	1010	260.00
102	NN3 S9N	0.8	10	1010	247.50
103	NN38 S119	0.8	10	1030	290.00
104	NN38 S119N	0.8	10	1030	285.00
105	NN38 S120	0.8	10	1030	310.00

Training and validation data for effective case depth prediction using NeuralWare Predict					
106	NN38 S120N	0.8	10	1030	290.00
107	NN38 S121	0.8	10	1030	290.00
108	NN38 S121N	0.8	10	1030	280.00
109	NN5 S13	0.8	10	1050	317.50
110	NN5 S13N	0.8	10	1050	310.00
111	NN5 S14	0.8	10	1050	315.00
112	NN5 S14N	0.8	10	1050	325.00
113	NN5 S15	0.8	10	1050	310.00
114	NN5 S15N	0.8	10	1050	317.50
115	NN23 S74	0.8	20	1010	312.50
116	NN23 S74N	0.8	20	1010	302.50
117	NN23 S75	0.8	20	1010	315.00
118	NN23 S75N	0.8	20	1010	310.00
119	NN23 S76N	0.8	20	1010	307.50
120	NN14 S40	0.8	20	1010	317.50
121	NN14 S40N	0.8	20	1030	322.50
122	NN14 S41	0.8	20	1030	330.00
123	NN14 S41N	0.8	20	1030	337.50
124	NN14 S42	0.8	20	1030	325.00
125	NN14 S42N	0.8	20	1030	327.50
126	NN11 S32	0.8	20	1030	357.50
127	NN11 S33	0.8	20	1050	372.50
128	NN11 S33N	0.8	20	1050	362.50
129	NN16 S46	0.8	30	1010	365.00
130	NN16 S46N	0.8	30	1010	372.50
131	NN16 S47	0.8	30	1010	372.50
132	NN16 S48N	0.8	30	1010	362.50
133	NN34 S107	0.8	30	1030	417.50
134	NN34 S107N	0.8	30	1030	420.00
135	NN34 S108	0.8	30	1030	407.50
136	NN34 S108N	0.8	30	1030	415.00
137	NN34 S109N	0.8	30	1030	405.00
138	NN18 S52	0.8	30	1050	422.50
139	NN18 S52N	0.8	30	1050	427.50
140	NN18 S53	0.8	30	1050	422.50
141	NN18 S53N	0.8	30	1050	425.00
142	NN18 S54	0.8	30	1050	425.00
143	NN18 S54N	0.8	30	1050	427.50

Appendix-6					
Training and validation data for total case depth prediction using NeuralWare Predict					
	Sample	Nitriding potential (bar - 1/2)	Cycle time (hrs)	Furnace temp (deg F)	Case depth at 40HRC (microns)
1	NN27 NN27A S95A	0.3	2.25	1010	220.0
2	NN27 NN27A S95AN	0.3	2.25	1010	200.0
3	NN28 S89	0.3	10	1010	247.5
4	NN28 S89N	0.3	10	1010	267.5
5	NN28 S90	0.3	10	1010	247.5
6	NN28 S90N	0.3	10	1010	247.5
7	NN28 S91	0.3	10	1010	242.5
8	NN28 S91N	0.3	10	1010	255.0
9	NN6 S16	0.3	10	1050	347.5
10	NN6 S16N	0.3	10	1050	342.5
11	NN6 S17	0.3	10	1050	347.5
12	NN27 S86	0.3	13	1010	327.5
13	NN27 S86N	0.3	13	1010	350.0
14	NN27 NN30 S95	0.3	17.75	1010	352.5
15	NN27 NN30 S95N	0.3	17.75	1010	347.5
16	NN10 S28	0.3	20	1010	337.5
17	NN10 S28N	0.3	20	1010	360.0
18	NN10 S29N	0.3	20	1010	352.5
19	NN25 S80	0.3	20	1030	362.5
20	NN25 S80N	0.3	20	1030	370.0
21	NN25 S81	0.3	20	1030	362.5
22	NN25 S81N	0.3	20	1030	362.5
23	NN25 S82	0.3	20	1030	372.5
24	NN25 S82N	0.3	20	1030	360.0
25	NN24 S77N	0.3	20	1050	397.5
26	NN31 S98N	0.3	30	1010	367.5
27	NN31 S99	0.3	30	1010	370.0
28	NN31 S99N	0.3	30	1010	362.5
29	NN31 S100	0.3	30	1010	367.5
30	NN31 S100N	0.3	30	1010	370.0
31	NN17 S49	0.3	30	1050	467.5
32	NN17 S49N	0.3	30	1050	465.0
33	NN17 S50	0.3	30	1050	472.5
34	NN17 S50N	0.3	30	1050	475.0
35	NN17 S51	0.3	30	1050	472.5
36	NN29 S92	0.45	10	1030	345.0
37	NN29 S92N	0.45	10	1030	342.5
38	NN29 S93	0.45	10	1030	350.0
39	NN29 S93N	0.45	10	1030	340.0
40	NN29 S94	0.45	10	1030	355.0
41	NN29 S94N	0.45	10	1030	337.5
42	NN35 S110	0.45	20	1010	355.0
43	NN35 S110N	0.45	20	1010	355.0
44	NN35 S112	0.45	20	1010	355.0
45	NN35 S112N	0.45	20	1010	345.0

Training and validation data for total case depth prediction using NeuralWare Predict					
46	NN36 S113	0.45	20	1030	362.5
47	NN36 S113N	0.45	20	1030	370.0
48	NN36 S114	0.45	20	1030	367.5
49	NN36 S114N	0.45	20	1030	360.0
50	NN36 S115	0.45	20	1030	360.0
51	NN32 S101	0.45	20	1050	442.5
52	NN32 S101N	0.45	20	1050	455.0
53	NN32 S102	0.45	20	1050	455.0
54	NN32 S102N	0.45	20	1050	465.0
55	NN32 S103N	0.45	20	1050	442.5
56	NN33 S104	0.45	30	1010	370.0
57	NN33 S105N	0.45	30	1010	370.0
58	NN33 S106N	0.45	30	1010	370.0
59	NN26 S83	0.6	6.6	1030	282.5
60	NN26 S84	0.6	6.6	1030	310.0
61	NN26 S84N	0.6	6.6	1030	315.0
62	NN26 S85	0.6	6.6	1030	292.5
63	NN26 S85N	0.6	6.6	1030	305.0
64	NN2 S4	0.6	10	1010	315.0
65	NN2 S6	0.6	10	1010	310.0
66	NN2 S6N	0.6	10	1010	307.5
67	NN22 S69	0.6	10	1050	360.0
68	NN22 S69N	0.6	10	1050	372.5
69	NN22 S70	0.6	10	1050	352.5
70	NN22 S70N	0.6	10	1050	362.5
71	NN22 S71	0.6	10	1050	365.0
72	NN22 S71N	0.6	10	1050	352.5
73	NN22 S72	0.6	10	1050	352.5
74	NN22 S72N	0.6	10	1050	352.5
75	NN22 S73	0.6	10	1050	367.5
76	NN22 S73N	0.6	10	1050	357.5
77	NN9 S25	0.6	20	1010	362.5
78	NN9 S27	0.6	20	1010	355.0
79	NN9 S27N	0.6	20	1010	362.5
80	NN37 S116N	0.6	20	1030	370.0
81	NN37 S117	0.6	20	1030	365.0
82	NN37 S117N	0.6	20	1030	365.0
83	NN37 S118N	0.6	20	1030	387.5
84	NN13 S37	0.6	20	1050	435.0
85	NN13 S38N	0.6	20	1050	435.0
86	NN13 S39	0.6	20	1050	457.5
87	NN13 S39N	0.6	20	1050	440.0
88	NN3 S7N	0.8	10	1010	352.5
89	NN3 S8	0.8	10	1010	347.5
90	NN3 S8N	0.8	10	1010	352.5
91	NN38 S119	0.8	10	1030	357.5
92	NN38 S119N	0.8	10	1030	360.0
93	NN38 S120	0.8	10	1030	360.0
94	NN5 S13	0.8	10	1050	367.5
95	NN5 S14	0.8	10	1050	370.0
96	NN5 S14N	0.8	10	1050	375.0

Training and validation data for total case depth prediction using NeuralWare Predict					
97	NN5 S15	0.8	10	1050	367.5
98	NN5 S15N	0.8	10	1050	370.0
99	NN23 S74	0.8	20	1010	365.0
100	NN23 S74N	0.8	20	1010	357.5
101	NN23 S75	0.8	20	1010	367.5
102	NN23 S75N	0.8	20	1010	367.5
103	NN23 S76N	0.8	20	1010	367.5
104	NN14 S40	0.8	20	1030	380.0
105	NN14 S40N	0.8	20	1030	412.5
106	NN14 S41	0.8	20	1030	387.5
107	NN11 S31	0.8	20	1050	465.0
108	NN11 S32	0.8	20	1050	460.0
109	NN11 S33	0.8	20	1050	490.0
110	NN11 S33N	0.8	20	1050	467.5
111	NN16 S46	0.8	30	1010	460.0
112	NN16 S46N	0.8	30	1010	465.0
113	NN16 S47	0.8	30	1010	462.5
114	NN16 S48N	0.8	30	1010	457.5
115	NN34 S108	0.8	30	1030	477.5
116	NN34 S108N	0.8	30	1030	480.0
117	NN18 S52	0.8	30	1050	485.0
118	NN18 S52N	0.8	30	1050	487.5
119	NN18 S53	0.8	30	1050	482.5
120	NN18 S53N	0.8	30	1050	487.5
121	NN18 S54	0.8	30	1050	487.5
122	NN18 S54N	0.8	30	1050	485.0

Appendix-7					
Training and validation data for Superficial hardness prediction using NeuralWare Predict					
	Sample	Nitriding potential (bar - 1/2)	Cycle time (hrs)	Furnace temp (deg F)	Superficial hardness (HR 15N)
1	NN27 NN27A S95A	0.3	2.25	1010	94.5
2	NN27 NN27A S95AN	0.3	2.25	1010	94.8
3	NN28 S89	0.3	10	1010	94.2
4	NN28 S89N	0.3	10	1010	94.2
5	NN28 S90	0.3	10	1010	94.2
6	NN28 S90N	0.3	10	1010	94.1
7	NN28 S91	0.3	10	1010	94
8	NN28 S91N	0.3	10	1010	94.2
9	NN6 S16	0.3	10	1050	94.1
10	NN6 S16N	0.3	10	1050	94.1
11	NN6 S17	0.3	10	1050	93.9
12	NN6 S17N	0.3	10	1050	93
13	NN6 S18	0.3	10	1050	90.8
14	NN6 S18N	0.3	10	1050	91.5
15	NN27 S86	0.3	13	1010	94.6
16	NN27 S86N	0.3	13	1010	94.6
17	NN27 NN30 S95	0.3	17.75	1010	94.1
18	NN27 NN30 S95N	0.3	17.75	1010	94
19	NN10 S28	0.3	20	1010	91.4
20	NN10 S28N	0.3	20	1010	93.4
21	NN10 S29	0.3	20	1010	90
22	NN10 S29N	0.3	20	1010	92.6
23	NN10 S30	0.3	20	1010	91.2
24	NN10 S30N	0.3	20	1010	90.6
25	NN25 S80	0.3	20	1030	93.8
26	NN25 S80N	0.3	20	1030	94.2
27	NN25 S81	0.3	20	1030	94.3
28	NN25 S81N	0.3	20	1030	94.4
29	NN25 S82	0.3	20	1030	93.9
30	NN25 S82N	0.3	20	1030	94.4
31	NN24 S77	0.3	20	1050	93.6
32	NN24 S77N	0.3	20	1050	94.2
33	NN24 S78	0.3	20	1050	93.6
34	NN24 S78N	0.3	20	1050	94
35	NN24 S79	0.3	20	1050	93.5
36	NN24 S79N	0.3	20	1050	93.9
37	NN31 S98	0.3	30	1010	91.2
38	NN31 S98N	0.3	30	1010	94.2
39	NN31 S99	0.3	30	1010	93.3
40	NN31 S99N	0.3	30	1010	91.9
41	NN31 S100	0.3	30	1010	93.6
42	NN31 S100N	0.3	30	1010	91.9
43	NN17 S49	0.3	30	1050	93.6
44	NN17 S49N	0.3	30	1050	94
45	NN17 S50	0.3	30	1050	92.6
46	NN17 S50N	0.3	30	1050	93.5
47	NN17 S51	0.3	30	1050	94
48	NN17 S51N	0.3	30	1050	93.3
49	NN29 S92	0.45	10	1030	94.3
50	NN29 S92N	0.45	10	1030	94.6
51	NN29 S93	0.45	10	1030	94.6
52	NN29 S93N	0.45	10	1030	94.6
53	NN29 S94	0.45	10	1030	94.2
54	NN29 S94N	0.45	10	1030	94.6
55	NN35 S110	0.45	20	1010	94.5

Training and validation data for Superficial hardness prediction using NeuralWare Predict					
56	NN35 S110N	0.45	20	1010	94.5
57	NN35 S111	0.45	20	1010	94.5
58	NN35 S111N	0.45	20	1010	94.5
59	NN35 S112	0.45	20	1010	94.4
60	NN35 S112N	0.45	20	1010	94.7
61	NN36 S113	0.45	20	1030	94.6
62	NN36 S113N	0.45	20	1030	94.6
63	NN36 S114	0.45	20	1030	94
64	NN36 S114N	0.45	20	1030	94.4
65	NN36 S115	0.45	20	1030	94.6
66	NN36 S115N	0.45	20	1030	94.7
67	NN32 S101	0.45	20	1050	94.3
68	NN32 S101N	0.45	20	1050	94.4
69	NN32 S102	0.45	20	1050	94.7
70	NN32 S102N	0.45	20	1050	94.3
71	NN32 S103	0.45	20	1050	93.2
72	NN32 S103N	0.45	20	1050	94.2
73	NN33 S104	0.45	30	1010	94.7
74	NN33 S104N	0.45	30	1010	94.6
75	NN33 S105	0.45	30	1010	94.6
76	NN33 S105N	0.45	30	1010	94.6
77	NN33 S106	0.45	30	1010	94.1
78	NN33 S106N	0.45	30	1010	94.7
79	NN2 S4	0.6	10	1010	92.7
80	NN2 S4N	0.6	10	1010	94.1
81	NN2 S6	0.6	10	1010	92.3
82	NN2 S6N	0.6	10	1010	92.5
83	NN26 S83	0.6	6.6	1030	94.6
84	NN26 S83N	0.6	6.6	1030	94.6
85	NN26 S84	0.6	6.6	1030	94.5
86	NN26 S84N	0.6	6.6	1030	94.8
87	NN26 S85	0.6	6.6	1030	94.6
88	NN26 S85N	0.6	6.6	1030	94.7
89	NN22 S69	0.6	10	1050	93.9
90	NN22 S69N	0.6	10	1050	94.4
91	NN22 S70	0.6	10	1050	94.1
92	NN22 S70N	0.6	10	1050	94.1
93	NN22 S71	0.6	10	1050	94.3
94	NN22 S71N	0.6	10	1050	94.5
95	NN22 S72	0.6	10	1050	94
96	NN22 S72N	0.6	10	1050	94.4
97	NN22 S73	0.6	10	1050	94
98	NN22 S73N	0.6	10	1050	94.2
99	NN9 S25	0.6	20	1010	92.3
100	NN9 S25N	0.6	20	1010	91.6
101	NN9 S27	0.6	20	1010	93.1
102	NN9 S27N	0.6	20	1010	94
103	NN37 S116	0.6	20	1030	92.9
104	NN37 S116N	0.6	20	1030	94.2
105	NN37 S117	0.6	20	1030	92.7
106	NN37 S117N	0.6	20	1030	93.1
107	NN37 S118	0.6	20	1030	93
108	NN37 S118N	0.6	20	1030	93.2
109	NN13 S37	0.6	20	1050	92.8
110	NN13 S37N	0.6	20	1050	89.2
111	NN13 S38	0.6	20	1050	92.4
112	NN13 S38N	0.6	20	1050	89.3
113	NN13 S39	0.6	20	1050	92.2
114	NN13 S39N	0.6	20	1050	90
115	NN3 S7	0.8	10	1010	91
116	NN3 S7N	0.8	10	1010	92.6

Training and validation data for Superficial hardness prediction using NeuralWare Predict					
117	NN3 S8	0.8	10	1010	93.6
118	NN3 S8N	0.8	10	1010	93.7
119	NN3 S9	0.8	10	1010	94.1
120	NN3 S9N	0.8	10	1010	93.5
121	NN38 S119	0.8	10	1030	92.7
122	NN38 S119N	0.8	10	1030	93.1
123	NN38 S120	0.8	10	1030	92.6
124	NN38 S120N	0.8	10	1030	92.9
125	NN38 S121	0.8	10	1030	93.2
126	NN38 S121N	0.8	10	1030	93.2
127	NN5 S13	0.8	10	1050	94.2
128	NN5 S13N	0.8	10	1050	94.1
129	NN5 S14	0.8	10	1050	94
130	NN5 S14N	0.8	10	1050	94.2
131	NN5 S15	0.8	10	1050	93.8
132	NN5 S15N	0.8	10	1050	94
133	NN23 S74	0.8	20	1010	93.8
134	NN23 S74N	0.8	20	1010	94.2
135	NN23 S75	0.8	20	1010	94
136	NN23 S75N	0.8	20	1010	94
137	NN23 S76	0.8	20	1010	91.4
138	NN23 S76N	0.8	20	1010	94.2
139	NN14 S40	0.8	20	1030	94.3
140	NN14 S40N	0.8	20	1030	94.6
141	NN14 S41	0.8	20	1030	93
142	NN14 S41N	0.8	20	1030	94.2
143	NN14 S42	0.8	20	1030	93.6
144	NN14 S42N	0.8	20	1030	94.1
145	NN11 S31	0.8	20	1050	91.6
146	NN11 S31N	0.8	20	1050	89.2
147	NN11 S32	0.8	20	1050	92.3
148	NN11 S32N	0.8	20	1050	90.2
149	NN11 S33	0.8	20	1050	92.5
150	NN11 S33N	0.8	20	1050	93.5
151	NN16 S46	0.8	30	1010	94
152	NN16 S46N	0.8	30	1010	94.8
153	NN16 S47	0.8	30	1010	93.5
154	NN16 S47N	0.8	30	1010	93.7
155	NN16 S48	0.8	30	1010	92.4
156	NN16 S48N	0.8	30	1010	94.6
157	NN34 S107	0.8	30	1030	94
158	NN34 S107N	0.8	30	1030	94.1
159	NN34 S108	0.8	30	1030	93.5
160	NN34 S108N	0.8	30	1030	94.5
161	NN34 S109	0.8	30	1030	92.8
162	NN34 S109N	0.8	30	1030	94.7
163	NN18 S52	0.8	30	1050	94.6
164	NN18 S52N	0.8	30	1050	94.9
165	NN18 S53	0.8	30	1050	94.7
166	NN18 S53N	0.8	30	1050	94.7
167	NN18 S54	0.8	30	1050	94.2
168	NN18 S54N	0.8	30	1050	94.5

Appendix-8					
Training and validation data for white layer thickness prediction using NeuralWare Predict					
	Sample	Nitriding potential (bar -1/2)	Cycle time (hrs)	Furnace temp (deg F)	White layer thickness in microns
1	NN27 NN27A S95A	0.3	2.25	1010	15.24
2	NN27 NN27A S95AN	0.3	2.25	1010	17.43
3	NN28 S89	0.3	10	1010	13.00
4	NN28 S89N	0.3	10	1010	17.95
5	NN28 S90	0.3	10	1010	13.99
6	NN28 S90N	0.3	10	1010	15.45
7	NN28 S91	0.3	10	1010	12.32
8	NN6 S16	0.3	10	1050	16.60
9	NN6 S16N	0.3	10	1050	16.08
10	NN6 S17	0.3	10	1050	13.57
11	NN6 S17N	0.3	10	1050	10.20
12	NN6 S18	0.3	10	1050	7.73
13	NN27 S86	0.3	13	1010	14.09
14	NN27 S86N	0.3	13	1010	17.43
15	NN27 NN30 S95	0.3	17.75	1010	13.47
16	NN27 NN30 S95N	0.3	17.75	1010	13.57
17	NN10 S28	0.3	20	1010	7.83
18	NN10 S28N	0.3	20	1010	14.30
19	NN10 S29N	0.3	20	1010	7.62
20	NN10 S30N	0.3	20	1010	12.42
21	NN25 S80	0.3	20	1030	10.86
22	NN25 S80N	0.3	20	1030	17.01
23	NN25 S81	0.3	20	1030	16.81
24	NN25 S81N	0.3	20	1030	17.85
25	NN25 S82	0.3	20	1030	13.47
26	NN25 S82N	0.3	20	1030	20.88
27	NN24 S77	0.3	20	1050	20.21
28	NN24 S77N	0.3	20	1050	17.54
29	NN24 S78	0.3	20	1050	14.41
30	NN24 S78N	0.3	20	1050	12.94
31	NN24 S79	0.3	20	1050	11.69
32	NN24 S79N	0.3	20	1050	13.67
33	NN31 S98	0.3	30	1010	15.34
34	NN31 S98N	0.3	30	1010	16.91
35	NN31 S99	0.3	30	1010	13.57
36	NN31 S99N	0.3	30	1010	16.39
37	NN31_S100N	0.3	30	1010	13.15
38	NN17 S49	0.3	30	1050	9.40
39	NN17 S49N	0.3	30	1050	16.81
40	NN17 S50	0.3	30	1050	15.03
41	NN17 S50N	0.3	30	1050	12.73
42	NN17 S51	0.3	30	1050	12.84

Training and validation data for white layer thickness prediction using NeuralWare Predict					
43	NN17_S51N	0.3	30	1050	13.36
44	NN29_S92	0.45	10	1030	16.39
45	NN29_S92N	0.45	10	1030	17.33
46	NN29_S93	0.45	10	1030	13.99
47	NN29_S93N	0.45	10	1030	18.68
48	NN29_S94	0.45	10	1030	12.53
49	NN29_S94N	0.45	10	1030	17.22
50	NN35_S110	0.45	20	1010	13.47
51	NN35_S110N	0.45	20	1010	15.14
52	NN35_S112	0.45	20	1010	14.72
53	NN35_S112N	0.45	20	1010	14.93
54	NN36_S113	0.45	20	1030	12.00
55	NN36_S113N	0.45	20	1030	17.85
56	NN36_S114	0.45	20	1030	15.14
57	NN36_S114N	0.45	20	1030	15.45
58	NN36_S115	0.45	20	1030	15.14
59	NN36_S115N	0.45	20	1030	18.68
60	NN32_S101	0.45	20	1050	11.69
61	NN32_S101N	0.45	20	1050	15.34
62	NN32_S102	0.45	20	1050	15.87
63	NN32_S102N	0.45	20	1050	16.28
64	NN32_S103	0.45	20	1050	12.11
65	NN32_S103N	0.45	20	1050	16.39
66	NN33_S104	0.45	30	1010	11.69
67	NN33_S104N	0.45	30	1010	15.34
68	NN33_S105	0.45	30	1010	16.60
69	NN33_S105N	0.45	30	1010	13.78
70	NN33_S106	0.45	30	1010	16.05
71	NN33_S106N	0.45	30	1010	16.70
72	NN2_S5	0.6	10	1010	5.69
73	NN2_S5N	0.6	10	1010	9.29
74	NN26_S83	0.6	6.6	1030	12.73
75	NN26_S83N	0.6	6.6	1030	16.60
76	NN26_S84	0.6	6.6	1030	13.47
77	NN26_S84N	0.6	6.6	1030	14.82
78	NN22_S69	0.6	10	1050	15.76
79	NN22_S69N	0.6	10	1050	17.33
80	NN22_S70	0.6	10	1050	12.42
81	NN22_S70N	0.6	10	1050	14.41
82	NN22_S71	0.6	10	1050	18.59
83	NN22_S71N	0.6	10	1050	13.88
84	NN22_S72	0.6	10	1050	12.94
85	NN22_S72N	0.6	10	1050	14.72
86	NN22_S73	0.6	10	1050	15.76
87	NN22_S73N	0.6	10	1050	16.91
88	NN9_S25	0.6	20	1010	10.86
89	NN9_S25N	0.6	20	1010	0.00
90	NN9_S26	0.6	20	1010	10.20

Training and validation data for white layer thickness prediction using NeuralWare Predict					
91	NN9 S26N	0.6	20	1010	7.60
92	NN37 S116	0.6	20	1030	13.15
93	NN37 S116N	0.6	20	1030	14.30
94	NN37 S117	0.6	20	1030	16.28
95	NN37 S117N	0.6	20	1030	15.97
96	NN37 S118	0.6	20	1030	11.27
97	NN37 S118N	0.6	20	1030	13.15
98	NN13 S38N	0.6	20	1050	6.37
99	NN13 S39	0.6	20	1050	19.10
100	NN13 S39N	0.6	20	1050	14.20
101	NN3 S7	0.8	10	1010	15.14
102	NN3 S7N	0.8	10	1010	13.99
103	NN3 S8	0.8	10	1010	0.00
104	NN3 S8N	0.8	10	1010	7.99
105	NN3 S9	0.8	10	1010	0.00
106	NN3 S9N	0.8	10	1010	18.48
107	NN38 S119	0.8	10	1030	16.08
108	NN38 S119N	0.8	10	1030	15.76
109	NN38 S120	0.8	10	1030	13.05
110	NN38 S120N	0.8	10	1030	14.20
111	NN38 S121	0.8	10	1030	15.45
112	NN38 S121N	0.8	10	1030	14.41
113	NN5 S13	0.8	10	1050	24.22
114	NN5 S13N	0.8	10	1050	21.19
115	NN5 S14	0.8	10	1050	19.52
116	NN5 S14N	0.8	10	1050	22.34
117	NN5 S15	0.8	10	1050	19.42
118	NN5 S15N	0.8	10	1050	19.83
119	NN23 S74	0.8	20	1010	17.23
120	NN23 S74N	0.8	20	1010	18.68
121	NN23 S75	0.8	20	1010	14.61
122	NN23 S76N	0.8	20	1010	10.61
123	NN14 S40	0.8	20	1030	19.83
124	NN14 S40N	0.8	20	1030	22.96
125	NN14 S41	0.8	20	1030	25.68
126	NN14 S41N	0.8	20	1030	18.89
127	NN14 S42	0.8	20	1030	18.06
128	NN14 S42N	0.8	20	1030	20.25
129	NN11 S31	0.8	20	1050	26.93
130	NN11 S31N	0.8	20	1050	30.79
131	NN11 S32	0.8	20	1050	25.57
132	NN11 S32N	0.8	20	1050	22.34
133	NN16 S46	0.8	30	1010	28.28
134	NN16 S46N	0.8	30	1010	22.86
135	NN16 S47	0.8	30	1010	12.84
136	NN16 S48	0.8	30	1010	15.76
137	NN16 S48N	0.8	30	1010	25.60
138	NN34 S107	0.8	30	1030	17.33
139	NN34 S107N	0.8	30	1030	19.62
140	NN34 S108	0.8	30	1030	19.21

Training and validation data for white layer thickness prediction using NeuralWare Predict					
141	NN34 S108N	0.8	30	1030	19.21
142	NN34 S109N	0.8	30	1030	19.11
143	NN18 S52	0.8	30	1050	25.99
144	NN18 S52N	0.8	30	1050	27.54
145	NN18 S53	0.8	30	1050	24.53
146	NN18 S53N	0.8	30	1050	27.77
147	NN18 S54	0.8	30	1050	27.98
148	NN18 S54N	0.8	30	1050	27.66

Appendix-9					
Training and testing data for case depth @ 60 HRC prediction using Radial Basis Function Neural Network					
	Sample	Nitriding potential (bar - 1/2)	Cycle time (hrs)	Furnace temp (deg F)	Case depth at 60HRC (microns)
1	NN27	0.3	2.25	1010	127.50
2	NN28	0.3	10	1010	144.58
3	NN6	0.3	10	1050	164.17
4	NN27A	0.3	13	1010	148.75
5	NN30	0.3	17.75	1010	167.50
6	NN10	0.3	20	1010	157.50
7	NN25	0.3	20	1030	171.67
8	NN24	0.3	20	1050	178.50
9	NN31	0.3	30	1010	160.00
10	NN17	0.3	30	1050	164.17
11	NN29	0.45	10	1030	168.33
12	NN35	0.45	20	1010	166.25
13	NN36	0.45	20	1030	170.00
14	NN32	0.45	20	1050	197.00
15	NN33	0.45	30	1010	208.33
16	NN2	0.6	10	1010	157.50
17	NN26	0.6	6.6	1030	165.83
18	NN22	0.6	10	1050	185.33
19	NN9	0.6	20	1010	203.33
20	NN37	0.6	20	1030	218.00
21	NN13	0.6	20	1050	227.25
22	NN3	0.8	10	1010	179.58
23	NN38	0.8	10	1030	193.33
24	NN5	0.8	10	1050	218.33
25	NN23	0.8	20	1010	211.50
26	NN14	0.8	20	1030	250.00
27	NN11	0.8	20	1050	272.50
28	NN16	0.8	30	1010	211.25
29	NN34	0.8	30	1030	240.00
30	NN18	0.8	30	1050	255.00

Appendix-10					
Training and testing data for effective case depth prediction using Radial Basis Function Neural Network					
	Sample	Nitriding potential (bar - 1/2)	Cycle time (hrs)	Furnace temp (deg F)	Effective case depth at 50HRC (microns)
1	NN27	0.3	2.25	1010	161.25
2	NN28	0.3	10	1010	211.25
3	NN6	0.3	10	1050	230.00
4	NN27A	0.3	13	1010	270.00
5	NN30	0.3	17.75	1010	280.00
6	NN10	0.3	20	1010	284.00
7	NN25	0.3	20	1030	306.25
8	NN24	0.3	20	1050	329.17
9	NN31	0.3	30	1010	312.50
10	NN17	0.3	30	1050	398.50
11	NN29	0.45	10	1030	248.33
12	NN35	0.45	20	1010	275.00
13	NN36	0.45	20	1030	301.25
14	NN32	0.45	20	1050	335.42
15	NN33	0.45	30	1010	320.00
16	NN2	0.6	10	1010	225.63
17	NN26	0.6	6.6	1030	225.83
18	NN22	0.6	10	1050	295.00
19	NN9	0.6	20	1010	292.50
20	NN37	0.6	20	1030	317.92
21	NN13	0.6	20	1050	333.75
22	NN3	0.8	10	1010	247.92
23	NN38	0.8	10	1030	290.83
24	NN5	0.8	10	1050	315.83
25	NN23	0.8	20	1010	309.50
26	NN14	0.8	20	1030	326.67
27	NN11	0.8	20	1050	364.17
28	NN16	0.8	30	1010	368.13
29	NN34	0.8	30	1030	413.00
30	NN18	0.8	30	1050	425.00

Appendix-11					
Training and testing data for total case depth prediction using Radial Basis Function Neural Network					
	Sample	Nitriding potential (bar - 1/2)	Cycle time (hrs)	Furnace temp (deg F)	Case depth at 40HRC (microns)
1	NN27	0.3	2.25	1010	210.00
2	NN28	0.3	10	1010	251.30
3	NN6	0.3	10	1050	345.80
4	NN27A	0.3	13	1010	338.80
5	NN30	0.3	17.75	1010	350.00
6	NN10	0.3	20	1010	349.90
7	NN25	0.3	20	1030	365.00
8	NN24	0.3	20	1050	380.00
9	NN31	0.3	30	1010	367.90
10	NN17	0.3	30	1050	470.50
11	NN29	0.45	10	1030	345.00
12	NN35	0.45	20	1010	352.50
13	NN36	0.45	20	1030	364.00
14	NN32	0.45	20	1050	452.00
15	NN33	0.45	30	1010	370.00
16	NN2	0.6	10	1010	310.80
17	NN26	0.6	6.6	1030	301.00
18	NN22	0.6	10	1050	359.50
19	NN9	0.6	20	1010	360.00
20	NN37	0.6	20	1030	371.90
21	NN13	0.6	20	1050	441.90
22	NN3	0.8	10	1010	350.80
23	NN38	0.8	10	1030	359.20
24	NN5	0.8	10	1050	370.00
25	NN23	0.8	20	1010	365.00
26	NN14	0.8	20	1030	393.30
27	NN11	0.8	20	1050	407.60
28	NN16	0.8	30	1010	461.30
29	NN34	0.8	30	1030	478.80
30	NN18	0.8	30	1050	485.80

Appendix-12					
Training and testing data for superficial hardness prediction using Radial Basis Function Neural Network					
	Sample	Nitriding potential (bar - 1/2)	Cycle time (hrs)	Furnace temp (deg F)	Average superficial hardness (HR 15N)
1	NN27	0.3	2.25	1010	94.65
2	NN28	0.3	10	1010	94.15
3	NN6	0.3	10	1050	92.90
4	NN27A	0.3	13	1010	94.60
5	NN30	0.3	17.75	1010	94.05
6	NN10	0.3	20	1010	91.53
7	NN25	0.3	20	1030	94.17
8	NN24	0.3	20	1050	93.80
9	NN31	0.3	30	1010	92.68
10	NN17	0.3	30	1050	93.50
11	NN29	0.45	10	1030	94.48
12	NN35	0.45	20	1010	94.52
13	NN36	0.45	20	1030	94.48
14	NN32	0.45	20	1050	94.18
15	NN33	0.45	30	1010	94.55
16	NN2	0.6	10	1010	92.90
17	NN26	0.6	6.6	1030	94.63
18	NN22	0.6	10	1050	94.19
19	NN9	0.6	20	1010	92.75
20	NN37	0.6	20	1030	93.18
21	NN13	0.6	20	1050	90.98
22	NN3	0.8	10	1010	93.08
23	NN38	0.8	10	1030	93.00
24	NN5	0.8	10	1050	94.05
25	NN23	0.8	20	1010	93.60
26	NN14	0.8	20	1030	93.97
27	NN11	0.8	20	1050	91.55
28	NN16	0.8	30	1010	93.83
29	NN34	0.8	30	1030	93.93
30	NN18	0.8	30	1050	94.60

Appendix-13					
Training and testing data for white layer thickness prediction using Radial Basis Function Neural Network					
	Sample	Nitriding potential (bar - 1/2)	Cycle time (hrs)	Furnace temp (deg F)	White layer thickness in microns
1	NN27	0.3	2.25	1010	16.34
2	NN28	0.3	10	1010	14.54
3	NN6	0.3	10	1050	12.39
4	NN27A	0.3	13	1010	15.76
5	NN30	0.3	17.75	1010	13.52
6	NN10	0.3	20	1010	10.54
7	NN25	0.3	20	1030	16.15
8	NN24	0.3	20	1050	15.08
9	NN31	0.3	30	1010	15.07
10	NN17	0.3	30	1050	13.47
11	NN29	0.45	10	1030	16.02
12	NN35	0.45	20	1010	14.56
13	NN36	0.45	20	1030	15.71
14	NN32	0.45	20	1050	14.61
15	NN33	0.45	30	1010	15.03
16	NN2	0.6	10	1010	5.64
17	NN26	0.6	6.6	1030	14.40
18	NN22	0.6	10	1050	15.27
19	NN9	0.6	20	1010	9.55
20	NN37	0.6	20	1030	14.02
21	NN13	0.6	20	1050	13.22
22	NN3	0.8	10	1010	13.90
23	NN38	0.8	10	1030	14.82
24	NN5	0.8	10	1050	21.09
25	NN23	0.8	20	1010	15.29
26	NN14	0.8	20	1030	20.95
27	NN11	0.8	20	1050	29.77
28	NN16	0.8	30	1010	21.07
29	NN34	0.8	30	1030	18.89
30	NN18	0.8	30	1050	26.91